การสังเคราะห์วัสดุประกอบแต่งของคาร์บอนนาโนทิวบ์และทังสเตนออกไซด์สาหรับประยุกต์ใช้เป็นเซนเซอร์ตรวจวัดก๊าซคาร์บอนไดออกไซด์

นางสาวศิริพร มนชยาพิสุทธิ์

วิทยานิพนธ์นี้เป็นส่วนหนึ่งของการศึกษาตามหลักสูตรปริญญาวิศวกรรมศาสตรมหาบัณฑิต
สาขาวิชาวิศวกรรมเคมี ภาควิชาวิศวกรรมเคมี
คณะวิศวกรรมศาสตร์ จุฬาลงกรณ์มหาวิทยาลัย
ปีการศึกษา 2554

SYNTHESIS OF CARBON NANOTUBE-TUNGSTEN OXIDE COMPOSITE FOR CARBON DIOXIDE SENSING APPLICATION

Miss Siriporn Monchayapisut

A Thesis Submitted in Partial Fulfillment of the Requirements
for the Degree of Master of Engineering Program in Chemical Engineering
Department of Chemical Engineering
Faculty of Engineering
Chulalongkorn University
Academic Year 2011

Thesis Title	SYNTHESIS OF CARBON NANOTUBE-TUNGSTEN OXIDE COMPOSITE FOR CARBON DIOXIDE SENSING APPLICATION
By	Miss Siriporn Monchayapisut
Field of Study	Chemical Engineering
Thesis Advisor	Associate Professor Tawatchai Charinpanitkul, D.Eng.
Thesis Co-advisor	Associate Professor Mana Sriyudthsak, D.Eng.

Accepted by the Faculty of Engineering, Chulalongkorn University in Partial Fulfillment of the Requirements for the Master's Degree

..... Dean of the Faculty of Engineering
(Associate Professor Boonsom Lerdhirunwong, Dr.Ing.)

THESIS COMMITTEE

..... Chairman
(Assistant Professor Apinan Soottitantawat, Ph.D.)

..... Thesis Advisor
(Associate Professor Tawatchai Charinpanitkul, D.Eng.)

..... Thesis Co-advisor
(Associate Professor Mana Sriyudthsak, D.Eng.)

..... Examiner
(Assistant Professor Varong Pavarajarn, Ph.D.)

..... Examiner
(Achariya Suriyawong, Ph.D.)

..... External Examiner
(Kajornsak Faungnavakij, D.Eng.)

ศิริพร มนชยาพิสุทธิ์ : การสังเคราะห์วัสดุประกอบแต่งของคาร์บอนนาโนทิวบ์และทังสเตนออกไซด์สาหรับประยุกต์ใช้เป็นเซนเซอร์ตรวจวัดก๊าซคาร์บอนไดออกไซด์. (SYNTHESIS OF CARBON NANOTUBE-TUNGSTEN OXIDE COMPOSITE FOR CARBON DIOXIDE SENSING APPLICATION) อ. ที่ปรึกษาวิทยานิพนธ์หลัก : รศ. ดร. ธวัชชัย ชรินพาณิชกุล, อ. ที่ปรึกษาวิทยานิพนธ์ร่วม : รศ. ดร. มานะ ศรียุทธศักดิ์, 97 หน้า.

วัสดุประกอบแต่งของคาร์บอนนาโนทิวบ์และทังสเตนออกไซด์เพื่อใช้สำหรับตรวจวัดก๊าซได้ถูกสังเคราะห์ขึ้นโดยวิธีตกตะกอนด้วยกรดตามด้วยการเผาภายใต้บรรยากาศของอากาศ กระบวนการทำวิจัยแบ่งออกเป็น 3 ขั้นตอนคือ การศึกษาการสังเคราะห์ทังสเตนออกไซด์ การสังเคราะห์วัสดุประกอบแต่งของคาร์บอนนาโนทิวบ์และทังสเตนออกไซด์ และการศึกษาความสามารถในการตอบสนองต่อก๊าซคาร์บอนไดออกไซด์ของวัสดุที่เตรียมขึ้น ในขั้นตอนการสังเคราะห์ทังสเตนออกไซด์ พบว่าสภาวะที่เหมาะสมในการสังเคราะห์ที่ให้ร้อยละผลได้สูงสุดเท่ากับ 71.4 คือ ความเข้มข้นของเกลือทังสเตนเท่ากับ 5.3 มิลลิโมลาร์ และความเข้มข้นของกรดไนตริกเท่ากับ 10 โมลาร์ ที่อุณหภูมิ 80 องศาเซลเซียส เป็นเวลา 30 นาที และเผาที่อุณหภูมิ 400 องศาเซลเซียส เป็นเวลา 1 ชั่วโมง ในขั้นตอนที่สอง วัสดุประกอบแต่งของคาร์บอนนาโนทิวบ์และทังสเตนออกไซด์ถูกสังเคราะห์ที่สัดส่วนโดยมวลที่แตกต่างกันโดยใช้สภาวะการสังเคราะห์ที่เหมาะสมดังกล่าว สัดส่วนของคาร์บอนนาโนทิวบ์ต่อทังสเตนออกไซด์ที่สังเคราะห์อยู่ในช่วง 0.4:100-8.5:100 ในขั้นตอนสุดท้ายวัสดุตอบสนองต่อก๊าซทั้ง 3 ชนิดคือ ทังสเตนออกไซด์ วัสดุประกอบแต่ง และ คาร์บอนนาโนทิวบ์ ถูกใช้เตรียมตัวตรวจวัดก๊าซแบบฟิล์มหนาที่เตรียมขึ้นได้เองโดยใช้วิธีการหยดและเคลือบอย่างง่าย ความสามารถในการตอบสนองต่อก๊าซของตัวตรวจวัดก๊าซทั้งหมดถูกทดสอบโดยใช้ก๊าซคาร์บอนไดออกไซด์ที่มีความเข้มข้น 500 ส่วนในล้านส่วน จากอุณหภูมิห้องจนถึงอุณหภูมิ 200 องศาเซลเซียส ตัวตรวจวัดก๊าซที่เตรียมจากทังสเตนออกไซด์ที่เผาที่อุณหภูมิ 400 องศาเซลเซียส แสดงความไวต่อการตอบสนองมากกว่าตัวตรวจวัดก๊าซที่เตรียมจากทังสเตนออกไซด์ที่เผาที่อุณหภูมิ 300 และ 600 องศาเซลเซียส สำหรับวัสดุประกอบแต่ง ตัวตรวจวัดก๊าซที่เตรียมขึ้นด้วยสัดส่วนคาร์บอนนาโนทิวบ์ต่อทังสเตนออกไซด์น้อยที่สุดคือ 0.4:100 มีความไวต่อการตอบสนองสูงเป็น 3 เท่าของตัวตรวจวัดก๊าซที่เตรียมจากทังสเตนออกไซด์ ด้วยสัดส่วนคาร์บอนนาโนทิวบ์ต่อทังสเตนออกไซด์ที่เหมาะสมคือ 1.5:100 พบว่าตัวตรวจวัดก๊าซที่เตรียมขึ้นตอบสนองต่อก๊าซคาร์บอนไดออกไซด์ได้ที่อุณหภูมิต่ำสุด 50 องศาเซลเซียส โดยมีความไวต่อการตอบสนองสูงถึงร้อยละ 41.0 และเวลาต่อการตอบสนองที่น้อยที่สุด 19.1 วินาที แสดงให้เห็นว่าอุณหภูมิในการตรวจวัดก๊าซสามารถลดลงได้ถึง 4 เท่า จาก 200 องศาเซลเซียส เป็น 50 องศาเซลเซียส เมื่อใช้วัสดุประกอบแต่งสัดส่วนดังกล่าว แทนการใช้ทังสเตนออกไซด์อย่างเดียว

ภาควิชา วิศวกรรมเคมี ลายมือชื่อนิสิต.....

สาขาวิชา วิศวกรรมเคมี ลายมือชื่อ อ.ที่ปรึกษาวิทยานิพนธ์หลัก.....

ปีการศึกษา 2554 ลายมือชื่อ อ.ที่ปรึกษาวิทยานิพนธ์ร่วม.....

5170659621 : MAJOR CHEMICAL ENGINEERING
KEYWORDS : TUNGSTEN OXIDE / CARBON NANOTUBE / CARBON DIOXIDE / GAS SENSOR / MWCNT-WO_3

SIRIPORN MONCHAYAPISUT : SYNTHESIS OF CARBON NANOTUBE-TUNGSTEN OXIDE COMPOSITE FOR CARBON DIOXIDE SENSING APPLICATION. ADVISOR : ASSOC. PROF. TAWATCHAI CHARINPANITKUL, D.Eng, CO-ADVISOR : ASSOC. PROF. MANA SRIYUDTHSAK, D.Eng, 97 pp.

For employing as sensing materials, multi-walled carbon nanotubes-tungsten oxide (MWCNT-WO_3) composites were synthesized by using acid precipitation method following by calcination under air atmospheres. The research procedure was divided into 3 steps including investigation of WO_3 synthesis, synthesis of MWCNT-WO_3 composites, and investigation of gas sensing ability of as-prepared sensing materials. In the step of synthesis of tungsten oxide nanoparticles, it was found that the suitable condition with the highest percent yield of 71.4 % was obtained from precipitation of 5.3 mM tungsten salt and 10 M nitric acid at 80 °C for 30 min and then calcine at 400 °C for 1 hour. In the second step, MWCNT-WO_3 composites were then synthesized with different mass ratio of MWCNTs to tungsten salt according to the suitable precipitation and calcination condition. The actual mass ratio (MWCNTs: WO_3) is in a range of 0.4:100 to 8.5:100. In the last step, three sensing materials including WO_3 nanoparticles, MWCNT-WO_3 composites, pristine MWCNTs were employed to prepare in-house fabricated thick film gas sensors by facile drop coating method. Sensing ability of all fabricated sensor were tested by exposure to CO_2 with concentration of 500 ppm at room temperature to 200 °C. Gas sensors prepared from WO_3 calcined at 400 °C would exhibit higher sensitivity to CO_2 than that calcined at 300 °C or 600 °C. For the composites as sensing materials, the fabricated sensor with the smallest ratio of MWCNTs to WO_3 (0.4:100) could provide three times sensitivity higher than the sensors prepared from WO_3 nanoparticles. With the optimum ratio of MWCNTs to WO_3 (1.5:100), the sensors could also respond to CO_2 at the lowest operating temperature of 50 °C with high sensitivity of 41.0% and the shortest response time of 19.1 seconds. It means that the operating temperature could be reduced four times from 200 °C to 50 °C when the composites at this ratio (1.5:100) were used instead of WO_3 nanoparticles.

Department : Chemical Engineering Student's Signature .....
Field of Study : Chemical Engineering Advisor's Signature .....
Academic Year : 2011 Co-advisor's Signature .....

ACKNOWLEDGEMENTS

I am very thankful to my thesis advisor and co-advisor, Assoc. Prof. Tawatchai Charinpanitkul, Department of Chemical Engineering and Assoc. Prof. Mana Sriyudthsak, Department of Electrical Engineering, Chulalongkorn University, for introducing me to this interesting project, and for their helpful and deep discussion and guidance throughout the course of this work. Furthermore, I am also thankful to Asst. Prof. Apinan Soottitantawat, Asst. Prof. Varong Pavarajarn, Dr. Achariya Suriyawong and Dr. Kajornsak Faungnavakij for their comments and participation as my thesis committee.

I would like to acknowledge the Centennial Fund of Chulalongkorn University and the 90th Year Chulalongkorn Scholarship for the partial financial support to this work. This work was also partially supported by Energy Research Institute, Chulalongkorn University.

Furthermore, I would like to thank Mr. Sakhon Ratchahat and Ms. Pusanisa Patrachotesawate and all members of Center of Excellence in Particle Technology for their help, suggestion and warm collaborations. I am also thankful to Prof. Hidetoshi Sekiguchi and all members of Sekiguchi's Laboratory, Tokyo Institute of Technology, Japan, for their support during my short research period in The Asia-Oceania Top University League on Engineering Program.

Finally, I would like to express my cordial and deep thanks to my family for their love and encouragement.

CONTENTS

Page

Page

LIST OF TABLES

LIST OF FIGURES

Page

Page

Page

CHAPTER I

INTRODUCTION

1.1 Motivation

Over the past several decades after the classic talk of Richard Feynman, 1959 Nobel laureate in Physics, about manipulating and controlling things on a small scale, great attention has been paid to nano-scale materials or nanomaterials due to their high potential for using in industrial, biomedical, catalysis, information storage, and electronic applications [1]. Nanomaterials are defined as materials (units, grains, particles, or fibers) with at least one dimension in the range of 1 – 100 nanometers (nm). They would cover metals, ceramics, polymeric, or composite materials [2]. Based on its extremely small feature size, nanomaterials exhibit different physical, chemical, electrical and magnetic properties from conventional materials. For example, some metal such as gold is yellow and is excellent conductor of heat and electricity at the bulk scale, but there is nothing happen when the light is shine onto a piece of gold. On the contrary, gold nanoparticles are red in color and start absorbing light and can turn that light into heat to act like miniature thermal scalpels that can kill unwanted cells in the body, such as cancer cells. Nanomaterials are also considered as good candidates for gas sensing applications due to their large surface area-to-volume ratio and size effects [3] which take an important role in sensing process by increasing sensor sensitivity. The general requirements of good sensor properties are high sensitivity, selectivity and stability [4, 5].

One of the well-known nanomaterials discovered in 1991 is carbon nanotubes (CNTs). They have attracted immense interest due to their unique structural, electronic and mechanical properties. CNTs are potential candidate for many applications such as catalysts, biological cell electrodes, nano-scale electronic and mechanical systems, and scanned probe microscope and electron field emission

tips [6, 7]. With their intrinsic properties such as high surface area, small size, hollow geometry, and chemical inertness [8], CNTs are suitable for using as sensing materials. Gas sensors based on pristine CNTs (including single-walled carbon nanotubes (SWCNTs), multi-walled carbon nanotubes (MWCNTs) and aligned CNTs) and the modification of CNTs (with functional groups, metals, metal oxides and polymers) for gas sensor have proved to work well at room temperature [9-13] which reduces the power consumption of the device and enables the safer detection of flammable gases [14-16]. Nevertheless, the slow and incomplete recovery process of carbon nanotubes-based gas sensors is a main disadvantage. Some reports reveal that the recovery time was very long on the order of 10-12 hours [15].

Meanwhile semiconductive metal oxides are also widely used as sensing materials. Metal oxide materials such as titanium dioxide (TiO_2), tin oxide (SnO_2), zinc oxide (ZnO), tungsten oxide (WO_3), indium oxide (In_2O_3) and others have been widely used for gas sensing [17-20]. Among the existing metal oxides, tungsten oxide (WO_3) has been proved to be a promising one for gas sensing applications. Several research studies have shown that it could be used for the detection of nitrogen oxide (NO and NO_2), ammonia (NH_3), hydrogen sulfide (H_2S), alcohol (e.g., methanol, ethanol, isopropanol and butanol) and ethylene gas [21-29]. However, the main drawback when using metal oxide (WO_3) as gas sensors is the rather high operating temperature (sensing temperature) that ranges between 200 and 800 °C. The aim of lowering the operating temperature is to prevent the long-term changes in response in metal oxide gas sensors [30]. Recently, mixture materials based on metal oxide and carbon nanotubes have been introduced as new gas sensitive materials with improved sensitivity. These works indicate that the detection of toxic gases at room temperature could be highly improved by adding suitable amount of carbon nanotubes into a metal oxide matrix [30].

However, in situ synthesis of carbon nanotube-tungsten oxide composites (hybridized materials) still has not known well in terms of how to synthesize, its microscopic characteristics, and its sensing ability to target gas. Therefore, the aim of this work is to in situ synthesis of multi-walled carbon

nanotube-tungsten oxide (MWCNT-WO_3) composites by using a facile/inexpensive acid precipitation method following by calcination under air atmospheres. Synthesis parameters including initial concentration of reactants, calcination temperature and time were thoroughly investigated to find a suitable condition. The as-prepared composites were then used as sensing materials for fabricating in-house thick-film sensors. Sensing ability of the fabricated sensors was tested by exposure to CO_2. Meanwhile effects of mass ratio of MWCNTs to WO_3 in the composites on sensing ability were also studied at different operating temperature.

1.2 Objectives

The objectives of this research are to synthesize multi-walled carbon nanotube-tungsten oxide (MWCNT-WO_3) composites by using a simple and inexpensive precipitation technique and to investigate sensing characteristics of the fabricated MWCNT-WO_3 composites which were formed as thick-film sensors to detect some greenhouse gas, such as carbon dioxide (CO_2).

1.3 Scopes

To achieve the objectives of this work, scopes of this work was outlined as follow;

1. Study effects of synthesis parameters on the characteristic of MWCNT-WO_3 composites by acid precipitation method

1.1 Effects of initial concentration of reacting agents (Ranged in 5-16 mM of tungsten salt and 1 – 10 M of nitric acid)

1.2 Effects of weight ratio of MWCNTs to WO_3 (Ranged in 1/100 to 1/1000 gram of CNTs /gram of WO_3)

1.3 Effects of calcination time and temperature (Ranged in 300 – 600 ℃ for 1 – 5 hours)

1.4 Analysis the physical properties of MWCNT-WO_3 composites

2. Study the sensing ability of fabricated MWCNT-WO_3 thick-film sensors

2.1 Preparation of MWCNT-WO_3 thick-film sensors by drop coating technique

2.2 Testing their sensing ability of MWCNT-WO_3 sensor to CO_2

1.4 Research Methodology

In this work, research methodology was divided into 8 steps as follow;

1. Conduct literature survey and review

2. Experimental set up (Chemicals and apparatus)

3. Prepare MWCNT-WO_3 composites by acid precipitation method

4. Characterize MWCNT-WO_3 composite properties by SEM, TEM, BET analyzer, XRD, TGA, FT-IR and Raman spectroscopy

5. Prepare MWCNT-WO_3 thick-film gas sensors by drop coating technique

6. Test and analyze the sensing ability of the fabricated sensors

7. Conclude the experimental results

8. Write thesis and prepare draft manuscript for journal publication

CHAPTER II

FUNDAMENTAL KNOWLEDGE AND LITERATURE REVIEWS

2.1 Fundamental Knowledge

This section focuses on the fundamental properties of nanostructured tungsten oxide and carbon nanotubes, including their promising properties, synthesizing method and fields of application. Also mentioned are fundamental knowledge relevant to principle of chemical gas sensor and its fabrication method.

2.1.1 Tungsten Oxide (WO_3)

Tungsten oxide is an n-type semiconductor with narrow band gap energy between 2.4-2.8 eV [21, 31-35]. WO_3 crystal structures are generally formed based on the corner and edge sharing of WO_6 regular octahedral with the O atom at the corner of each octahedron to produce a highly symmetrical three-dimensional network with cubic symmetry as shown in Figure 2.1 [36, 37].

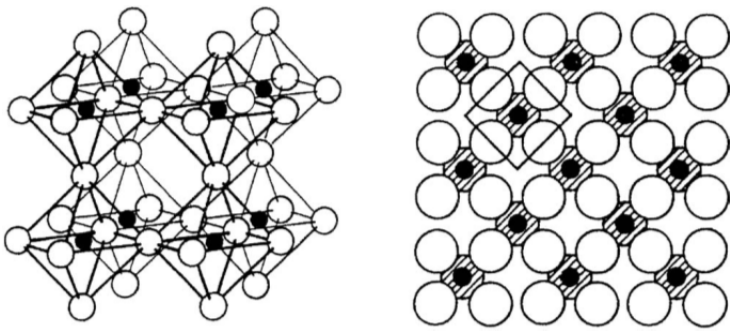

Figure 2.1 Crystal structure of tungsten oxide, illustrated by space model and in projection: W atoms are black and O atoms shown as rings [37]

WO_3 has exceptional chromic properties [36], it exhibits high coloration efficiency and a high cyclic stability compared to other transition metal oxides [38]. It has been widely used to construct electrochromic, optochromic, and gasochromic material such as electrochromic windows, infrared switching devices,

writing–reading–erasing optical devices, reflectance variable mirrors and information displays [38, 39]. WO_3 is a good candidate for gas sensing application, this material in the sub-stoichiometric configuration has weakly bounded electrons created from oxygen vacancies on the surface that can be attributed to the change in electrical conductivity when the composition of the surrounding atmosphere is changed. The electrical properties of WO_3 are greatly changed by means of physisorption, chemisorption and catalytic reaction of gaseous molecules such as H_2, NO_x, H_2S, CO, SO_2, NH_3 and O_3 with the film surface [40]. Moreover, it also has been used as catalysts and photocatalysts [39]. WO_3 has a conduction band edge positioned slightly more positive than H_2/H_2O reduction potential and a valence band edge much more positive than the H_2O/H_2 oxidation potential, which makes WO_3 capable of efficiently photo-oxidizing a wide range of organic compound. It can be irradiated blue region of the visible solar spectrum and stable in acidic environments, making it a promising candidate for treatment of water contaminated by organic acids [36].

Many different approaches have been used for synthesizing nanostructured WO_3 including thermal evaporation, radio frequency magnetron sputtering, chemical vapor deposition (CVD), sol-gel synthesis [22, 26, 41], precipitation [21, 25, 27, 31], hydrothermal reaction [3, 42, 43], electrochemical [44] and template assisted method [22, 36, 45]. Compared to other precipitation method is attractive because of its cost effectiveness and the ease of material preparation [45].

2.1.2 Acid precipitation technique [46]

Chemical precipitation has been widely used to synthesize the oxide powders since only simple glasswares are required. It is a common technique for the synthesis of nanosize particles. Moreover, chemical synthesis permits the manipulation of the matter at the molecular level. Because of mixing at that level, good chemical homogeneity can be achieved. The particle size, shape and size distribution can be controlled by manipulating the parameter such as concentration, temperature and pH of the solution.

The general procedure involves chemical reactions in aqueous or non-aqueous solutions containing the soluble salts. Once the solution becomes supersaturated, a precipitate is formed by either homogeneous or heterogeneous nucleation. Homogeneous and heterogeneous nucleations refer to the formation of stable nuclei with or without foreign species, respectively. After the nuclei are formed, their growth usually proceeds by diffusion. In diffuse controlled growth, concentration gradient and the temperature are important factors in determining the growth rate. Process variables that influence on the precipitation process include temperature of the solution, concentration of the reaction, order of mixing, time of reaction, effect of anions, pH, solvent, rate of mixing, atmosphere, and washing.

2.1.3 Carbon nanotubes

Carbon nanotubes (CNTs) are a group of one-dimensional nanoscale materials composed of carbon atoms with fullerene structure, in which each carbon atom is sp^2 hybrid and every carbon atom is covalently bonded to another three adjacent carbon atom [15]. CNTs can be classified into 2 types according to their wall layer, single-walled carbon nanotubes (SWCNTs) which can be considered as a layer of graphite (see Figure 2.2 (a)) rolled-up into a cylinder and multi-walled carbon nanotubes which can be considered as a collection of concentric SWCNTs with different diameters and interlayer distance close to that of graphite (0.34 nm) [15, 47]. The basic structures of CNTs are shown in Figure 2.2.

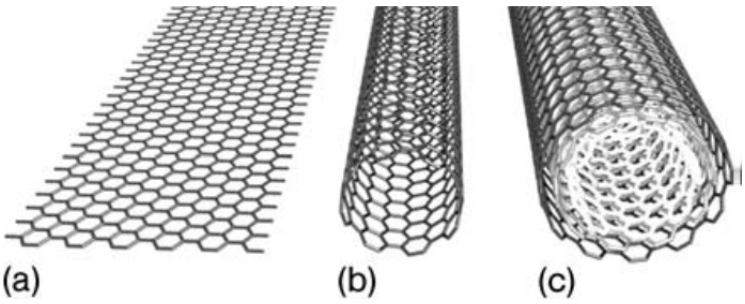

Figure 2.2 Structure of a single layer of graphite (graphene) (a), single-walled carbon nanotube (b) and a multi-walled carbon nanotube with three shells (c) [48]

A single-walled carbon nanotube can be considered as a rolled up graphene strip. Its structure can be specified or indexed by its circumferential periodicity (C_h), as described using the chiral vector (AA in Figure 2.3). In this way, the SWCNT's geometry is completely specified by a pair of integers (n, m), denoting the relative position $C_h = na_1 + ma_2$ of the pair of atoms on a graphene strip which form a tube when rolled onto each other. This chiral vector C_h also defines a chiral angle θ, which is the angle between C_h and the zigzag direction of the graphene sheet [49].

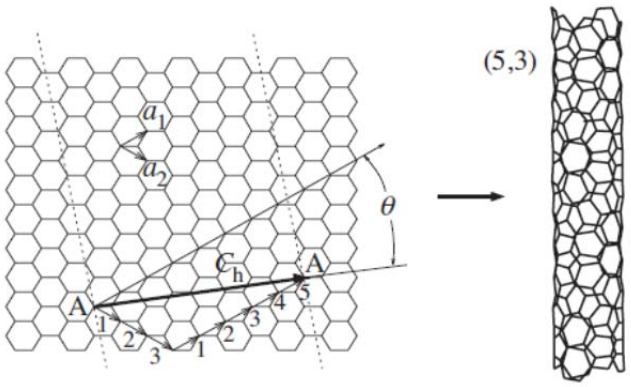

Figure 2.3 Schematic showing a possible wrapping of the 2D graphene sheet into a tubular form [49]

CNTs can be classified into 3 types by using their chiral vector C_h and chiral angle θ, as shown in Table 2.1.

Table 2.1 Classification of carbon nanotubes

Type	Chiral vector (C_h)	Chiral angle (θ)
Armchair	n = m	30°
Zigzag	n or m =0	0°
Chiral	n, m	0°<θ<30°

2.1.4 Fabrication of carbon nanotubes

Carbon nanotubes can be synthesized by two main methods as follows:

1. Arc discharge and laser ablation **[48]**

Arc discharge and laser ablation rely on the evaporation of a graphite target to create gas-phase carbon fragments that recombine to form CNTs. The temperatures reached in these processes are in the range 2000 – 3000 °C, more than sufficient for the carbon atoms to rearrange into the tube structure. In order to increase the yield of nanotubes in the carbon material created, several different metals in concentrations of the order of 1% are incorporated into the target material that is evaporated. The metals evaporate with the carbon and coalesce into clusters that form a base from which the nanotubes can grow.

Under optimized conditions, both of these processes produce nanotubes with the highest achievable crystallinity due to the high temperature during formation. Unfortunately, a large amount of unwanted non-nanotube graphitic and amorphous carbon material is also produced, and a cleaning process is necessary before the nanotubes can be used.

2. Catalyst-enhanced chemical vapor deposition (CCVD) **[48]**

Catalyst-enhanced chemical vapor deposition utilizes small metal catalyst clusters in the gas phase or on surfaces to decompose a carbon containing feedstock gas, such as methane or acetylene. The resulting carbon dissolves in, or is adsorbed on, the catalyst particle and is released in the form of a nanotube starting with a buckyball-type cap when the concentration exceeds the maximum solubility. The nanotube continues to grow as long as carbon continues to be delivered at the right rate and the form of the catalyst does not change. The growth temperature depends on the type of nanotube to be grown and the catalyst composition and lies in the range 400 – 1100 °C, lower than the temperatures in the arc discharge or laser

ablation processes. For this reason, it is believed that CCVD tubes have a higher density of defects.

The advantage of CCVD nanotube production is the possibility of structuring the catalyst particles and, hence, selectively growing the nanotubes where they are required. Further, under the right conditions only nanotubes are produced and no unwanted graphitic material. Using this CCVD method, SWCNTs and MWCNTs can be grown on semiconductor wafers with semiconductor production equipment without almost any equipment modifications using carbon-containing gases such as methane or acetylene.

2.1.5 Properties of carbon nanotubes

Table 2.2 shows some physical properties of CNTs compared to other materials.

Table 2.2 Physical properties of carbon nanotubes [50]

Property	CNTs	Comparison material
Thermal conductivity [W/mK]	>3000	2000 for natural diamond and the basal plane of graphite
Young's modulus [TPa]	~0.64	~0.66 for silicon carbide nanofibers
Strength [GPa]	~37	~53 for silicon carbide nanorods

2.1.6 Conductivity gas sensors [51]

Conductivity gas sensors work on the principle that a change in some property of the material resulting from interaction with a gas/odor leads to a change in resistance in the sensor. The mechanisms that lead to these resistance changes are different for each material type; however, the structure and layout of conductivity sensors prepared using these materials are essentially the same. A schematic of a typical conductivity sensor design is shown in Figure 2.4.

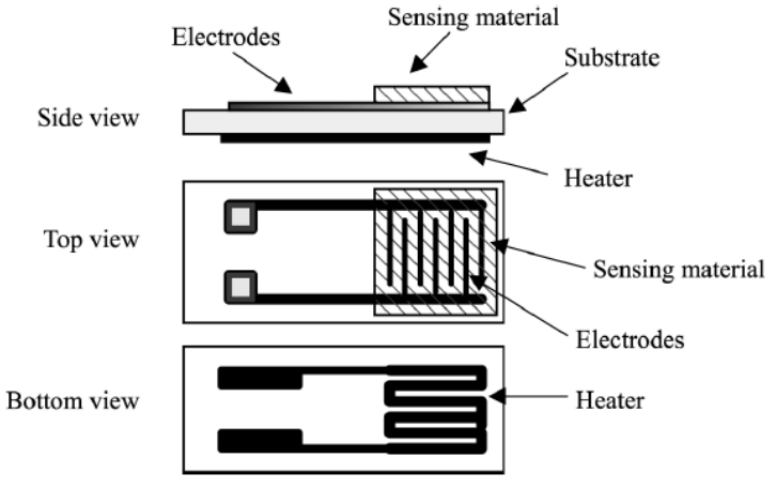

Figure 2.4 Typical structure of a conductivity sensor

The sensing material is deposited over interdigitated or two parallel electrodes, which form the electrical connections through which the relative resistance change is measured. The heater is required when metal oxides are used as the sensing material because very high temperatures are required for effective operation of metal oxide sensors.

The principle of operation of metal oxide sensors is based on the change in conductance of the oxide on interaction with a gas and the change is usually proportional to the concentration of the gas. There are two types of metal oxide sensors; n-type (zinc oxide, tin dioxide, titanium dioxide or iron (III) oxide) and p-type (nickel oxide, cobalt oxide). The n-type sensor operates as follows: oxygen in the air reacts with the surface of the sensor and traps any free electrons on the surface or at the grain boundaries of the oxide grains. This produces large resistance in these areas due to the lack of carriers and the resulting potential barriers produced between the grains inhibit the carrier mobility. However, if the sensor is introduced to a reducing gas like H_2, CH_4, CO, C_2H_5 or H_2S the resistance drops because the gas reacts with the oxygen and releases an electron. This lowers the potential barrier and allows the electrons to flow, thereby increasing the conductivity.

Thick and thin film fabrication methods have been used to produce metal oxide gas sensors. The metal oxide films are deposited using screen printing, spin coating, RF sputtering or chemical vapor deposition onto a flat or tube type substrate made of alumina, glass, silicon or some other ceramic. Gold, platinum, silver or aluminium electrodes are deposited onto the substrate using the same methods. A heating element is printed onto the back of the substrate to provide the high temperatures required for metal oxides to operate as gas sensors, typically 200 – 500 °C. The sensitivity of the metal oxide sensor depends on the film thickness and the temperature at which the sensor is operated. The sensitivity can be improved by adding a catalytic metal to the oxide; however excessive doping can reduce sensitivity. The grain size of the oxide also affects the sensitivity and selectivity to particular gases as the grain boundaries act as scattering centers for the electrons.

2.2 Literature Reviews

This section aims to present the previous research which relates to synthesizing of CNT-WO_3 composite by various methods. Also discussed is the application of composite as chemical gas sensor and their sensing capabilities**.**

Many published papers about synthesizing of CNT-WO_3 composite and their applications in various fields from 2005 – 2012 are showed in Figure 2.5. Application as gas sensor is of interest for many researchers, some research works relevant to preparation and application of composite as gas sensor are as follows:

2.2.1 Preparation of CNT-WO_3 nanocomposites

Pietruszka et al. [52] fabricated WO_3/carbon nanotube (CNT) catalysts with different WO_3 loadings by wet impregnation with ammonium paratungstate as precursor. TEM images show that the inner volume of the MWCNTs was completely filling with paratungstate solution during the impregnation step due to capillary forces.

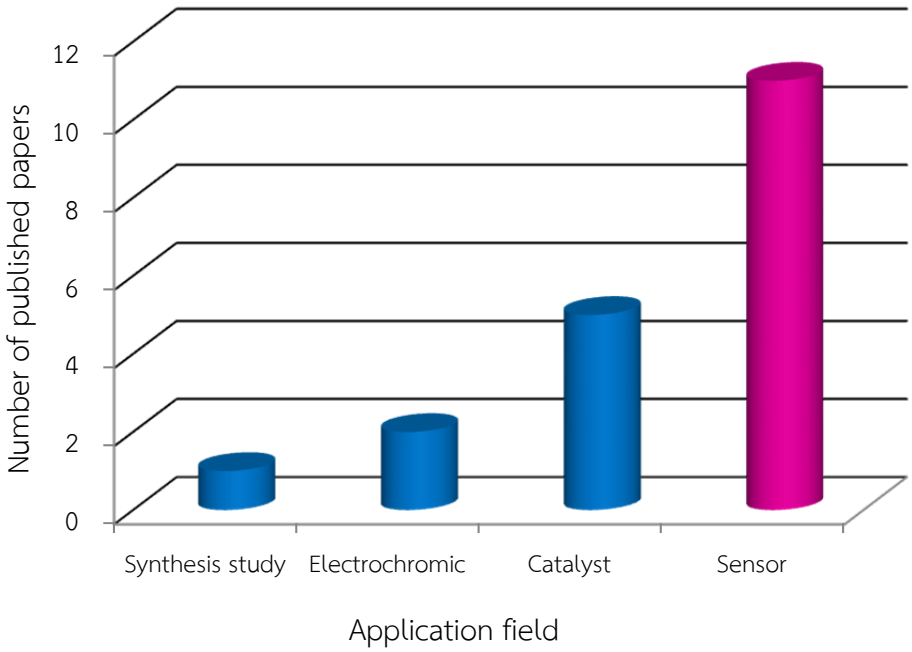

Figure 2.5 Publication papers relevant to CNT-WO_3 composite from 2005 – 2012 [8-11, 14, 30, 32, 33, 38, 40, 52-61]

Bittencourt et al. [11] fabricated hybrid WO_3–CNT (carbon nanotube) films in two steps: oxygen plasma functionalized multi-walled CNTs was drop coated on silicon substrate and then deposited the layer of WO_3 nanoparticles over the MWCNT film by using an advanced evaporation method. The WO_3 nanoparticles are formed by condensation. SEM and TEM images show that their morphology reveals that the MWCNT are cover by WO_3 particles and the CNTs act as internal pillars. This morphology increases the surface area which is an important characteristic for gas sensing.

Wang et al. [56] prepared Multi-walled carbon nanotube (MWCNT)-supported tungsten trioxide (WO_3) composite by liquid-phase process and thermal treatment in air at 500 °C. The results show that WO_3 nanoparticles grew on the inner and outer surface of MWCNTs. WO_3 inside the tube was explained by the ability to wet and fill nanotubes of the elements and compounds with surface tension lower than 190 mN/m such as water (72 mN/m).

2.2.2 Application of CNT-WO_3 nanocomposites as gas sensors

Bittencourt et al. [10] prepared active layers for gas sensing applications by adding oxygen plasma functionalized multi-walled carbon nanotubes (MWCNTs) to WO_3 and using the drop-coating deposition method. Two different ratios of MWCNTs in WO_3 (1/100 and 1/1000) were considered and the response of these sensors towards toxic gases such as nitrogen dioxide, carbon monoxide and ammonia was compared with that of WO_3 and MWCNTs gas sensors. The results indicate that the addition of a suitable quantity of MWCNTs in a WO_3 film can lower the sensor operating temperature to room temperature. The response of the hybrid films to NO_2 was found to increase when only a few MWCNTs were added into the WO_3 films. Furthermore, hybrid films were able to detect ammonia which is very difficult to detect by using pure WO_3 and MWCNTs gas sensors, when operated at 150 °C.

Espinosa et al. [30] investigated response to NO_2 of three different type of metal oxide (SnO_2, WO_3 or TiO_2) prepared by adding a low amount of oxygen-functionalized MWCNTs into them. The results show that the responsiveness towards NO_2 of these metal oxide/MWCNT hybrid films is considerably improved. In particular, the sensors based on hybrid SnO_2/MWCNTs films present excellent sensitivity towards NO_2 when operated at room temperature. The results suggest that there should be an optimum amount of carbon nanotubes to be added to each specific metal oxide in order to enhance sensitivity.

Balazsi et al. [54] prepared hybrid composite of hexagonal tungsten oxide (hex-WO_3) nanopowders and multi-walled carbon nanotubes (MWCNTs) by drop coating both hex-WO_3 and MWCNTs onto silicon based microhotplates. Hex-WO_3 nanopowders prepared by acidic precipitation from a sodium tungstate solution and MWCNTs were modified by adding metallic nanocluster (Ag, Au) for improving the gas sensing properties of the films. The results show that the addition of MWCNTs lowered the temperature range of sensitivity of the hex-WO_3 nanocomposites to NO_2. In comparison, the sensitivity of hex-WO_3 to NO_2 was in the

temperature range between 150 °C and 250 °C, while the hex-WO_3/MWCNTs composites were sensitive to NO_2 gas at room temperature.

Hashishin et al. [8] prepared CNT-WO_3 composite by directly growing CNTs on Au microgap electrode by means of thermal CVD and drop coating the suspension of H_2WO_3 on the surface of as-grown CNTs. After calcinations in argon at 400 °C for 3 hours, the composite was achieved and the sensor responses to NO_2 were measured. The CNTs-WO_3 composite sensor showed the fairly good sensor response (R_a/R_g = 3.8 at 200 °C, whereas R_a is the resistance of sensor in air and R_g is that in NO_2-containing atmosphere). The sensor response was greatly improved with CNTs-WO_3 composite, comparing with that of CNT sensor (R_a/R_g = 1.05) which can be explained by formation of p-n junction, between CNT(p) and WO_3(n), and thus improvement of NO_2 adsorption.

Sedlackova et al. [57] embedding a low amount of gold-decorated carbon nanotubes into the hex-WO_3 matrix prepared by acidic precipitation from sodium tungstate solution. The results show that the addition of MWCNTs lowered the temperature range of sensitivity of hex-WO_3 nanocomposites to NO_2 hazardous gas. The sensitivity of hex-WO_3 with Au-decorated MWCNTs to NO_2 is at the temperature range between 25 °C and 250 °C. The composite were able to detect a very low concentration of NO_2 gas (only 100 ppb) at room temperature.

Ghasempour et al. [40] fabricated the WO_3/multi-walled carbon nanotubes (MWNTs) hybrid films by spin-coating on an alumina substrate and investigated their response to hydrogen. Results show that WO_3 nanoparticles were nucleated on oxygenated functionalized MWNTs in hybrid suspension. After coating and annealing the films at 350 °C, the hybrid WO_3/MWNTs films present rather linear gas sensitivity as a function of hydrogen concentrations (from 24 to 12000 ppm) at 300 °C. As the result of increasing of surface area as well as developing of two types of Schottky potential barrier height, one at the n-WO_3/p-MWNTs hetero-junction and the other at WO_3 grain boundaries.

CHAPTER III

RESEARCH METHODOLOGY

In this research, experimental work was divided into two main parts. The first part is to synthesize of MWCNT-WO_3 composites as sensing materials by using acid precipitation method. The second part is to fabricate thick-film sensors and then test their sensing ability to CO_2.

3.1 Synthesis of MWCNT-WO_3 composites by acid precipitation method

In order to synthesize MWCNT-WO_3 composites with high sensing ability, characteristics of the composites, such as surface area and crystallite size of WO_3 nanoparticles would be investigated. In this work, synthesis conditions of WO_3 nanoparticles would be examined to determine a suitable condition, such as reactant concentration, calcination time, and calcination temperature.

3.1.1 Raw materials and equipment

Chemicals and raw materials required for synthesizing WO_3 nanoparticles and MWCNT-WO_3 composites by using acid precipitation process were shown in Table 3.1.

Table 3.1 Chemicals used for preparation of WO_3 nanoparticles and MWCNT-WO_3 composites

Chemical	Formula	Manufacturer	Country
Ammonium tungstate parapentahydrate (ATP)	$(NH_4)_{10}W_{12}O_{41}.5H_2O$	Wako Pure chemicals industries Ltd.	Japan
Nitric acid	HNO_3	Merck	USA
Multiwalled carbon nanotubes (MWCNTs, Baytubes®)	-	Bayer	Germany
De-ionized water	H_2O	Purelab classic DI, ELGA	UK

Ordinary laboratory equipment used in this research was shown in Table 3.2.

Table 3.2 Equipment used for preparation of WO_3 nanoparticles and MWCNT-WO_3 composites

Equipment	Manufacturer	Remark
Hotplate stirrer	IKA	Stirred at maximum speed
Cooling Bath	HETO	
Hot air oven	Memmert	
Vacuum pump	Daikawa VP-35L	
Digital muffle furnace	Human Lab/DMF-12	Do not set heating rate

3.1.2 Experimental

WO_3 nanoparticles were synthesized via the facile acid precipitation route which according to Suphothina et al. [31] method. 150 mL of designated concentration of tungstate salt solution was heated in the three-neck round bottom flask connected with reflux system, dropping funnel, and thermometer. The solution was kept at isothermal temperature of 80 °C. Schematic of experimental setup is shown in Figure 3.1.

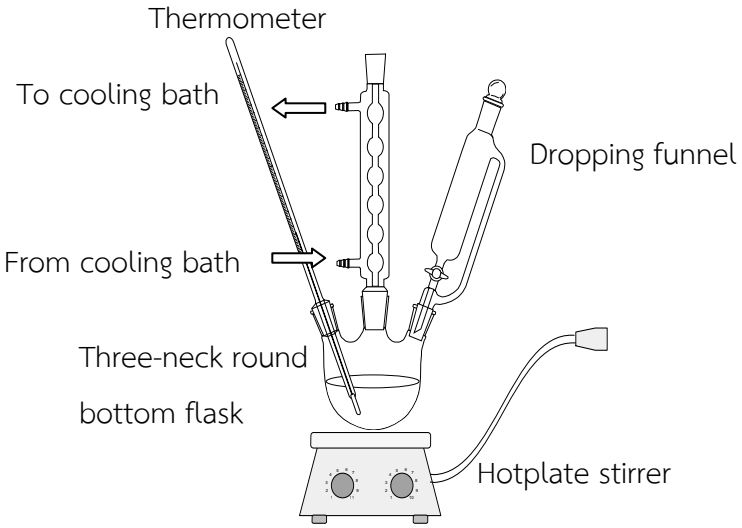

Figure 3.1 Experimental setup for synthesizing WO_3 nanoparticles

25 mL of predetermined concentration of nitric acid was added dropwise to accommodate the hydrolysis reaction of tungstate salt. The mixed solution was kept under stirring and reflux condition for 30 minutes after dropping to ensure the completion of reaction. Subsequently, the solution is cooled to room temperature naturally and kept with static conditions for one day. The precipitated product was washed with deionized water and filtrated through nylon membrane with diameter of 0.45 μm until pH of the washed effluent equal to 7 and dried in hot air oven at 100 ℃ overnight. The as-prepared solid product was weighted to determine percent yield. The dried products were calcined under air atmosphere with various target temperature of 300 – 600 ℃ with holding time of 1 – 5 hours. Finally, the obtained WO_3 nanoparticles were kept in desiccators for preventing them from the ambient moisture.

Similarly, MWCNT-WO_3 composites were also synthesized according to the same procedures with adding a predetermined amount of MWCNTs into the tungstate salt solution at the beginning of the reaction and calcined in muffle furnace at the referable condition examined from experimental mentioned above.

3.2 Gas response study of the fabricated MWCNT-WO_3 composites

To study the sensing ability of the composite, paste of various ratios of MWCNTs to WO_3 composite was prepared and tested its sensitivity toward carbon dioxide by using in-house fabricated gas testing kit.

3.2.1 Raw materials

In this section, in-house thick film sensors were fabricated from the as-prepared sensing materials. The sensors were then tested by exposure to CO_2. Some chemicals and gases used in this preparation were listed in Table 3.3.

Table 3.3 Chemicals used for making paste of composite

Chemical	Formula	Manufacturer	Country
Absolute ethyl alcohol	C_2H_5OH	Merck	Germany
High purity nitrogen	$N_{2\ (g)}$	Thai Industrial Gas	Thailand
High purity carbon dioxide	$CO_{2\ (g)}$	Thai Industrial Gas	Thailand

3.2.2 Experimental

The calcined WO_3 nanoparticles, MWCNT-WO_3 composites, pristine MWCNTs were formed into paste by mixing them with absolute ethyl alcohol and sonicated in sonicate bath for 30 minutes. Thick film sensors were formed by dropping the paste on the electrode coated on the glass substrate and dried in hot-air oven overnight for evaporating of organic vehicle (ethanol). The electrode was prepared by evaporating a 50 nm-thick titanium layer, followed by a 100 nm-thick platinum layer on the glass slide using electron beam evaporation (ULVAC, EBV-6DH). The bare (electrode) and pasted sensors were shown in Figure 3.2.

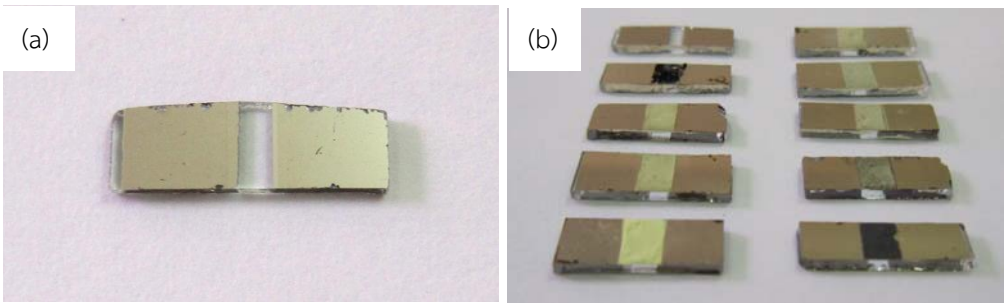

Figure 3.2 (a) electrode and (b) pasted sensors

The sensing characteristics test was carried out in testing chamber for exposing the sensor to CO_2 at isothermal temperature ranging from room temperature to high temperature (200 °C). The measuring equipment was set up according to Figure 3.3, this system included sensor holder and heater (a), chamber (b), digital multimeter AT-9995 with RS232 connecting port (c), transformer (d), digital thermocouple (e), computer with RS232 port for data collection (f), and digital multimeter for monitoring bias voltage across heater (g).

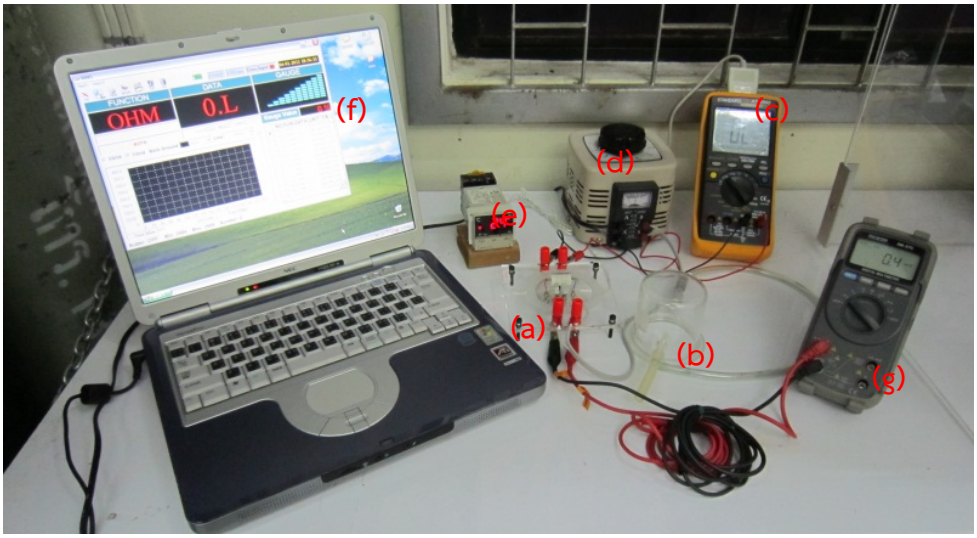

Figure 3.3 Experimental setup for sensing characteristic measurement

The fabricated sensors were installed in a 200 cm^3-measuring chamber (as shown in Figure 3.4 and 3.5) under nitrogen flowing with volumetric flow rate of 100 ml/min as carrier gas. The sensors were heated to target operating temperature ranging from room temperature (25 °C) to 200 °C, waited until the base line was stable. For each measurement, 100 ml/min of CO_2 (500 ppm) was introduced into measuring chamber for 195 seconds and allowed the sensors recovered back to initial stage for 195 seconds after CO_2 gas was offed. The testing was repeated for 3 times. The resistance change of sensors was measured with respect to exposure time using digital multimeter AT-9995 connected to computer for data collection.

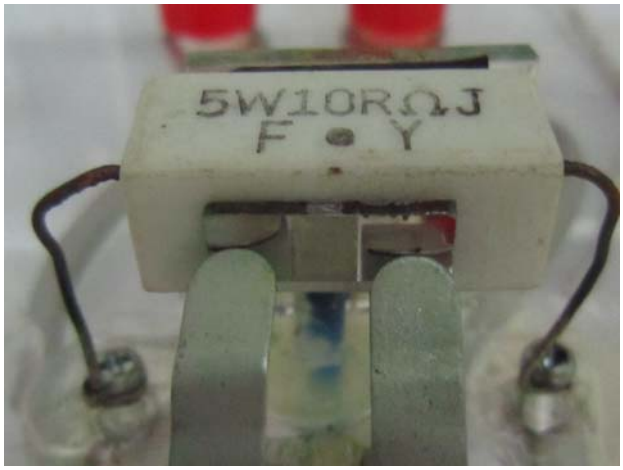

Figure 3.4 Sensor installation to heating system within measuring chamber

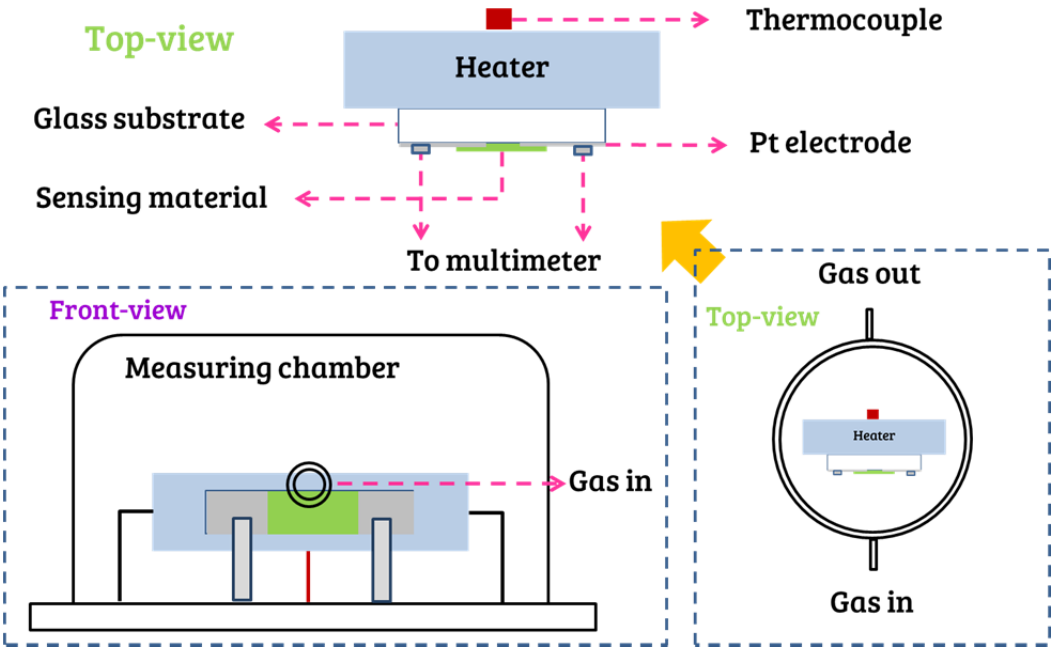

Figure 3.5 Schematic diagrams of experimental setup of measuring system

The sensitivity, *S* was defined as S (%) = $((R_t-R_0)/R_0) \times 100$, where R_0 and R_t was the resisitivity of the sensor at its initial and exposure states, respectively (as shown in Figure 3.6). The response time (τ_{res}) is defined as the time required for the sensor to reach 90% of the stabilized value of its resistance in the presence of the test gas (as shown in Figure 3.7).

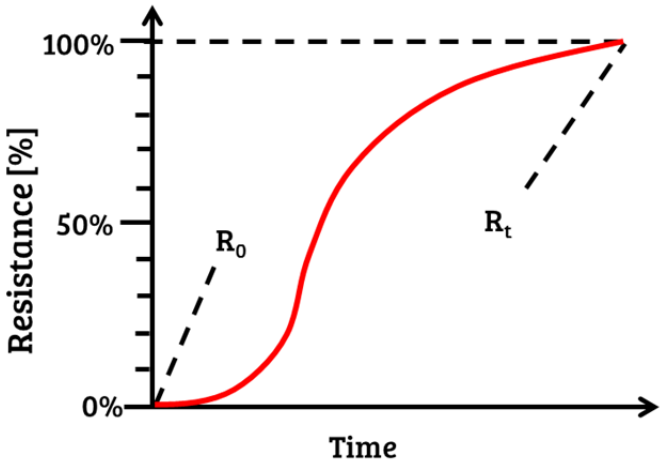

Figure 3.6 Determination of sensitivity

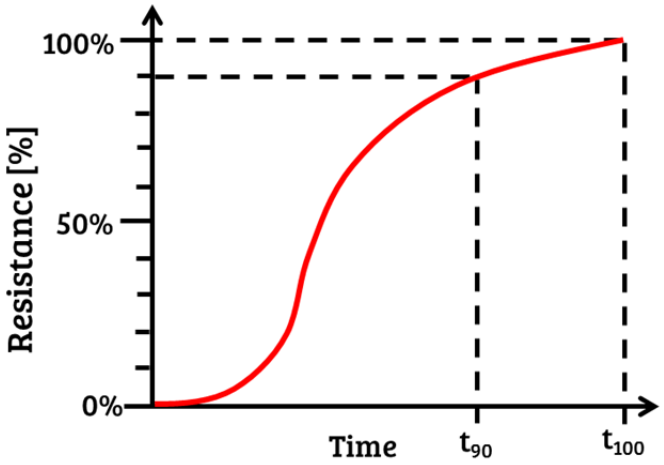

Figure 3.7 Determination of response time

3.3 Analytical instruments

In this research work, various analytical instruments were employed to determine physical and chemical properties of synthesized products, such as functional groups, microstructure, internal structure, porosity, crystallinity, thermal decomposition, etc. Some detail and specifications of that analytical instrument were shown below.

3.3.1 Fourier transform-infrared spectroscopy (FT-IR)

Functional groups on surface of WO_3 nanoparticles, pristine MWCNTs and MWCNT-WO_3 composites were analyzed by FT-IR spectrometer (Spectrum one, Perkin Elmer) using KBr pellets as shown in Figure 3.8. The scanning was commenced at wavenumbers ranging from 4000 to 450 cm^{-1} at 4.0 cm^{-1} resolution and number of scan 16.

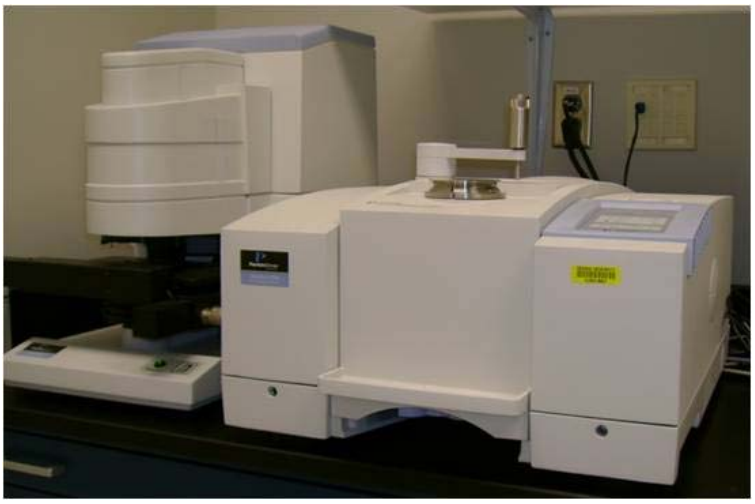

Figure 3.8 Fourier transform-infrared spectroscopy *(Spectrum one, Perkin Elmer)*

3.3.2 Scanning electron microscope (SEM)

Scanning Electron Microscope as shown in Figure 3.9 (*SEM, JEOL: JSM-5410LV, Japan*) was used to visually observe WO_3 nanoparticles, pristine MWCNTs and MWNCT-WO_3 composites by placing them onto conductive carbon tape. Morphologies and shapes of the particles, therefore, were characterized and illustrated.

Figure 3.9 Scanning Electron Microscope (*SEM, JEOL: JSM-5410LV, Japan*)

3.3.3 Transmission electron microscope (TEM)

Internal microstructures of WO_3 nanoparticles, MWCNTs and MWCNT-WO_3 composites were analyzed by using Transmission Electron Microscope (*TEM, JEOL JEM-2100*) as shown in Figure 3.10. The JEM-2100 has been developed to achieve the highest image quality and the highest analytical performance in the 200kV class analytical TEM with a probe size under 0.5 nm.

Figure 3.10 Transmission Electron Microscope (*TEM, JEOL JEM-2100*)

3.3.4 X-ray diffractometer (XRD)

Structure and crystallinity of WO_3 nanoparticles and MWCNT-WO_3 composites both before and after calcination were characterized by X-ray diffraction analysis (*XRD, SIEMENS D 5000, Japan*) as shown in Figure 3.11 using Cu$K\alpha$ radiation with Ni filter in the 2q range of 20-70 degrees resolution 0.04°. The crystallite size was calculated from by using Scherrer's equation.

Figure 3.11 X-ray diffraction analyzer (*XRD, SIEMENS D 5000, Japan*)

3.3.5 Porosity measurement (BET)

Porous structure of WO_3 nanoparticles, MWCNTs and MWCNT-WO_3 composites both before and after carbonization process was characterized by nitrogen adsorption-desorption at -196 ℃ (*BEL: BELSORP-mini, Japan*) as shown in Figure 3.12. In brief, the sample (~0.1 g) was pretreated at 100 ℃ under vacuum for 3 hours in order to remove moisture and gaseous residual. BET surface area (S_{BET}) was determined by BET equation.

Figure 3.12 N_2 adsorption-desorption analyzer (*BEL: BELSORP-mini, Japan*)

3.3.6 Raman spectroscopy

Raman spectrometer as shown in Figure 3.13 (DXR, Thermo Scientific) was also employed for recording Raman spectra of the synthesized products. Raman shift spectra were used to determine existence of carbonaceous materials in the composites as well as spectra of WO_3 nanoparticles.

Figure 3.13 Raman spectrometer (DXR, Thermo Scientific)

3.3.7 Thermo gravimetric analyzer (TGA)

Thermal decomposition of MWCNTs, WO_3 and the mass ratio of MWCNTs to WO_3 nanoparticles were determined by thermo gravimetric analyzer (*Model TGA/DSC1, METTLER TOLEDO*) as shown in Figure 3.14. Thermal decomposition was determined under air atmospheres with heating rate of 10 °C/min.

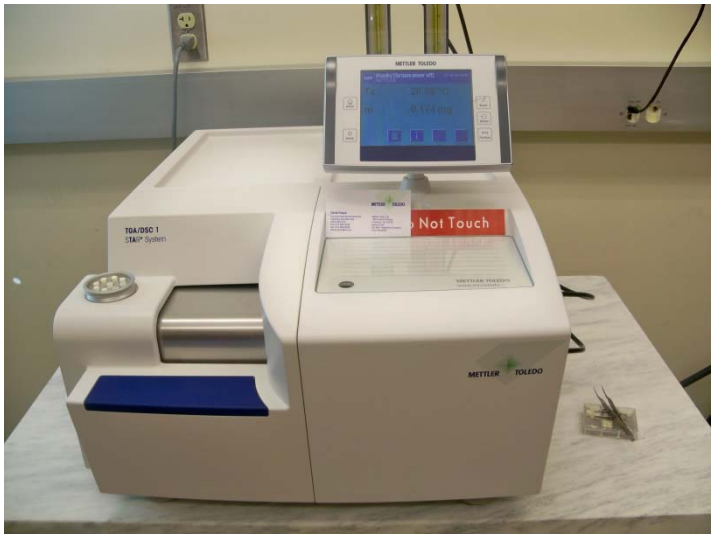

Figure 3.14 Thermo gravimetric analyzer (*Model TGA/DSC1, METTLER TOLEDO*)

CHAPTER IV

SYNTHESIS OF TUNGSTEN OXIDE (WO_3) NANOPARTICLES

In order to obtain the suitable conditions for synthesizing of multi-walled carbon nanotube-tungsten oxide (MWCNT-WO_3) composites, tungsten oxide (WO_3) nanoparticles were synthesized solely to determine the highest yield and the optimal calcination conditions which have strong effect to the properties of sensing material. Subsequently, various ratios of tungsten oxide and multi-walled carbon nanotube composites were synthesized and then fabricated as thick film sensors. Finally such thick-film sensors were tested to study their sensing capabilities when exposed to greenhouse gas such as carbon dioxide (CO_2) at various operating temperature varying from room temperature to higher temperature (200 °C).

4.1 Synthesis of tungsten oxide (WO_3) nanoparticles

4.1.1 Acid precipitation of ATP (hydrolysis reaction)

Tungsten oxide nanoparticles were synthesized with facile consecutive two steps including acid precipitation and calcination process. In acid precipitation, ammonium tungstate para pentahydrate [$(NH_4)_{10}W_{12}O_{41}.5H_2O$, ATP], used as tungsten precursor, was precipitated by nitric acid (HNO_3) with designated mole ratio at constant isothermal precipitation temperature of 80 °C and fixed precipitation time of 30 minutes. During such acid precipitating step, the color of mixture was gradually changed from clear solution to light yellow and finally dark yellow suspension along the increasing of precipitation time clearly seen in Figure 4.1 (a) – (e). It is known that this color-change phenomenon is attributed to the precipitation of polyoxometallates ions to solid nanoparticle products which is hydrated tungsten oxide or metatungstic acid ($H_2WO_4.nH_2O$) [62, 63].

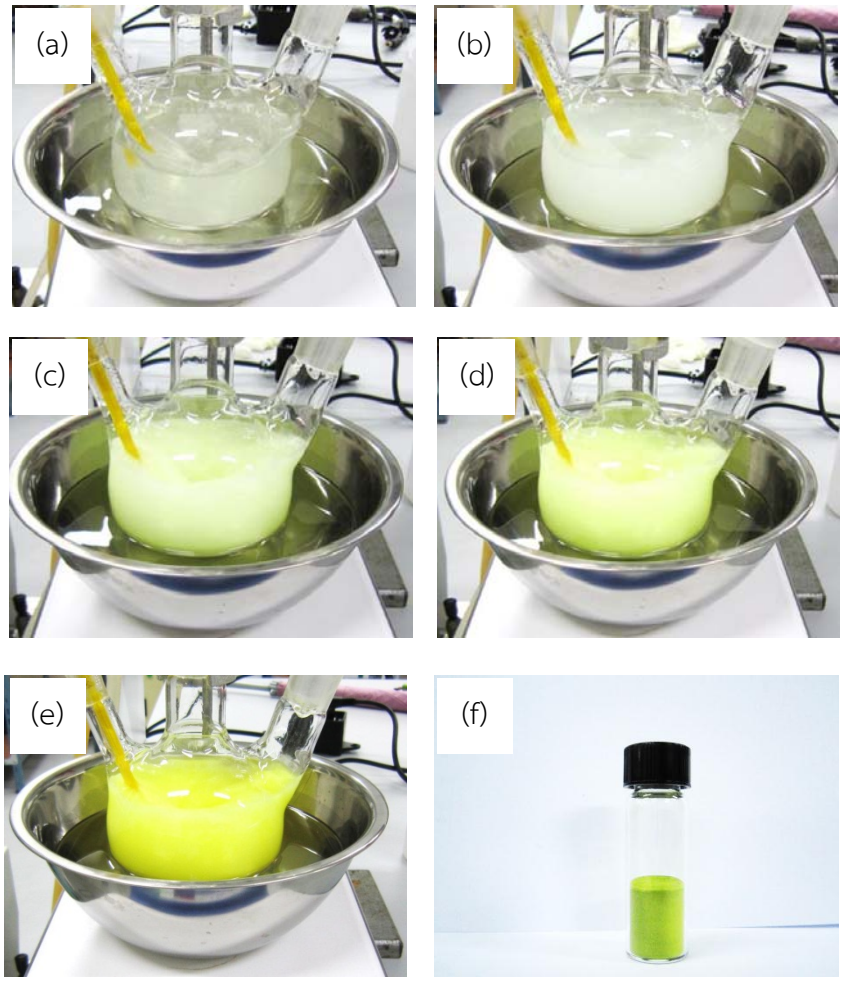

Figure 4.1 Color changing during precipitation of WO_3 nanoparticles and the dried precipitated WO_3 nanoparticles

Such acid precipitation mechanism was generally attributed to hydrolysis reaction of ammonium tungstate para pentahydrate (ATP) in an excess acid environment. It is well known that the aqueous chemistry of high-valent cations such as MO^{VI}, W^{VI}, and V^{V} is dominated by the formation of polyoxometallates (i.e. paratungstate ions) that usually exhibit compact, highly symmetrical molecular structures. At high pH, W^{VI} gives tetrahedral oxoanions $[WO_4]^{2-}$. Protonation of such tetrahedral oxoanions leads to the formation of hydroxy species [62]. To deep understand such acid precipitation, the hydrolysis reaction of ATP would be comprehensively discussed.

Firstly ATP was isothermally dissolved by deionized water in a closed re-condensable system to obtain paratungstate ions like $[W_{12}O_{41}]^{10-}$, $[H_2W_{12}O_{42}]^{10-}$ and $[H_2W_{12}O_{40}]^{6-}$ as shown in equation (4.1). Such paratungstate ions could be generally formed in solution with the pH range of 7–4 [63]. Although a wide range of polyoxotungstates is observed, only two of them are thermodynamically stable; the paratungstate B $[H_2W_{12}O_{42}]^{10-}$ formed around pH ≈ 6 and the α-metatungstate $[H_2W_{12}O_{40}]^{6-}$ formed around pH ≈ 4 [62]. Meanwhile it is known that tetrahedral oxoanions $[WO_4]^{2-}$ are stable in an alkaline solution (pH ~ 12) [22]. In addition, the pH of solution would be higher due to ammonium ion (NH_4^+) from ATP. Therefore the $[W_{12}O_{41}]^{10-}$ was further hydrolyzed to form $[WO_4]^{2-}$ ions as shown in equation (4.2). Similarly the paratungstate B $[H_2W_{12}O_{42}]^{10-}$ and the α-metatungstate $[H_2W_{12}O_{40}]^{6-}$ are also hydrolyzed to $[WO_4]^{2-}$ as shown in equation (4.3-4.4). However the pH of mixture would be continuously decreased when nitric acid was dropwise added to the mixture due to hydronium ions $[H^+]$ as shown in equation (4.5). With such decrease in pH values, $[WO_4]^{2-}$ ions could not be able to stand in lower pH system, consequently they would be protonated to metatungstic acids (H_2WO_4) prevail in the pH range of 4–1 as shown in equation (4.6) [22, 63]. It was suggested that an excess acid would play an important role in not only protonating of $[WO_4]^{2-}$ ions but also providing low pH environment. Such metatungstic acid is first obtained in a clear solution. The solution subsequently becomes yellow-color nanoparticles' suspension because of rapid transformation of a formed gel to a crystalline $WO_3.nH_2O$ [23, 62, 63]. The overall reaction of such hydrolysis reaction was shown in equation (4.7) [31].

$$(NH_4)_{10}W_{12}O_{41}.5H_2O + 2H_2O \longrightarrow [W_{12}O_{41}]^{10-} + 10NH_4^+ + 7H_2O \quad (4.1)$$

$$[W_{12}O_{41}]^{10-} + 7H_2O \longrightarrow 12WO_4^{2-} + 14H^+ \quad (4.2)$$

$$[H_2W_{12}O_{42}]^{10-} + 6H_2O \longrightarrow 12WO_4^{2-} + 12H^+ \quad (4.3)$$

$$[H_2W_{12}O_{40}]^{6-} + 8H_2O \longrightarrow 12WO_4^{2-} + 18H^+ \quad (4.4)$$

$$10HNO_3 \longrightarrow 10H^+ + 10NO_3^- \quad (4.5)$$

$$12WO_4^{2-} + 14H^+ + 10H^+ \rightarrow 12H_2WO_4.nH_2O \quad (4.6)$$

$$(NH_4)_{10}W_{12}O_{41}.5H_2O + 10HNO_3 + 2H_2O \rightarrow 12H_2WO_4.nH_2O + 10NH_4^+ + 10NO_3^- \quad (4.7)$$

The nuclei of hydrated tungsten oxide nanoparticles would be initially formed when supersaturation condition would be able to achieve. With increase in precipitation time, such hydrated tungsten oxide nanoparticles would gradually grow to obtain final products suspended in the mixture. Meanwhile the precipitation rate attributed to acid concentration could be explained based on the activation energy (ΔG^*) [21, 31]. Such activation energy is required to form a critical nucleus of the solid of radius r* which is defined as in equation (4.8),

$$\Delta G^* = 16\pi\sigma^3 M^3/3(\rho RT\ln S)^2 \quad (4.8)$$

where σ is the interfacial tension between the precipitate and its surroundings, ρ is the precipitate density, M is the molecular weight of the precipitate, and S is the supersaturation, which is defined by:

$$S = c/c^* \quad (4.9)$$

where c is the concentration of the paratungstate ions such as $[W_{12}O_{41}]^{10-}$, $[H_2W_{12}O_{42}]^{10-}$, $[H_2W_{12}O_{40}]^{6-}$, $[W_6O_{20}(OH)]^{5-}$, $[W_{12}O_{39}]^{6-}$ or $[W_{12}O_{38}(OH)_2]^{6-}$ depending on the solution's pH and concentration, and c* is the concentration of the solution at equilibrium. It is obviously seen that the activation energy in equation (4.8) could be decreased by increasing supersaturation of the solution (S). Therefore nucleation would be strongly promoted. In this system, the degree of supersaturation would be increased with increase in nitric acid concentration (reducing pH).

4.1.2 Calcination of hydrated tungsten oxide

After the acid precipitation completed, the as-synthesized yellow suspension was filtered through ultra-high small pore size filter papers by suction filtration apparatus to gain solid products. This hydrated tungsten oxide would be turned to $WO_3.H_2O$ when heated around 100 °C [64]. Therefore the wet solid product ($H_2WO_4.nH_2O$) was carefully dried overnight at isothermal temperature of 100 °C to

obtain hydrated WO_3 nanoparticles ($WO_3.H_2O$) with bright yellow color as shown in Figure 4.1 (f). In such drying step, water molecules (nH_2O) were removed by evaporation mechanism to finally obtain the hydrated products. This drying mechanism is described by the drying equation shown in equation (4.10).

$$12H_2WO_4.nH_2O \longrightarrow 12WO_3.H_2O + nH_2O \quad (4.10)$$

However since there is some water molecules in such hydrated sample, it would need further treatment at higher temperature (i.e. calcination process). In calcination process, the hydrated WO_3 nanoparticles ($WO_3.H_2O$) were calcined under air atmosphere at elevated temperature (300 – 600 °C) to transform hydrated WO_3 to dehydrated one. The dehydration phenomenon in calcination process would attribute to removal of water molecules chemically absorbed in nanostructure of hydrated WO_3. After such calcination process, dehydrated tungsten oxide (WO_3) nanoparticles were obtained as shown in equation (4.11)

$$12WO_3.H_2O \longrightarrow 12WO_3 + 12H_2O \quad (4.11)$$

4.2 Effect of reactant concentrations on percent yield of hydrated WO_3 nanoparticles

Theoretical yield of hydrated tungsten oxide ($WO_3.H_2O$ or H_2WO_4) was defined based on the precipitation equation and the drying equation as shown in equation (4.7) and (4.10), respectively. To obtain 12 moles of hydrated tungsten oxide, one mole of tungstate salt (ATP) would completely react with 10 moles of nitric acid (HNO_3). Therefore theoretical yield is defined as shown in equation (4.12). Meanwhile actual yield of hydrated tungsten oxide products is defined in equation (4.13). It is an actual mass of hydrated tungsten oxide after drying process. Therefore percent yield of hydrated tungsten oxide is defined as a ratio of actual yield to theoretical yield as shown in equation (4.14).

$$\text{Theoretical yield [g]} = 12 \cdot \text{mol ATP} \cdot MW_{H_2WO_4} \quad (4.12)$$

$$\text{Actual yield [g]} = \text{Mass of hydrated } WO_3 \quad (4.13)$$

Percent yield [%] = (Actual yield/Theoretical yield) · 100% (4.14)

In 2007 and 2008 Supothina et al. [21, 31] studied on high yield synthesis of tungsten oxide by acid precipitation method. It was evidenced that percent yields of precipitated WO_3 nanoparticles depended on initial concentrations of both tungstate salt (ATP) and nitric acid (HNO_3). In this work percent yields of synthesized products were also systematically investigated by varying both initial concentrations of tungstate salt and nitric acid. The percent yields of synthesized products calculated by equation (4.14) were shown in Figure 4.2. With constant tungstate salt concentration of 5.3 mM, it was found that percent yield is likely to slightly increase with increase in concentration of nitric acid. The highest percent yield of 71.4% was obtained at acid concentration of 10 M.

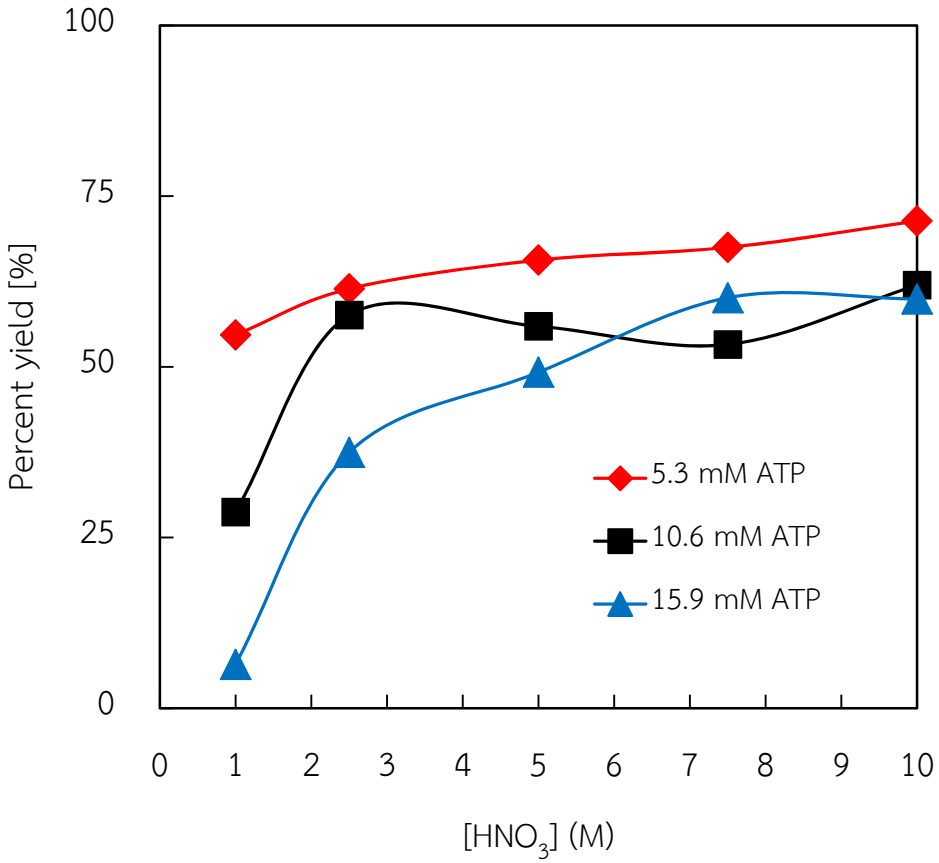

Figure 4.2 Effect of initial concentration of reactants to percent yield of as-precipitated WO_3 nanoparticles

However percent yield dramatically increased six times (from 6.4 % to 37.5%) when tungstate salt of 15.9 mM precipitated with increase in nitric acid concentration from 1 M to 2.5 M. It was suggested that the excess nitric acid plays an important role in precipitation phenomenon of tungstate salt. Moreover the percent yield still constantly increased with further increase in acid concentration from 2 M to 7.5 M. Since the excess of nitric acid could help reduce in pH system, supersaturate condition was obtained. Nevertheless percent yield seemed to be constant when acid concentration increased from 7.5 M to 10 M as shown in Figure 4.2. It was inferred that tungsten salt was completely consumed to yield precipitated WO_3. Similarly with constant concentration of 10.6 mM, percent yield also rapidly increased two times (from 28.7% to 57.6%) with increase in acid concentration from 1 M to 2.5 M. With further increase in acid concentration, percent yield could be slight increase. However it was found that percent yield slight decreased from 57.6% to 53.3% and finally increase to 62.0%. The fluctuated percent yield could be from some unidentified factor from experimental conditions which needs further investigation.

On the other hand, percent yield dramatically decreased while the concentration of tungstate salt increased from 5.3 mM to 15.9 mM with constant acid concentration of 1 M. It was suggested that the dissolved tungstate salt partially precipitated with limit amount of nitric acid due to acid is limiting reactant resulting in small amount of percent yield. This experimental result was also observed when concentration of tungstate salt increase with constant acid concentration.

In sum, the maximum percent yield was obtained at initial concentration of tungstate salt and nitric acid of 5.3 mM and 10 M, respectively. Therefore this initial concentration condition was chosen as a suitable condition for synthesizing pure tungsten oxide nanoparticles (WO_3) as well as multi-walled carbon nanotube-tungsten oxide (MWCNT-WO_3) composites. Subsequently both pure WO_3 nanoparticles and MWCNT-WO_3 composites would be used for fabricating thick-film sensors. Meanwhile their sensing ability to pollutant gas would be comparatively investigated which is mentioned in detail in chapter VI.

4.3 Effect of calcination conditions on WO_3 characteristics

To investigate calcination effect on properties of dehydrated WO_3 nanoparticles, the hydrated WO_3 nanoparticles was calcined under air atmosphere with different points of calcination temperature and calcination time. Subsequently the properties of both hydrated and dehydrate WO_3 nanoparticles were characterized by various analytical techniques to thoroughly investigate WO_3 existence, morphology, dehydration behavior, crystallite size, and specific surface area.

4.3.1 Confirmation of WO_3 existence in the as-prepared products

Figure 4.3 illustrates the XRD diffraction patterns of the as-prepared particulate products dried in hot-air oven at 100 ℃ following by calcination in ambient air at various calcination temperatures (300, 400, 600 ℃). Based on these XRD results, the dried precipitate and that calcined at 300 ℃ could be identified as tungsten oxide monohydrate ($WO_3.H_2O$ or H_2WO_4), having orthorhombic structure (JCPDS# 43-0679) which is indicated by diffraction peaks at 2θ = 25.6. This diffraction peak is ascribed to (1 1 1) plane [31, 63, 64]. Meanwhile the precipitates calcined at 400 and 600 ℃ show diffraction peaks at 2θ = 23.1, 23.7, 24.5, 26.7, 28.8, 34.2, 41.8, 50.0, and 55.7 which are ascribed to (0 0 2), (0 2 0), (2 0 0), (1 2 0), (0 2 1), (2 0 2), (2 2 2), (0 0 4), and (2 4 0), respectively. These diffraction peaks were used to identify the sample as WO_3. However three main diffraction peaks at 2θ = 23.1, 23.7, 24.5 which were identified as WO_3 having monoclinic structure (JCPDS# 43-1035) [31, 45, 65]. It should also be noted from XRD patterns that degree of crystallinity increased from orthorhombic phase to monoclinic phase upon increasing calcination temperature. It was suggested that the calcination temperature should be more than 300 ℃ in order to obtain monoclinic phase. Consequently the calcination temperature of 400 ℃ should be a suitable temperature for calcination process to anneal hydrated WO_3 to monoclinic WO_3. However it would be great that further investigation could be carried out to ensure the characteristics of monoclinic WO_3.

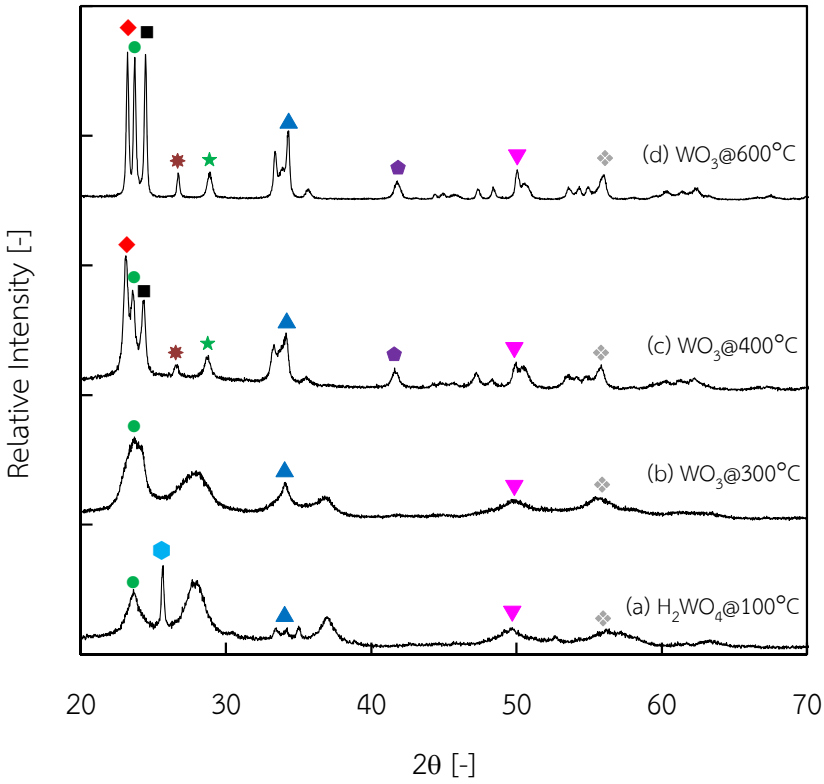

Figure 4.3 XRD patterns of (a) hydrated WO_3 (H_2WO_4) and dehydrated WO_3 at various calcination temperatures ((b)-(d)): ◆ (0 0 2), ● (0 2 0), ■ (2 0 0), ✸ (1 2 0), ★ (0 2 1), ▲ (2 0 2), ⬟ (2 2 2), ▼ (0 0 4), ❖ (2 4 0), ⬢ (1 1 1)

Although these XRD results could verify the synthesized products as tungsten oxide (WO_3) and identify their crystallinity, it could not determine whether water molecules would be completely removed from the as-prepared products after calcination process. Raman measurements were performed since this technique is well known to give the 'fingerprint" of WO_3 material [66]. Therefore not only the calcined product at 400 °C but also the dried precipitates were subjected to Raman spectroscopic analysis to verify the removal of water molecules from the hydrated WO_3. Raman spectra in Figure 4.4 reveal W-O stretching and bending vibrations locating between 700–800 cm^{-1} and 250–400 cm^{-1}, respectively. Meanwhile the band around 950 cm^{-1} is assigned to the stretching mode of the terminal W=O bonds at the surface of clusters [67, 68].

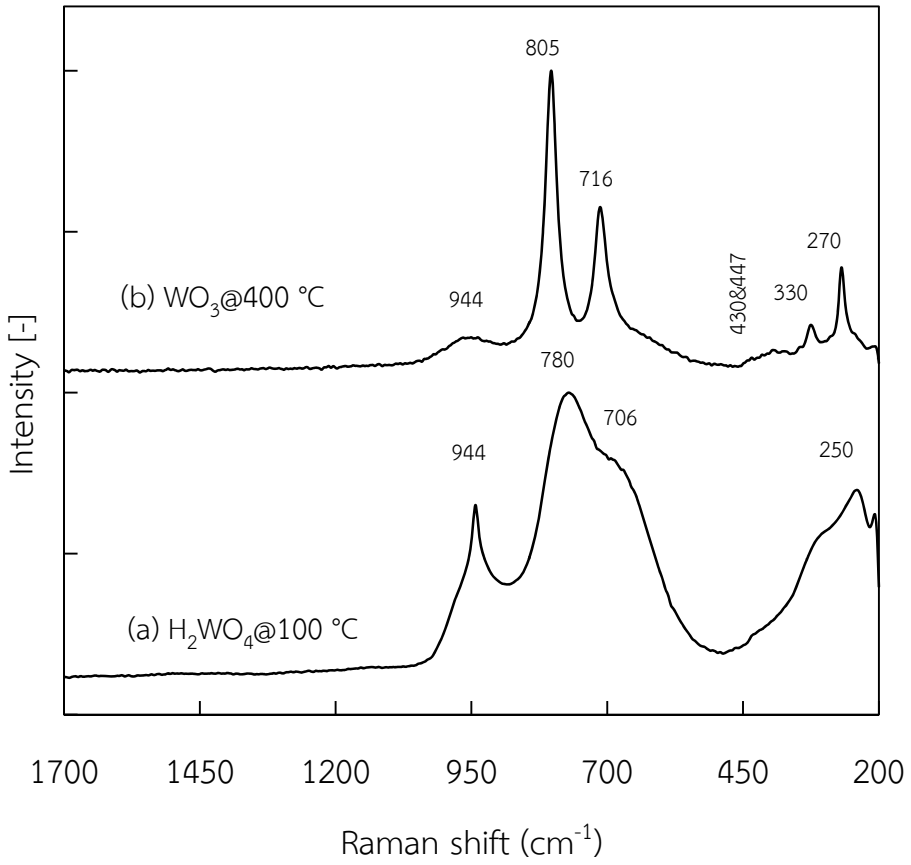

Figure 4.4 Raman spectra of hydrated WO_3 and dehydrated WO_3 at 400 °C

Raman shifts at 250, 706, 780 and 944 cm^{-1} characterize the Raman spectrum of the sample dried at 100°C. The band around 944 cm^{-1} is assigned to the stretching mode of the terminal W=O bond; this mode is common for all types of tungsten trioxide hydrates. Following the vibration assignments by Daniel et al., the band at 706 cm^{-1} should be attributed to stretching O-W-O modes of the bridging oxygens in the residual hydrated tungsten oxide, since very similar bands were observed for $WO_3.H_2O$ (or H_2WO_4) [69]. This assignment is tentative and requires further confirmation by IR measurements. However, the spectrum of the sample dried at 100 °C cannot be attributed to any specific crystalline tungsten oxide or hydrated oxide. Evidently, this spectrum has all the characteristics of an amorphous tungsten oxide (*a*-WO_3), namely all bands are broad and their relative band intensities are characteristic of *a*-WO_3. With the increase in calcination temperature to

400 °C, Raman bands shifted to higher wavenumber and became sharper. The broad band centered at ca. 780 cm^{-1} most probably could be deconvoluted into several Raman peaks, including the strongest peaks at 716 and 805 cm^{-1} of a monoclinic WO_3. Indeed, the increase in calcination temperature to 400 °C resulted in the decreased intensity of the stretching mode of the terminal W=O bond at 944 cm^{-1}, with the simultaneous appearance of six new bands at 270, 330, 430, 447, 716, and 805 cm^{-1}. The spectrum of the sample treated at 400 °C was very strong, with well-defined Raman bands at 270, 330, 716, and 805 cm^{-1}. These bands fall very close to the wavenumbers of the four strongest modes of monoclinic tungsten oxide (*m*-WO_3) [67, 69, 70]. The bands at 270 and 330 cm^{-1} correspond to O-W-O bending modes of the bridging oxygen and the bands at 716 and 805 cm^{-1} are the corresponding stretching modes. The shorter O-W-O bonds are responsible for the stretching mode at 805 cm^{-1}, while longer bonds are the source of the 716 cm^{-1} peak [67, 69]. The typical bands around 430 and 447 cm^{-1} together with the lattice modes below 200 cm^{-1} (134 and 184 cm^{-1}) are attribute to the crystalline WO_3. In this work, due to the notch filter cutoff, the lattice vibrations could not be investigated.

In summary, a typical Raman spectrum of a WO_3 sample where four well-resolved peaks could be observed (270, 330, 716 and 805 cm^{-1}). The comparison of the Raman spectra recorded on the as-prepared WO_3 samples with those reported in the literature [20, 67, 69, 70] suggested that they have the monoclinic phase and are formed by O-W-O microcrystalline clusters connected to each other by O-W-O bonds, with the terminal W=O bonds at the surface of the clusters. The peaks at 805 and 716 cm^{-1} are assigned as O-W-O stretching frequencies. The peaks at 270 and 330 cm^{-1} could be ascribed to the O-W-O bending mode of the bridging oxygen.

However due to uncompleted information on the band at 706 cm^{-1} of stretching O-W-O modes of the bridging oxygens in the residual hydrated tungsten oxide, further confirmation by IR measurements are required. Therefore the synthesized products including the hydrated and dehydrated WO_3 were analyzed by Fourier Transform Infrared Spectrometer (FT-IR) to determine W-O functional groups

of WO_3 nanoparticles and O-H groups of water molecules as well as observing transformation of the hydrated WO_3 to dehydrated WO_3 by calcination process.

Figure 4.5 shows the comparison between FT-IR spectra of hydrated and dehydrated WO_3 nanoparticles. The broad absorption band of hydrated WO_3 at 710 cm^{-1} assigned to W-O stretching and slightly shifted to 750 cm^{-1} when such hydrated WO_3 was calcined at 400 ℃ for 1 hour. It was suggested that both hydrated and dehydrated products have characteristics of WO_3. The broad absorption bands between 3200 and 3600 cm^{-1}, which is clearly observed in the hydrated sample, could be assigned to O-H vibration of physically absorbed water molecules. Other peak at 1620 cm^{-1} is assigned to O-H bond of chemically bond water (water of crystallization) in the hydrated products. After calcination process of hydrated products at 400 ℃, the intensity of transmittance at such wave numbers (3200, 3600, 1620 cm^{-1}), however, is likely to decrease due to removal of physical and chemical adsorbed water molecules. This experimental result was confirmed that the calcination process at 400 ℃ for 1 hour could be a suitable calcination condition to eliminate water molecules to yield dehydrated WO_3. The dehydration behavior of hydrated WO_3 is also observed in many research works [39, 71]. Meanwhile there is evidence that ammonia residue from ATP reactants partially exists in the hydrated products. In other word the absorption band around 3000 cm^{-1} and the sharp absorption peak around 1400 cm^{-1} is due to the stretching and rotational vibration of N-H bond in ammonia which is also disappeared upon heating in calcination process at 400 ℃ for 1 hour, respectively [71].

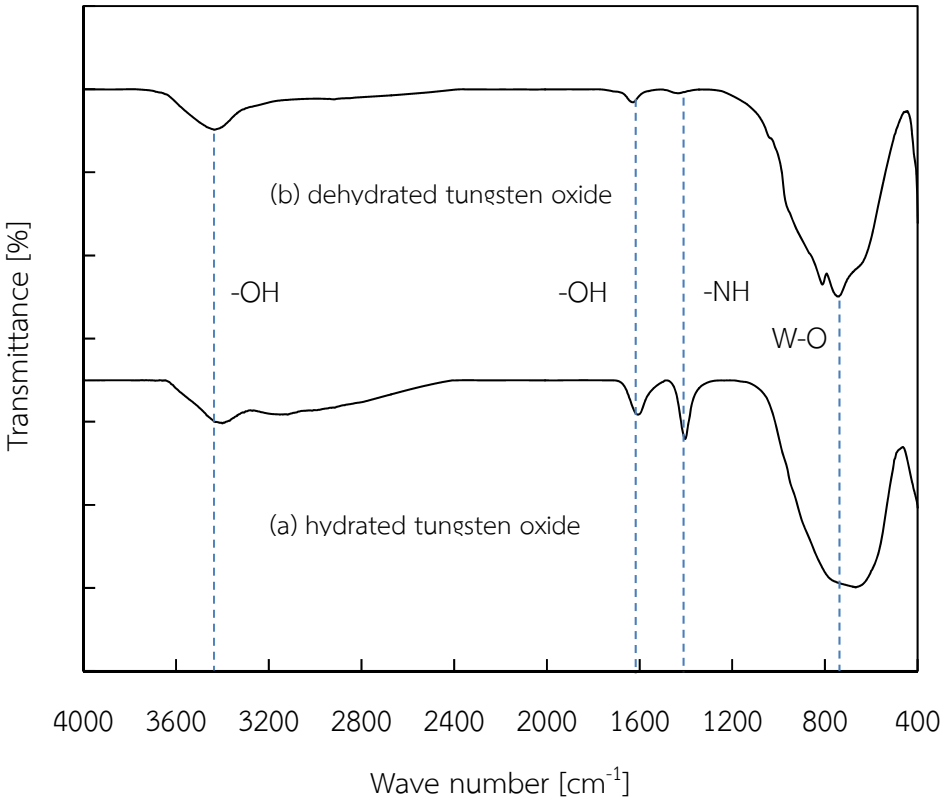

Figure 4.5 IR spectrums of (a) hydrated tungsten oxide (H_2WO_4) and (b) dehydrated tungsten oxide (WO_3)

4.3.2 Dehydration behavior of hydrated WO_3 nanoparticle

In order to investigate dehydration behavior of hydrated WO_3 during calcination process, mass change during heating condition of the hydrated products was analyzed by Thermo Gravimetric Analyzer (TGA) under oxygen atmosphere at a scan rate of 10°C/min. The weight loss of hydrated products in Figure 4.6 was clearly observed with three steps in the region 25 – 400 °C including first step from 25 – 120 °C, second step from 120 – 300 °C and the last steps from 300 – 400 °C. In first step of weight loss, it was evidenced that the physical water molecules adsorbed in the hydrated products was firstly removed with the percent weight loss of 1.95%. Meanwhile the chemical water molecules adsorbed in the product was further dehydrated at higher temperature with the major percent weight loss of 5.29%. The last step is final decomposition of water molecules and simultaneous transformation

of amorphous WO_3 to crystalline WO_3 with the percent weight loss of 0.45%. A total weight loss of 7.69% has been observed and this close to the calculated weight loss of 7.2% based on the loss of H_2O from H_2WO_4 [31]. The higher weight loss observed maybe due to the loss of ammonium ion [56] which correspond to FT-IR result. The complete weight loss of adsorbed water after treatment at 900 °C is 8.1% slightly higher than total weight loss at 400 °C. Hence the three-step decomposition could be attributed to stepwise removal of physically adsorbed water in the range of 25-120°C, chemically adsorbed water from 120-300 °C and final removal during crystalline phase formation between 300-400°C. This TGA analytical result was useful for determining suitable temperature for calcination process. Although slight water molecules remain in the WO_3 sample after calcination at 400 °C, it was suggested that this temperature gives WO_3 nanoparticles with monoclinic phase (XRD results), crystalline characteristics (Raman results), and acceptable slight water molecules in structure (IR and TGA results). Therefore the appropriated temperature for calcination process would be 400 °C. However the effects of calcination temperature and time on surface area and crystallite size of WO_3 nanoparticles would be further investigated in the last section of this chapter.

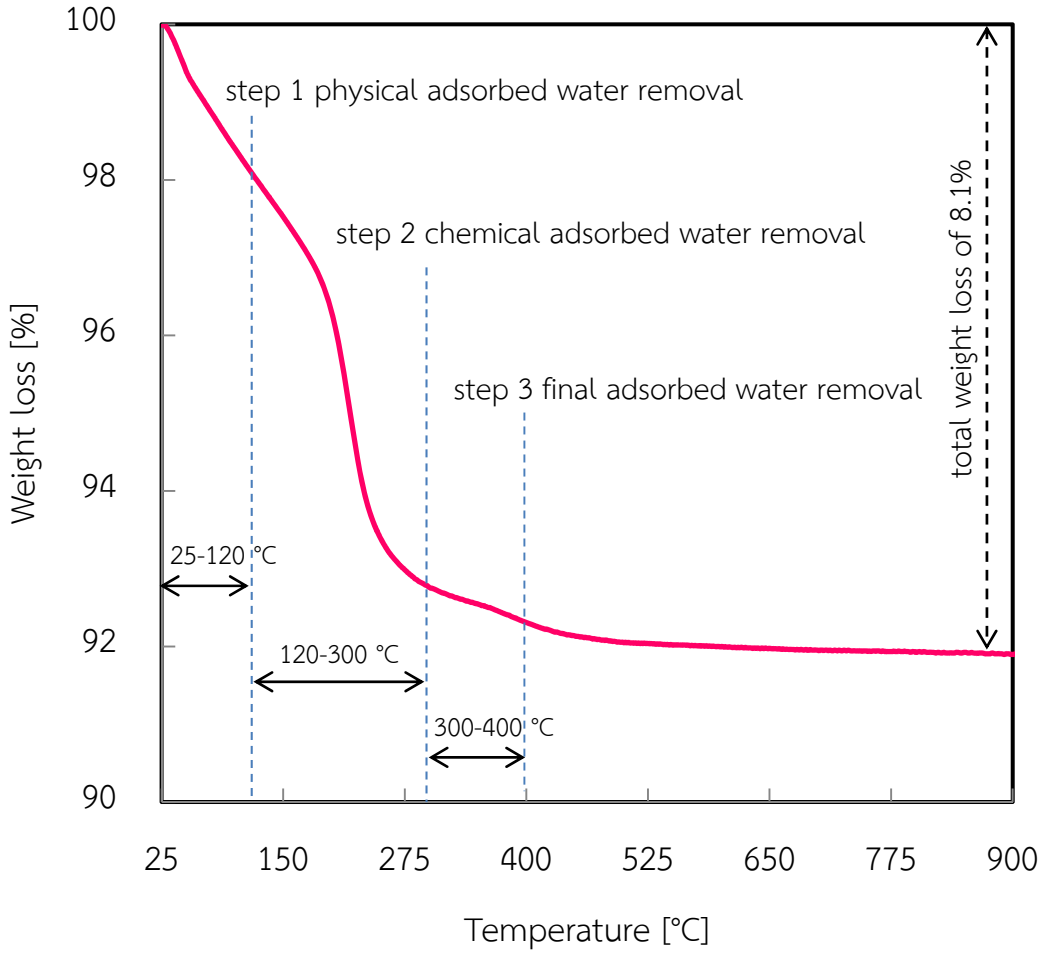

Figure 4.6 Thermo gravimetric analysis of H_2WO_4

4.3.3 Morphology of hydrated and dehydrated WO_3 nanoparticles

Morphology of synthesized products was visually observed by Scanning Electron Microscope (SEM). Typical SEM micrographs of hydrated products were shown in Figure 4.7. Morphologies reveal that the as-prepared H_2WO_4 and WO_3 nanoparticles calcined at various temperatures exhibit agglomerating grain-like morphology with nominal size in a range of 100–200 nm. SEM micrographs also show that the higher the calcination temperature, the larger the nominal particle size.

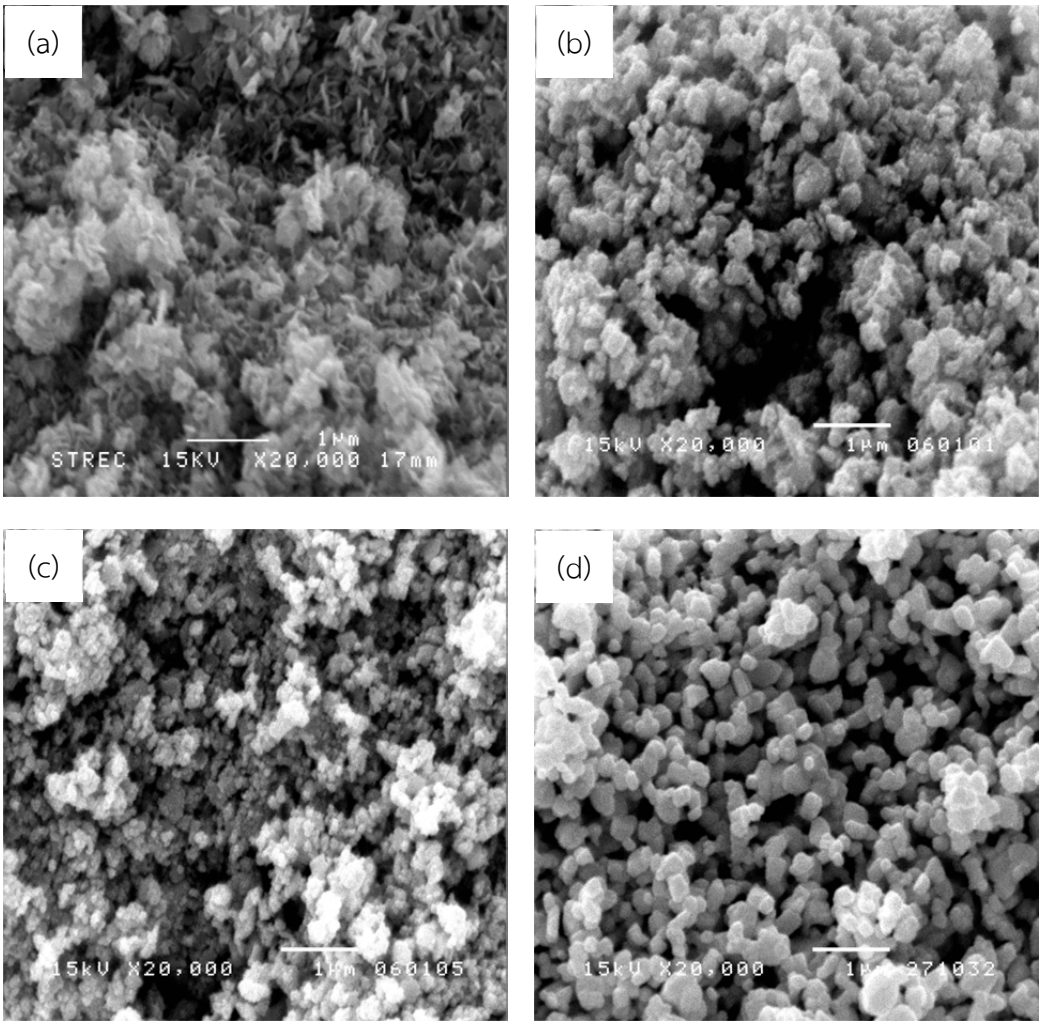

Figure 4.7 Typical SEM micrographs of (a) H_2WO_4, (b) WO_3@300 ℃, (c) WO_3@400 ℃, and (d) WO_3@600 ℃

The primary particles of WO_3 nanoparticles were observed by Transmission Electron Microscope (TEM). It was found that the primary particle of WO_3 nanoparticles would be in the range of 10-65 nm. TEM micrographs also show that the higher the calcination temperature, the larger the primary particle size.

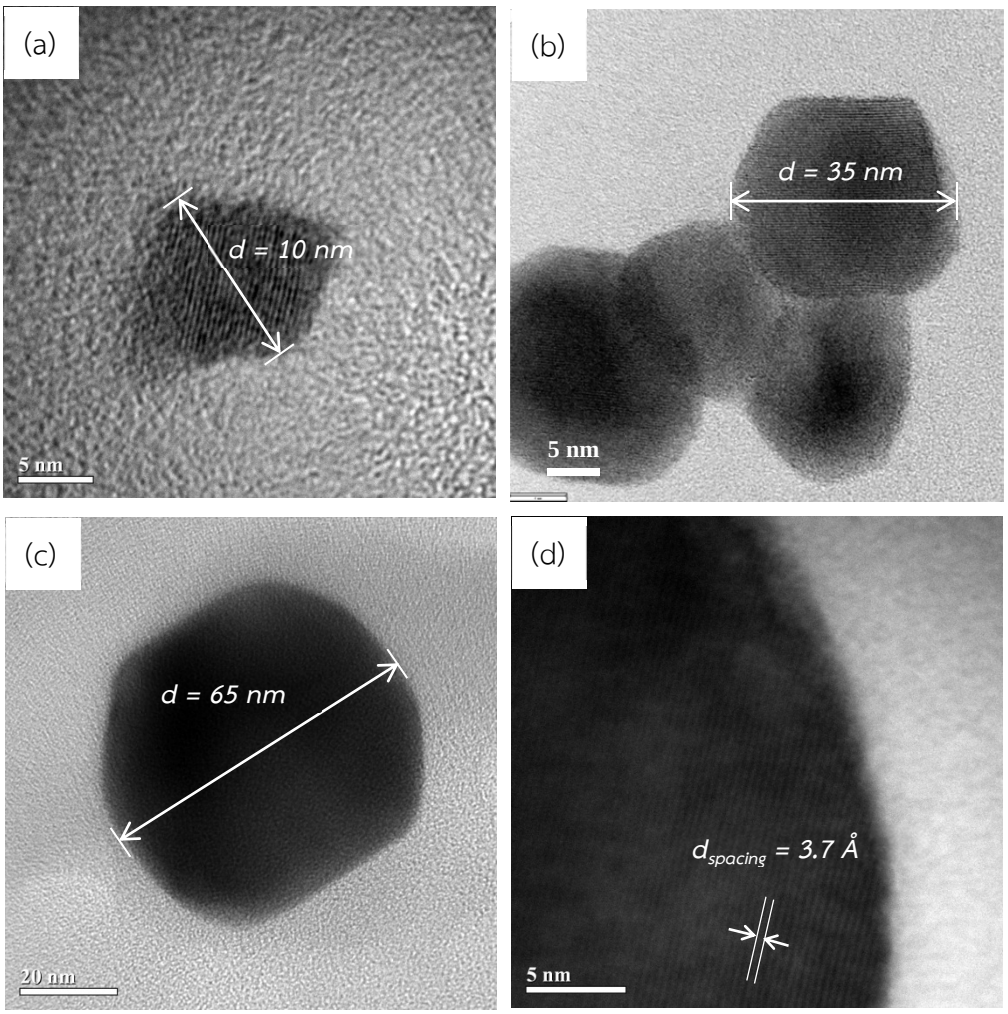

Figure 4.8 Typical TEM micrograph of (a) WO_3@300 °C, (b) WO_3@400 °C (c) WO_3@600 °C, and (d) $d_{spacing}$ of WO_3@600 °C

4.3.4 Specific surface area and crystallite site

One of the desirable characteristics of gas sensing material is its high surface area. The higher surface area of the sensing material implies a larger amount of sites available for gas adsorption. Not only high surface area but also small crystallite size of WO_3 nanoparticles would be required for good sensitivity of sensing materials. Since crystallite size and specific surface area of WO_3 nanoparticles are two main characteristics which play an important role for sensing application, they were analytically investigated in both hydrated and all dehydrated WO_3 calcined at different temperature. In general it is known that the heating condition in calcination

process would reduce specific surface area but increase crystallite size of WO_3 nanoparticles. Therefore suitable temperature and time for calcination of WO_3 nanoparticles would be required to determine.

Specific surface areas of all calcined and dried products were evaluated by nitrogen adsorption-desorption analysis and calculated the specific surface area by the BET method. Figures 4.9 and 4.10 show the nitrogen adsorption/desorption isotherms of the samples before and after calcinations and their corresponding pore-size distributions, respectively. The isotherm corresponding to the un-calcined sample is of type IV (BDDT classification) with one capillary condensation step, implying the unimodal pore-size distributions in the mesoporous region. The hysteresis loop in lower relative pressure range ($0.4 < P/P_0 < 0.8$) is related to finer intra-aggregated pore within the agglomerated particles, and that in higher relative pressure range ($0.8 < P/P_0 < 1$) is associated with larger inter-aggregated pore between the aggregated particles [39]. This unimodal mesopore size distribution is confirmed by the corresponding pore-size distributions (see Figure 4.10). The powders contain slight mesopores with a peak pore diameter of *ca.* 3.3 nm. Calcination temperatures obviously influence the pore structures and BET surface areas of the samples. With increasing calcination temperatures, the isotherms corresponding to the samples obtained at 300 °C show higher absorption at low relative pressure (P/P_0) range ($0.4 < P/P_0 < 0.8$), indicating the formation of more mesopores and/or the increase of pore volume. It was that the pore diameter was constant at *ca.* 3.3 nm but this calcination temperature gives more pore volume as shown in Figure 4.10. With higher calcination temperature of 400 °C, the isotherm showed higher absorption at high relative pressure (P/P_0) range (approaching 1), indicating the formation of more mesopores with larger pore size of *ca.* 9.2 nm. Further observation indicates that the hysteresis loop in low relative pressure range gradually disappears while that in high relative pressure range gradually become larger, suggesting that the pore-size distributions of intra-aggregated pores tend to decrease but inter-aggregated ones tend to increase, as confirmed in Figure 4.10. This is associated with the growth of the crystallites, phase transformation and re-

structures of particles and the shrinkage of the aggregates, resulting in the increase of intra-aggregated pores and decrease of inter-aggregated ones, respectively. When calcination temperatures are above 600 °C, the hysteresis loop in low relative pressure range completely disappears and the areas of hysteresis loop decrease greatly, implying the decrease of pore volume and the collapse of intra-aggregated pores, which is confirmed by the corresponding small pore volume (Figure 4.10).

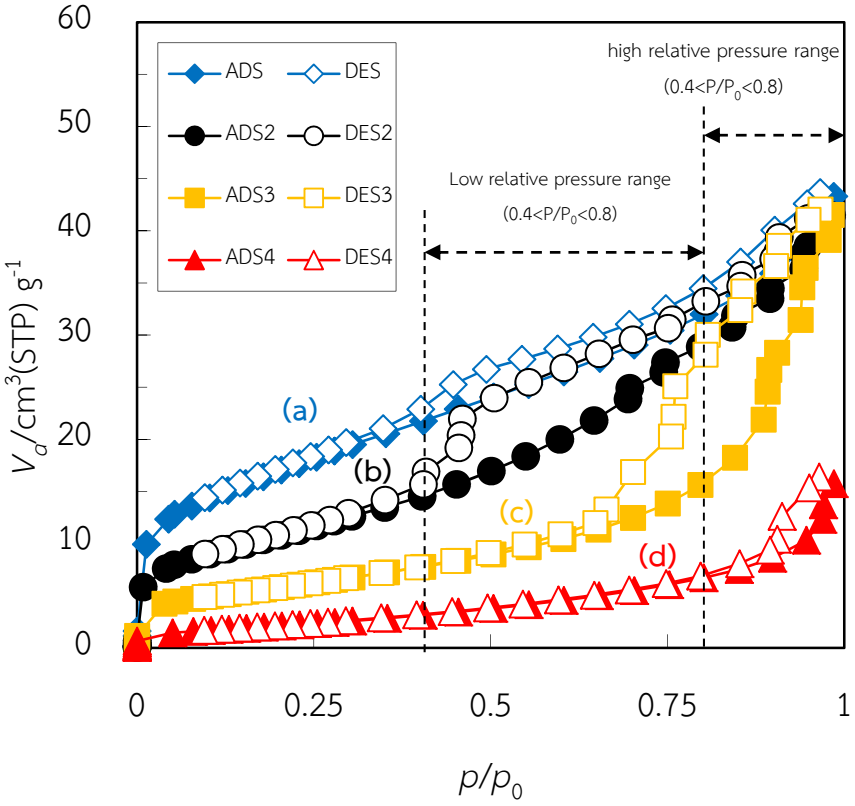

Figure 4.9 Nitrogen adsorption/desorption isotherms of (a) H_2WO_4, (b) WO_3@300 °C, (c) WO_3@400 °C, (d) WO_3@600 °C

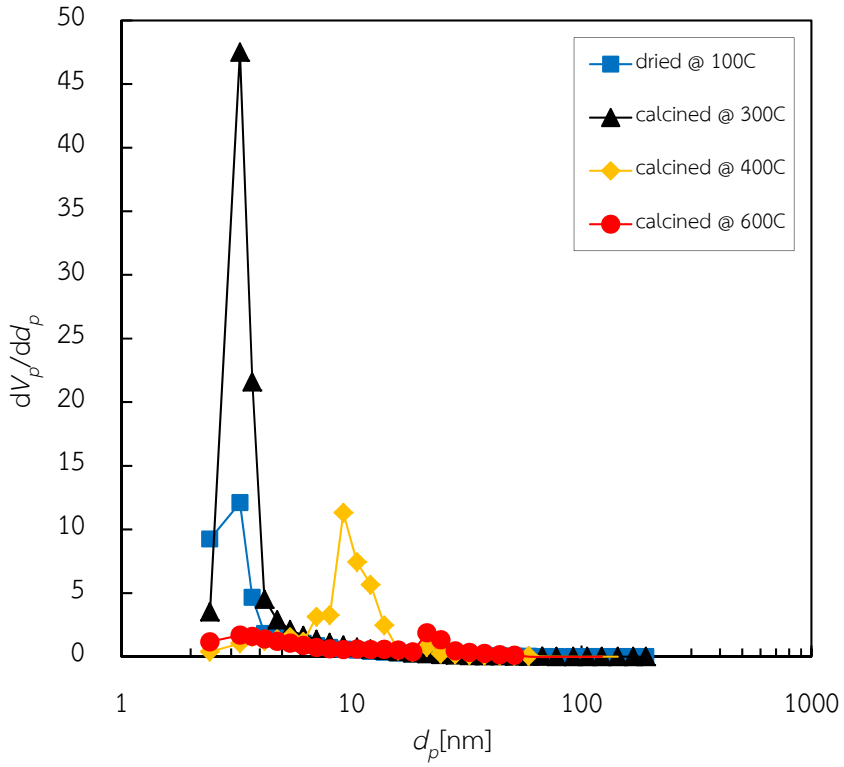

Figure 4.10 Pore-size distribution curves of (a) H_2WO_4, (b) WO_3@300 °C, (c) WO_3@400 °C, (d) WO_3@600 °C

An increase in the calcination temperature exerts large effect on a decrease in specific surface area of products as shown in Figure 4.11. This result is attributed to the larger crystallite size of the WO_3 powders calculated from the broadening of the (0 0 2), (0 2 0) and (2 0 0) peaks of XRD patterns. The higher calcination temperature lead to the crystal growth and partial collapsed of WO_3 structure, resulting in larger grain size [3].

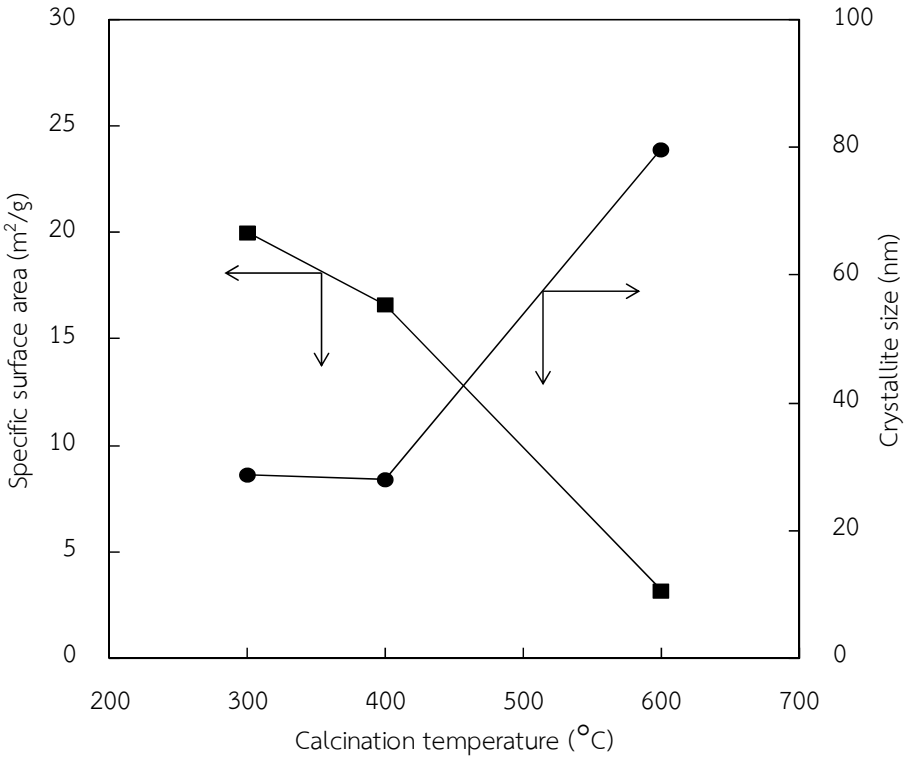

Figure 4.11 Specific surface area of synthesized product calcined at various temperatures for 1 hour

When consider the effect of calcination time to specific surface area and crystallite size of WO_3 nanoparticles, WO_3 nanoparticles calcined at 600 ℃ for 1, 3, and 5 hours were observed. Figure 4.12 reveals that calcination time exerts only small effect on both specific surface area and crystallite size. The longer calcination time examined in this work would be insufficient to effect to the crystal growth, resulting in crystal with stable size. Tamaki et al. [72] reported that crystallite size could be controlled by choosing calcination or sintering temperature. The rates of response and recovery of WO_3 were affected by crystallite size, increasing in crystallite size decreasing and increasing rate of response and recovery, respectively. In order to improved sensitivity to gas the mean crystallite size should be about 25 nm.

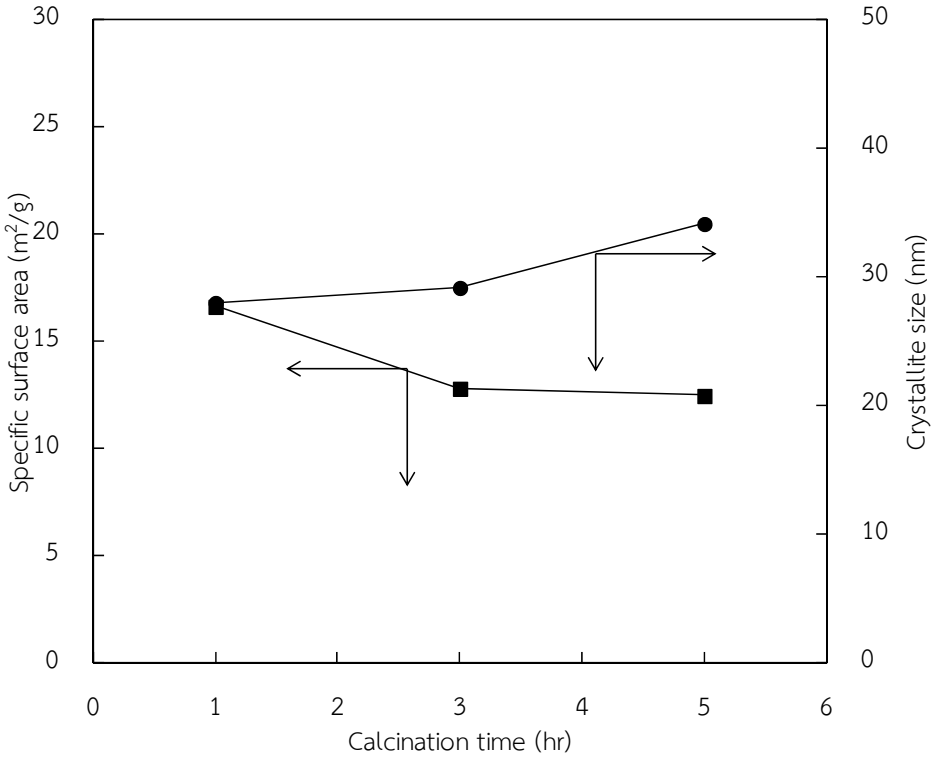

Figure 4.12 Specific surface area of synthesized products at 400 °C for various calcination times

4.4 Conclusion

In order to obtain the suitable conditions for synthesizing the MWCNT-WO_3 composites, tungsten oxide (WO_3) nanoparticles were synthesized solely to determine the highest yield and the optimal calcination conditions which have strong effect to the properties of sensing materials. The WO_3 nanoparticles were synthesized with facile consecutive two steps including acid precipitation and calcination process. In acid precipitation, the color of mixture was changed from clear solution to light yellow and finally dark yellow suspension attributed to the precipitation of polyoxometallates ions to solid nanoparticles. Such acid precipitation mechanism was generally attributed to hydrolysis reaction of tungstate salt (ATP) in an excess acid environment. The excess acid would play an important role in not only protonating of $[WO_4]^{2-}$ ions but also providing low pH environment. The increase in acid concentration would promote supersaturation of WO_3 nuclei. Percent yields

of WO_3 products were investigated by varying both initial reactant concentrations. The maximum percent yield was obtained at initial concentration of tungstate salt and nitric acid of 5.3 mM and 10 M, respectively. Therefore this condition was chosen for synthesizing WO_3 nanoparticles as well as MWCNT-WO_3 composites. In calcination process, effects of calcination temperature and calcination time on WO_3 characteristics, such as water molecules remain, crystallite size, surface area were investigated. From view point of microscopic analysis from XRD and BET, it was found that higher temperature and longer time would provide the lager crystallite size and lower surface area. With further supported observation from TGA Raman and FITR, it was confirmed that the calcination temperature of 400 °C and calcination time of 1 hour would be suitable condition to obtain appropriate WO_3 characteristics. With SEM observations, the agglomerating grain-like morphology with nominal size in a range of 100–200 nm. SEM micrographs also show that the higher the calcination temperature, the larger the nominal particle size. The primary particles of WO_3 nanoparticles observed by TEM would be in the range of 10-65 nm. TEM micrographs also show that the higher the calcination temperature, the larger the primary particle size.

CHAPTER V

SYNTHESIS OF MWCNT-WO_3 COMPOSITES

In many research works published previously, multi-walled carbon nanotubes (MWCNTs) were directly mixed with tungsten oxide nanoparticles (WO_3) to fabricate sensing materials [10, 30, 54, 55]. Because of its high surface area and electrical conductivity, carbon nanotubes would help to increase surface area for high adsorption of target gas as well as to decrease its sensing temperature. However such physically mixed preparation would not be sufficient for incorporating its useful nano-characteristics of carbon nanotubes and tungsten oxide nanoparticles. To cooperate such characteristics of tungsten oxide nanoparticles (WO_3) and multi-walled carbon nanotubes (MWCNTs), thus the second aim of this research work is to in situ synthesize WO_3 nanoparticle composited with MWCNTs by acid precipitation process. The mass ratio of MWCNTs to ATP reactants was varied to study their effects on sensing ability of fabricated thick-film sensor.

5.1 In situ synthesis of MWCNT-WO_3 composite by acid precipitation method

In previous chapter of synthesis of WO_3 nanoparticles, the appropriated concentrations of both ATP and nitric acid (ATP = 5.3 mM, nitric acid = 10 M) were experimentally investigated to obtain the highest yield of 71.4%. Meanwhile the WO_3 nanoparticles prepared from this condition were further used to investigate the suitable calcination temperature and time of 400 °C and 1 hour, respectively. Therefore only such condition was used to further prepare MWCNT-WO_3 composites. Consequently in situ synthesis of MWCNT-WO_3 composites were carried according to acid precipitate synthesis of WO_3 nanoparticles. Briefly, designated amount of MWCNTs was firstly put into ATP solution constantly heated at 80 °C following addition of dropwise nitric acid to precipitate ATP to H_2WO_4 nanoparticles simultaneously composited with those MWCNTs.

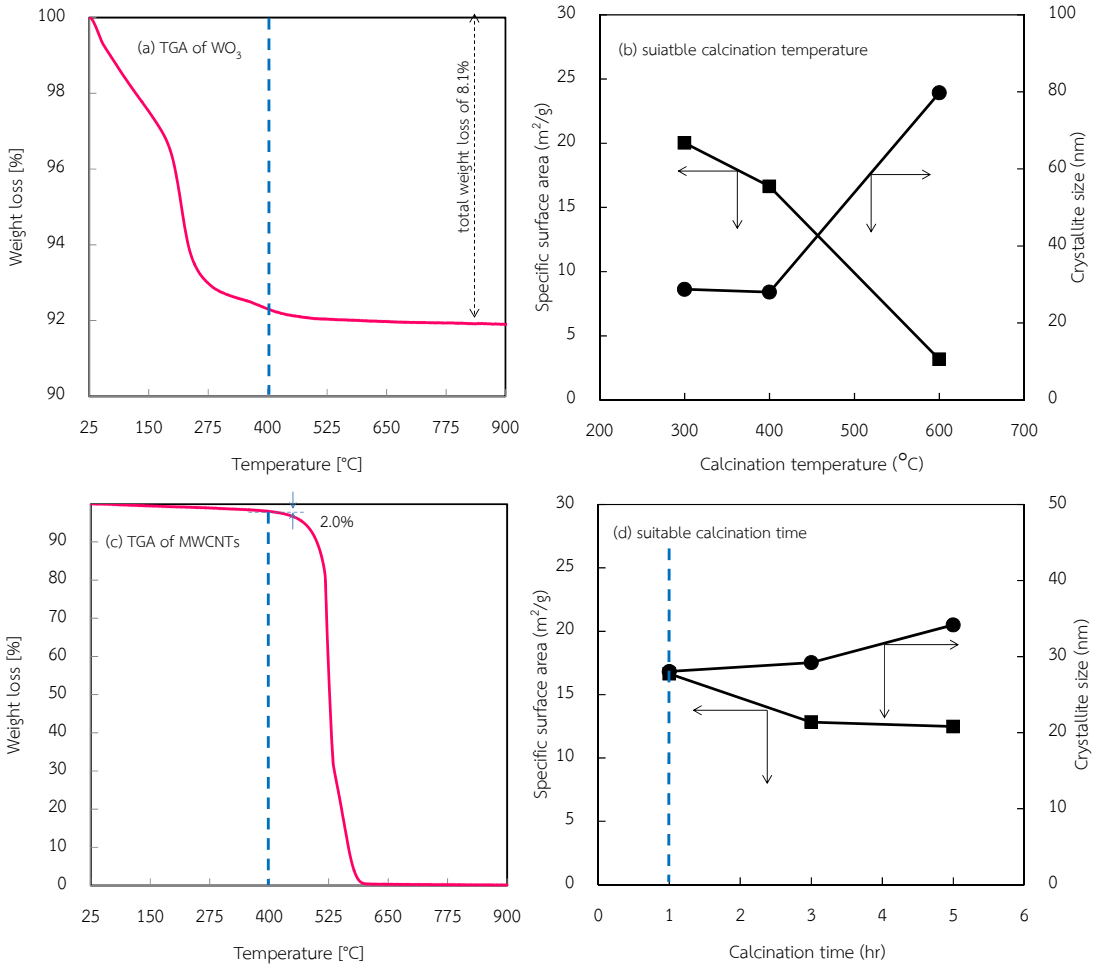

Figure 5.1 Thermo gravimetric analyses of (a) WO_3 nanoparticles, (c) pristine MWCNTs and specific surface area and crystallite size of WO_3 nanoparticles with (b) different calcination temperature and (d) different calcination time

However calcination process of the composite samples would be carefully considered. Since calcination process was performed under air atmospheres, carbon nanotubes in the composite samples would be completely decomposed at high temperature treatment under such atmospheres. Meanwhile WO_3 nanoparticles would be also required sufficient calcination temperature and time in both removal of water molecules and transformation of monoclinic phase. According to previous chapter, calcination temperature of 400 °C could almost remove water molecules in WO_3 nanoparticles as confirmed by TGA analysis in Figure 5.1 (a). Meanwhile specific surface area seemed to slightly decrease and crystallite

size also likely to constant after calcined at 400 °C for 1 hour as shown in Figure 5.1 (b). The effects of calcination time on specific surface area and crystallite size of WO_3 nanoparticles would be also investigated. It was found that calcination time of 1 hour would be sufficient in calcination process of WO_3 nanoparticles as shown in Figure 5.1 (d). With TGA analysis of pristine multi-walled carbon nanotubes in Figure 5.1 (c), it was found that MWCNTs were completely decomposed at temperature of 580. It was implied that calcination temperature of composite should not excess such temperature. However it was found that only weight loss of 2% was observed at temperature of 400 °C. Form this analytical results, it was suggested that calcination temperature of 400 °C would be suitable for calcination process of the composites.

5.2 Determination of composition of MWCNT-WO_3 composites

After determination of the appropriate condition for acid precipitation synthesis and the suitable calcination condition of MWCNT-WO_3 composites, the effects of mass ratio of MWCNTs to WO_3 nanoparticles on its characteristics were experimentally investigated. Such mass ratio was varied by changing mass ratio of MWCNTs to ATP with five ratios including 0.252:100, 0.5:100, 1:100, 2:100, and 5:100. Meanwhile actual mass ratios of MWCNTs to WO_3 nanoparticles of as-synthesized composites were analyzed by thermo gravimetric analyzer as shown in Figure 5.2.

Figure 5.2 (a) revealed three decomposition steps of WO_3 nanoparticles. This decomposition behavior was employed to determine amount of MWCNTs in the as-prepared composites. After water molecules would be removed at low temperature (< 400 °C), the last decomposition step would imply the decomposition of MWCNTs. Therefore an actual mass of MWCNTs in each as-prepared composite was calculated as shown in Figure 5.2 (b) - (f). These mass ratios would be used to infer the effects of MWCNTs on sensing ability when such composites would be employed to prepare a fabricated thick-film sensor for sensing CO_2 thoroughly discussed in chapter 6.

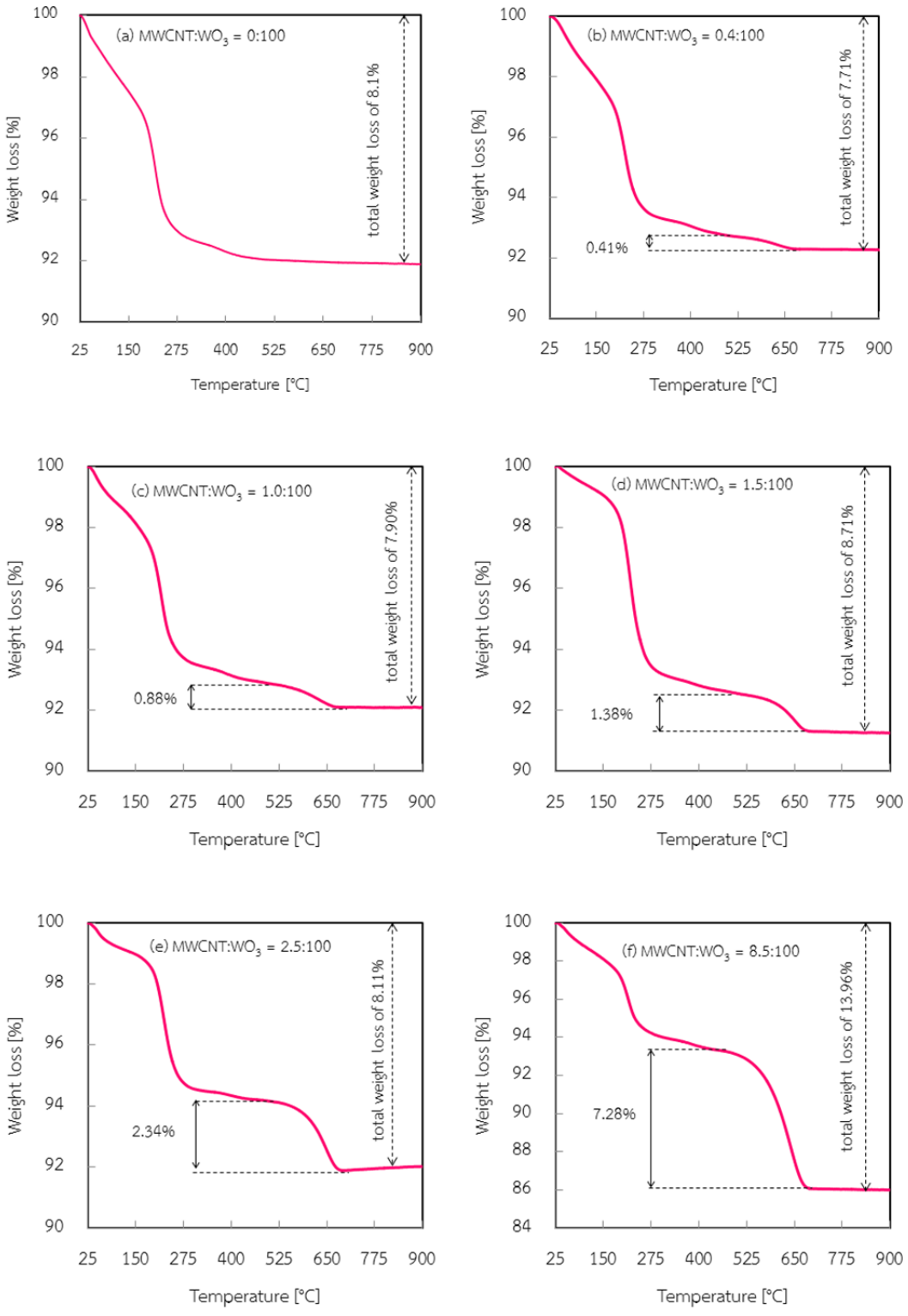

Figure 5.2 Thermo gravimetric analyses of (a) MWCNT:WO_3 = 0:100, (b) MWCNT:WO_3 = 0.4:100, (c) MWCNT:WO_3 = 1.0:100, (d) MWCNT:WO_3 = 1.5:100, (e) MWCNT:WO_3 = 2.5:100, (f) MWCNT:WO_3 = 8.5:100

Actual mass ratio of MWCNTs to WO_3 nanoparticles were plot against mass ratio of MWCNTs to ATP as shown in Figure 5.3. A second power equation was used to fit data. With the r-square value of 0.9936, it was suggested that this equation would be good agreement with the data. An obtained equation from this plot would be expect to use for tailor predication of actual mass ratio when the composite synthesis by acid precipitation method would be performed in a mass ratio (MWCNT:ATP [g/g]) range of 0.252:100 to 5:100.

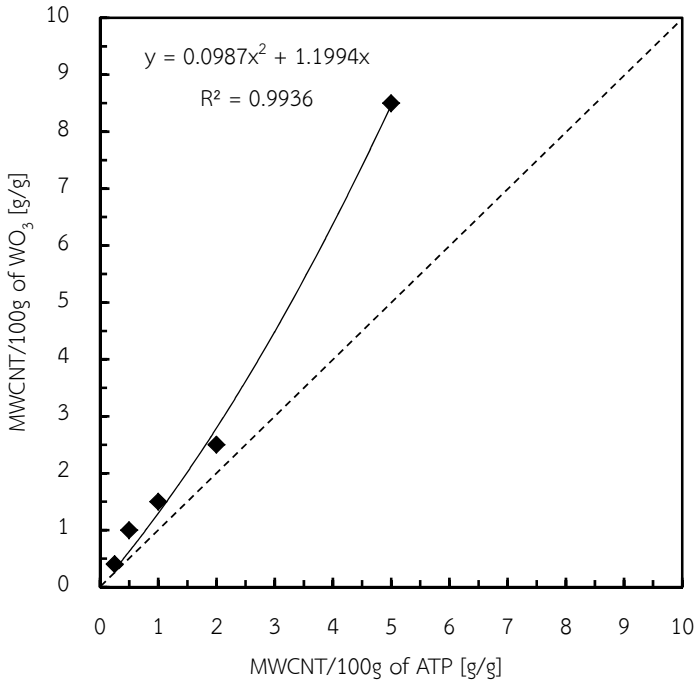

Figure 5.3 Mass ratio of MWCNT:WO_3 in the as-prepared composite compared with mass ratio of MWCNT:ATP

5.3 Morphology of MWCNT-WO_3 composites

In this work, commercial multi-walled carbon nanotubes were employed to in situ synthesizes the composite with WO_3 nanoparticles. To understand formation of composites, pristine MWCNTs were solely characterized by many analytical techniques. Therefore morphology of pristine MWCNTs was analyzed by scanning electron microscope (SEM). The entangled nanotubes were visually demonstrated in Figure 5.4 (a). Further morphology observation was performed by

transmission electron microscope (TEM) to reveal their internal structures as shown in Figure 5.4 (b) – (d). It was found that typical nominal diameter of nanotubes is 16 nm with the wall width of *ca.* 5 nm as shown in Figure 5.2 (c). With high magnification observation, the spacing between two graphitic layers is *ca.* 0.34 nm.

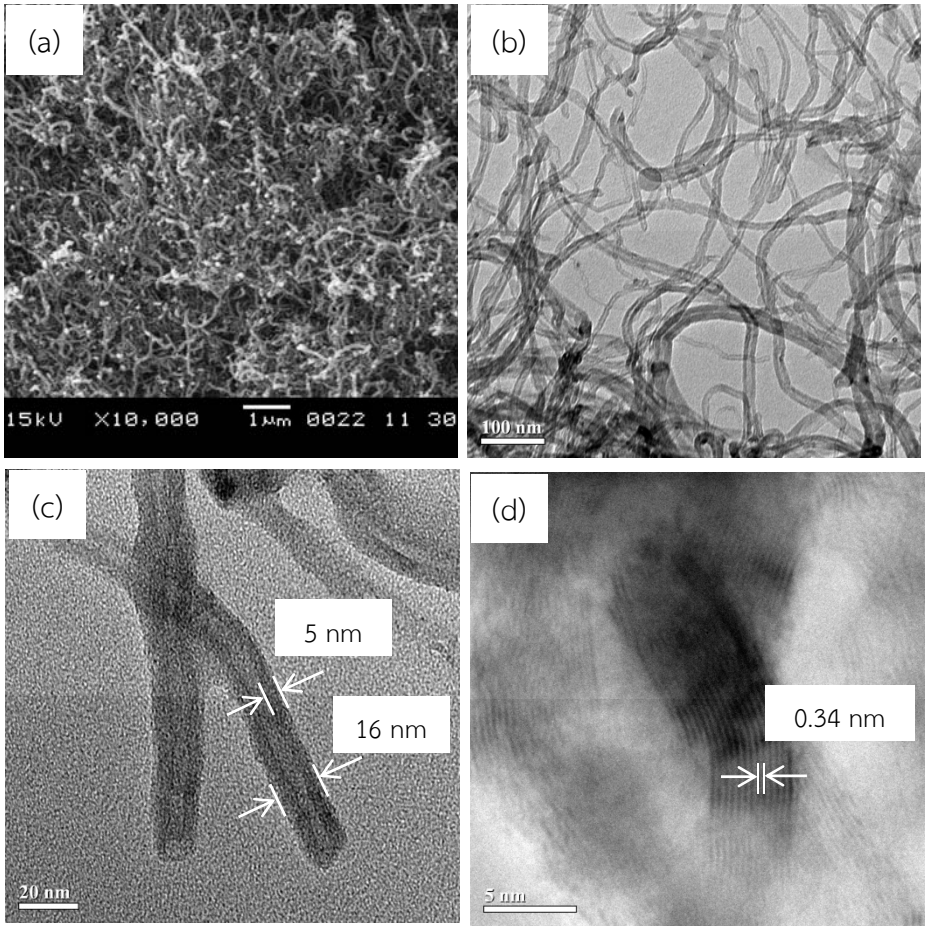

Figure 5.4 Typical (a) SEM micrograph and TEM micrograph of (b) pristine multi-walled carbon nanotubes, (c) individual nanotube (d) high resolution of graphene sheets

Meanwhile morphology of the MWCNT-WO_3 composite was also observed to visually demonstrate the existence of MWCNTs in WO_3 nanoparticles. A typical composite with mass ratio of 1:100 was thus analyzed by SEM as shown in Figure 5.5. It was found that MWCNTs would be visually observed in the composite. MWCNTs entangled with agglomerated WO_3 nanoparticles as shown in Figure 5.5 (a).

A schematic of the composite was illustrated to shown how to they incorporate together as shown in Figure 5.5 (b).

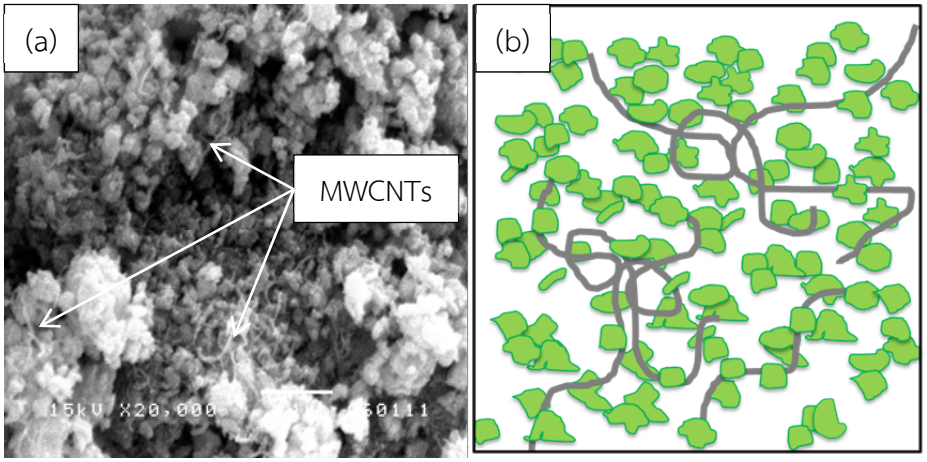

Figure 5.5 Typical (a) SEM micrograph and (b) model schematic of the MWCNT-WO_3 composites prepared with the ratio of MWCNT:WO_3 [g/g] = 1.0:100

Further observations of internal structure of as-prepared composites were performed by transmission electron microscope (TEM). With such high magnification observation, high density of WO_3 nanoparticles would be easily seen contrast with MWCNTs as shown in Figure 5.6 (a). In more high magnification in Figure 5.6 (b), it was found that the composite would be composed of MWCNTs decorated with WO_3 nanoparticles on its surface. It was suggested that WO_3 nanoparticles would randomly grow through surface of MWCNTs. This composite structure would be suitable for using as sensing materials. In other observation point of composites in Figure 5.6 (c), it was found that WO_3 nanoparticles also embed on surface of nanotubes. Meanwhile typical nominal diameter and wall width of MWCNTs would be same as pristine one as shown in Figure 5.6 (d). It was suggested that structure of MWCNTs would be not affected by acid precipitation method. Typical particle size of WO_3 nanoparticles was *ca.* 25 – 30 nm as shown in Figure 5.6 (d) – (f).

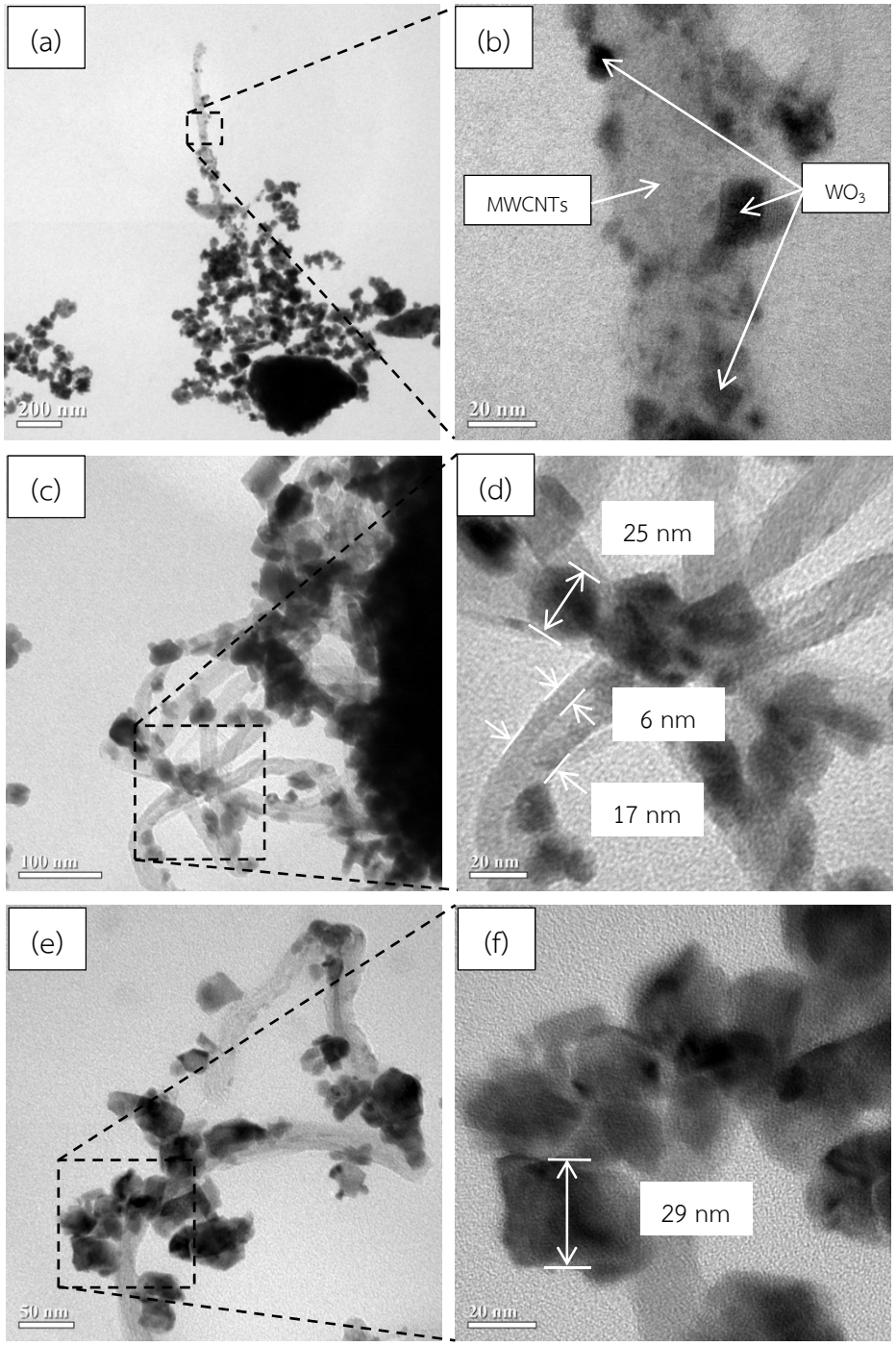

Figure 5.6 Typical TEM micrograph of the MWCNT-WO_3 composites prepared with the ratio of MWCNT:WO_3 [g/g] = 1.0:100

5.4 Existence of MWCNTs in the bulk MWCNT-WO_3 composite

With microscopic observations by SEM and TEM, MWCNTs decorated with WO_3 nanoparticles would be clearly seen as mentioned in previous section. However it would be great if bulk composites would be further characterized in order to confirm existence of MWCNTs thoroughly dispersed in the composites. Therefore the existence of MWCNTs in the bulk composite was confirmed by Raman spectroscopic technique. The WO_3 nanoparticles could be characterized by Raman spectroscope as mentioned in previous chapter. Meanwhile carbonaceous materials would be usually analyzed by this technique. The characterization would be employed to indicate amorphous and crystalline property by the intensity ratio of disorder band (D-band) and graphitic band (G-band).

With this advantages, thus the bulk composite were also analyzed by Raman technique. The Raman shifts of pure WO_3 nanoparticles, pristine MWCNTs, and the as-prepared composite were comparatively shown in Figure 5.7. It was found that D-band and G-band characteristics could not be observed in pure WO_3 samples. Meanwhile such D-band and G-band characteristics of the MWCNT-WO_3 composite would be clearly observed in Raman shifts of 1598 and 1279 cm^{-1}, respectively. It was suggested that the bulk property of composite would be composed with MWCNTs and WO_3 nanoparticles.

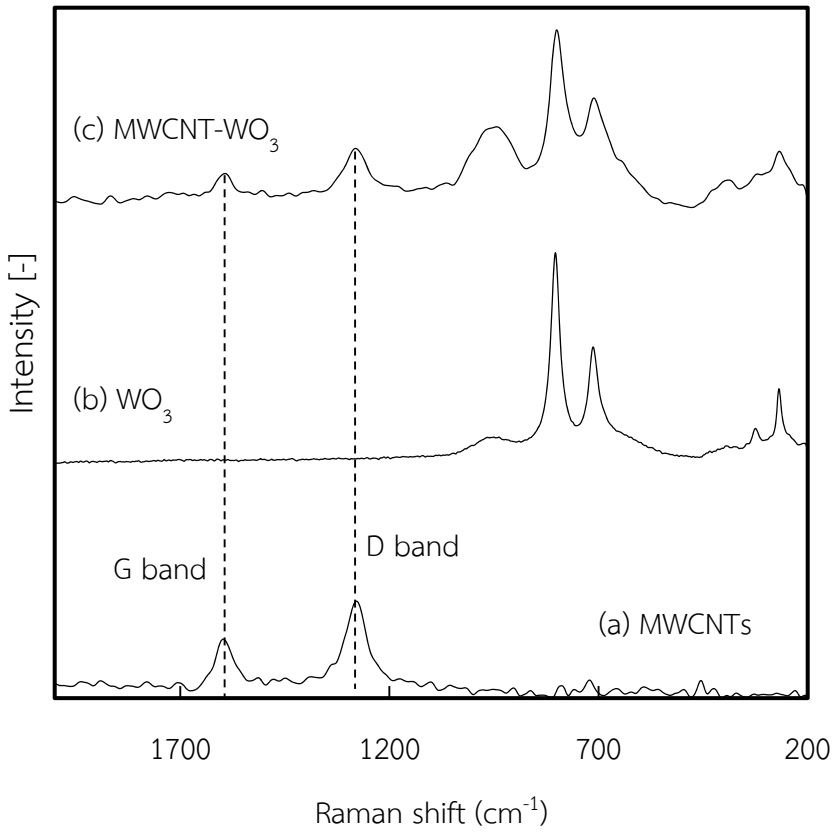

Figure 5.7 Raman shifts of (a) pristine MWCNTs, (b) WO_3, and (c) MWCNT-WO_3 composites

5.5 Crystallite site and specific surface area of composite

According to previous chapter, crystallite site and specific surface area would be main characteristics for sensing materials. Therefore crystallite site and specific surface area of pure WO_3 nanoparticles were investigated with different calcination temperature and time. Subsequently the suitable condition for calcination process was determined. This calcination condition was also employed to calcine the as-prepared composites. The effects of MWCNTs on crystallite size of WO_3 nanoparticles were investigated and analyzed by XRD technique. It was found that crystallite size of WO_3 nanoparticles seemed to be constant in size as shown in Figure 5.8. From such crystallite size results, it was suggested that amount of MWCNTs would not involve in formation of WO_3 nanoparticles.

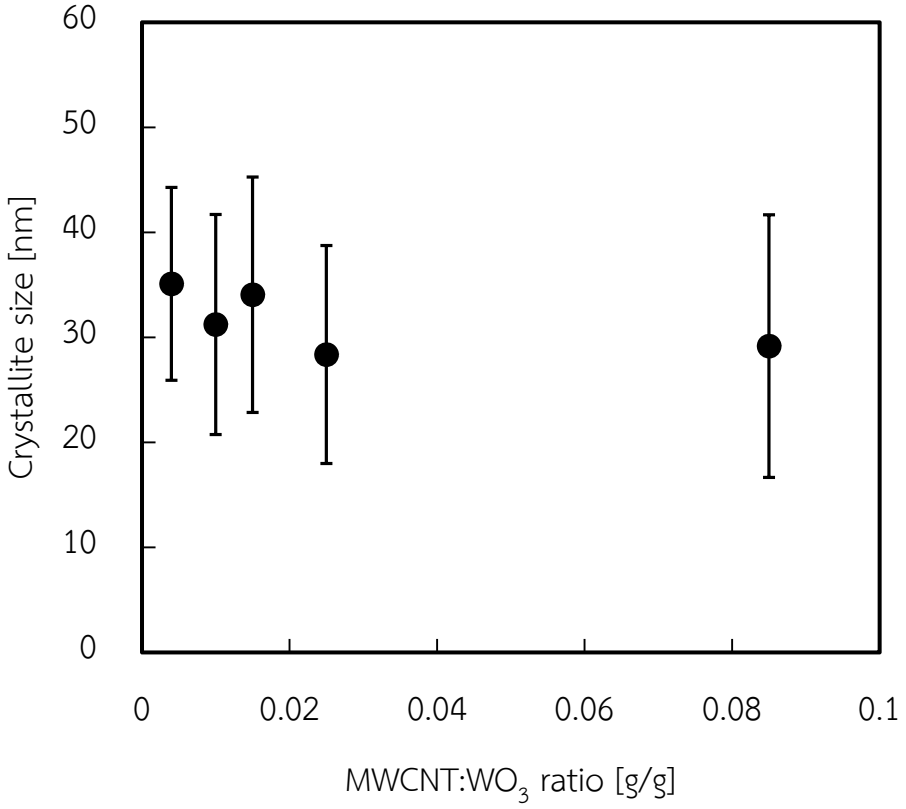

Figure 5.8 Crystallite size of WO_3 nanoparticles in the composites synthesized with different ratios of MWCNT:WO_3

One of important characteristics of composites for sensing materials is its surface area for adsorption of target gas. High surface area of MWCNTs would be expected to increase surface area of as-prepared composites. Therefore BET surface area of the as-synthesized composites after calcination process was analyzed by BET technique. The BET specific surface areas of the composite with different ratio were shown in Figure 5.9. It was found that surface area would increase with increase in amount of MWCNTs. It was suggested that high surface area of MWCNTs would be incorporated in the composites. Such high surface area characteristic would increase sensing ability of sensing materials. Meanwhile high electrical conductivity of MWCNTs would help reduce sensing temperature because low resistance of sensing material.

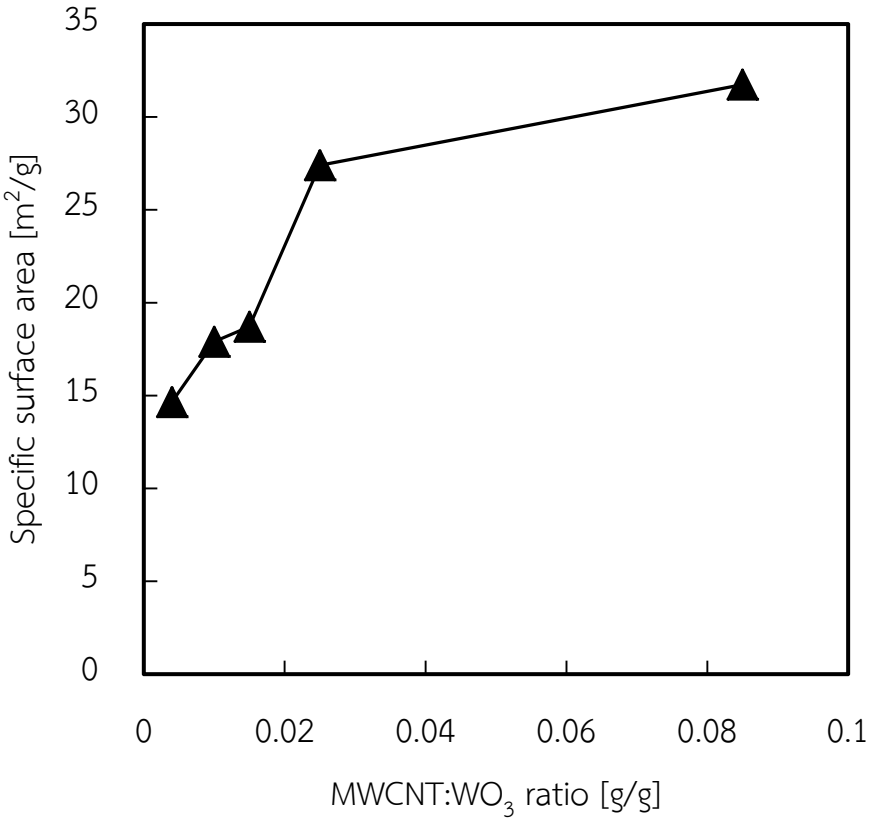

Figure 5.9 Specific surface area of the composites synthesized with different ratio of MWCNT:WO_3

5.6 Conclusion

This work is based on the assumption that physically mixed preparation of MWCNTs and WO_3 would not be sufficient for incorporating their useful nano-characteristics. To incorporate high surface area and good electrical conductivity of MWCNTs to WO_3, MWCNT-WO_3 composites, therefore, were in situ synthesized by acid precipitation method instead of only physically mixed together for fabricating sensing materials. With the chosen precipitation and calcination condition mentioned previously, mass ratio of MWCNTs to ATP was varied to investigate their effects on sensing ability of fabricated thick-film sensors. However actual mass ratio of MWCNTs to WO_3 was determined by TGA analysis. The actual mass ratio and MWCNT:ATP ratio were used to calculate an equation. The obtained equation (y=0.0987X2+1.1994X) would be expect to predict actual mass ratio of the

composite synthesis by precipitation method. Meanwhile the observation of composite morphology by SEM revealed that MWCNTs entangled with agglomerated WO_3 nanoparticles. Further observations of internal structure by TEM, it was found that WO_3 nanoparticles decorated on MWCNTs' surface and some of them embed on surface of nanotubes. Typical diameter and wall width of MWCNTs would be same as pristine MWCNTs. It was suggested that morphology of MWCNTs would be not affected by acid precipitation method. Meanwhile typical particle size of WO_3 nanoparticles was *ca.* 25 nm. The bulk composites would be further characterized by Raman to confirm existence of MWCNTs thoroughly dispersed in the composites. D-band and G-band characteristics, which used to characterize carbonaceous materials, were clearly observed in the composite samples as well as the band characteristics of WO_3. It was suggested that the bulk property of composite would be composed with MWCNTs and WO_3 nanoparticles. Because crystallite size and surface area are main characteristics of sensing materials, they were also characterized. With XRD result, it was that crystallite size of WO_3 was changed insignificantly. However, surface area of the composites increased upon increase in MWCNT ratio.

CHAPTER VI

SENSING ABILITY OF FABRICATED THICK-FILM SENSOR

The main objective of this work is to investigate sensing ability of in-house fabricated thick-film sensors. By using drop coating method, the in-house fabricated thick-film sensors were prepared from three sensing materials including as-synthesized WO_3 nanoparticles, pristine MWCNTs, MWCNT-WO_3 composites. In many previous research works, it is known that the WO_3 sensors could only perform effectively in a range of high operating temperature (200 – 800 °C) [5, 21, 24, 28, 72-74]. Because of its high resistance at low operating temperature, the WO_3 sensors could not detect a target gas. Such high operating temperature would be main disadvantage of the sensors prepared from only WO_3 nanoparticles. Therefore the goal of this work is to synthesize MWCNT-WO_3 composites for fabricating gas sensors which could response to a target gas at lower operating temperature (< 200 °C) than that prepared from only WO_3 nanoparticles. Sensing ability at lower operating temperature would be attributed to high electrical conductivity and high surface area from additional MWCNTs. However, thick-film sensors fabricated from both as-synthesized WO_3 nanoparticles and pristine MWCNTs were also prepared as reference samples to compare their sensing ability with that from the composites.

In the as-synthesized composites, amount of MWCNTs would play an important role in increase in surface area and electrical conductivity, resulting in sensing ability at lower temperature. To investigate effects of MWCNTs' amount in the composites on sensing ability, the as-prepared composites with different mass ratios of MWCNTs to WO_3 nanoparticles were prepared to comparatively test using carbon dioxide (CO_2) as a model target gas. The operating temperature for testing sensor ability was in a range from room temperature (25 °C) to higher temperature (200 °C). Meanwhile main sensing abilities in this work are response, sensitivity (S), and response time (τ_{res}). They would be examined in each fabricated sensor in order to verify a good sensor (suitable amount of MWCNTs in the composites) in term of low operating temperature and/or high sensitivity and/or fast response time.

6.1 Fabrication and measurement of thick-film sensors

As mentioned earlier in chapter III, an in-house fabricated gas sensing kit (IFG kit) was easily assembled to examine sensing ability of as-synthesized sensing materials. Briefly, the IFG kit composed of three main components including fabricated thick-film sensor, small integrated heater, and measuring chamber. The fabricated thick-film sensors were prepared by drop coating method of a paste onto electrodes following 100 ℃-overnight drying. The paste is a homogeneous mixture of sensing materials (i.e. WO_3 nanoparticles) and organic vehicle (absolute ethyl alcohol) with designated ratio (see chapter III). The electrode was prepared by evaporating a 50 nm-thick titanium layer, followed by a 100 nm-thick platinum layer on a glass slide using electron beam evaporation.

The fabricated thick-film sensors were installed in a 200 cm^3-measuring chamber under nitrogen flowing with volumetric flow rate of 100 ml/min as carrier gas. The sensors were heated by the small integrated heater to target operating temperature ranging from room temperature (25 ℃) to higher temperature (200 ℃). When the target operating temperature was reached and constant, a base line of resistance was monitored and waited until it became stable before introducing target gas. For each measurement, 100 ml/min of CO_2 (500 ppm) as target gas was introduced into the measuring chamber for 195 seconds and allowed the sensor recovered back to initial stage for 195 seconds after CO_2 gas was offed. Resistance change of the sensor was measured and recorded with respect to exposure time using digital multimeter connected to computer for data collection.

6.2 Sensing ability of gas sensing materials

In order to characterize performance of gas sensors, many sensing parameters are generally used, such as response, sensitivity, response time, recovery time, working temperature, selectivity, stability, detection limit, life cycle and etc. Meanwhile an ideal sensor would possess high sensitivity, dynamic range, selectivity and stability; low detection limit; good linearity; small hysteresis and response time; and long life cycle. However many research works usually make efforts to approach

only some of these ideal characteristics, disregarding the others. This is because the task of creating an ideal sensor for some gases is extremely difficult. And real applications usually do not require sensors with all perfect characteristics. Therefore in this work only three main sensing abilities including response, sensitivity (S), and response time (τ_{res}) were investigated.

Sensitivity is a change of measured signal per analyte concentration unit. The sensitivity, *S* was defined as follow;

$$S\ (\%) = ((R_t-R_0)/R_0) \times 100 \qquad (6.1)$$

where R_0 and R_t was the resistance of the sensor at its initial and exposure states, respectively.

Response time is the time required for sensor to respond to a step concentration change from zero to a certain concentration value. In this work, the response time (τ_{res}) is defined as the time required for the sensor to reach 90% of the stabilized value of its resistance in the presence of the test gas.

6.3 Responses of fabricated thick-film sensors

Responses of fabricated thick-film sensors were examined by exposing toward carbon dioxide with fixed concentration of 500 ppm (100 ml/min) at designated operating temperature. For example, thick-film sensors fabricated from MWCNT-WO_3 composites with five different mass ratios were exposed to CO_2 at operating temperature of 200 °C. Their responses to CO_2 were shown in Figure 6.1 (a) – (e). The responses are a change in resistance of sensors due to adsorption/desorption of CO_2 gas onto/out from their surface and nanostructure. It was found that the resistance (response) increased upon time of exposure and vice versa. It is clearly indicated that these fabricated sensors are n-type semiconductor sensors where the majority charge carriers are electrons [75, 76]. This observation was also corresponded to many previous research works on preparation gas sensors from WO_3 nanoparticles for oxidizing gas detection [74, 77].

With close observation in degree of responses in each sensor fabricated from the composites, the response degree varies significantly according to increase in mass ratio of MWCNTs to WO_3. It was suggested that MWCNTs would play an important role in CO_2 adsorption onto surface of the composites. However this effect would be further discussed in later section.

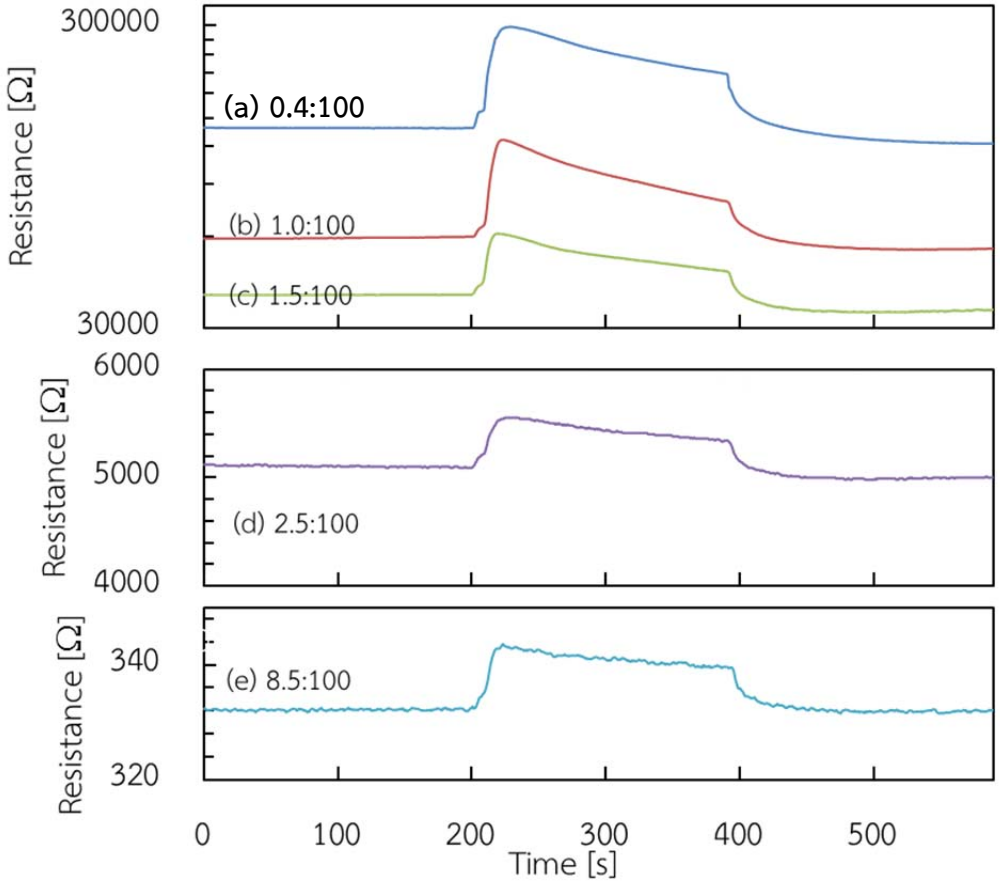

Figure 6.1 Responses of MWCNT-WO_3 composite to CO_2 at 200 °C at various ratio of MWCNT:WO_3 (a) 0.4:100 (b) 1.0:100 (c) 1.5:100 (d) 2.5:100 and (e) 8.5:100

The responses of all fabricated sensors would be measured and recorded with fixed CO_2 concentration at different operating temperatures. Although they would not be all shown in every sample, they would be used to calculate sensitivity and response time of the sensors according to definition mentioned previously.

6.4 Sensitivity of fabricated thick-film sensors

As mentioned earlier, sensitivity (S) would be calculated from its response according to equation (6.1). To investigate sensing ability of the sensors fabricated from different sensing materials, three main sensing materials including the as-synthesized WO_3 nanoparticles (see chapter IV), pristine MWCNTs (commercial), and the as-prepared MWCNT-WO_3 composites (see chapter V) were used to fabricate the in-house sensors.

6.4.1 Sensitivity of the sensors fabricated from WO_3 nanoparticles

As comprehensively discussed (in chapter IV) in search of suitable characteristics of as-synthesized WO_3 nanoparticles for fabricating sensors, the main characteristics for gas sensing materials are small crystallite size and high specific surface area. It was found that the appropriate condition was precipitation of 5.3 mM (ATP) with 10 M (HNO_3) for 30 min at 80 °C, which could give the highest yield of 71.4%. Meanwhile the calcination at 400 °C for 1 hour was the suitable condition, which could maintain small crystallite size and acceptable specific surface area. However the WO_3 nanoparticles which calcined at three different points of temperature (300 °C, 400 °C, and 600 °C) were all employed to fabricate the sensors. The all three sensors would be tested to ensure the effects of crystallite size and surface area on their sensitivity. The sensitivity of sensors were calculated and plotted in Figure 6.2. It was found that all sensors could not detect CO_2 at low operating temperature (25 °C and 50 °C). It is known that the resistance of WO_3 nanoparticles was extremely high at low operating temperature [78] and metal oxide gas sensors behaved as insulators rather than semiconductors [79] due to the density of electrons at their surface which were increased with increasing temperature [29]. It is also known that for granular metal oxides, the formation of a depletion layer at the surface of grains and grain boundaries leads to the formation of Schottky barriers between the oxide crystallites, as depicted in Figure 6.2. At low temperature, these potential barriers are very high and obstruct the transportation of charge across grain boundaries leads to the high resistivity. Increasing temperature causes more powerful

charges, due to high activation energy, that could be transport cross these barriers resulting in lower resistivity. These experimental results were also corresponded with other research works.

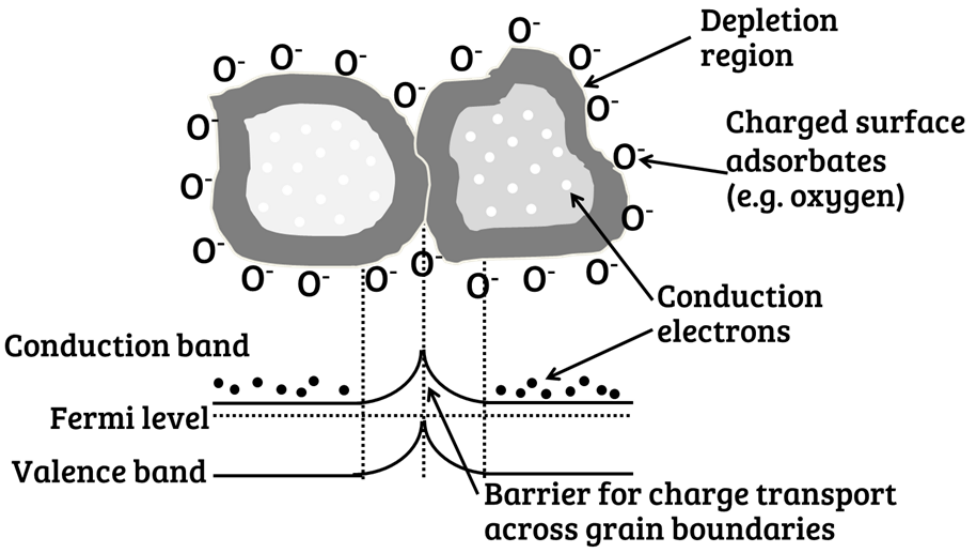

Figure 6.2 Schematic diagram of the formation of interparticle Schottky barriers between the oxide crystallites

Moreover the WO_3@300 °C sensor (prepared from WO_3 calcined at 300 °C) could still not sensitive to CO_2 until operating temperature above 200 °C. Although this WO_3 sensor possesses small crystallite size and high surface area, the content of water molecules in its crystal still high which is evident from TGA result (see chapter IV). Due to the electronic conduction in WO_3 structure is done by the clusters linked together by O-W-O bonds, presence of water molecule causes the terminal W=O bond resulting in high resistance of the sensor and limit the sensing ability. Therefore it could perform only at higher operating temperature of 200 °C as shown in Figure 6.3.

The two sensors including WO_3@400 °C sensor and WO_3@600 °C sensor denote the sensors prepared from WO_3 calcined at 400 °C and 600 °C, respectively. However their sensitivity could be observed from operating temperature of 100 °C. And they increased upon increase in operating temperature. It was

suggested that the higher operating temperature would enhance chemical reactions of target gas (CO_2) on the surface of sensing materials (WO_3 nanoparticles) [26]. This experimental result is also corresponded to previous research works on WO_3 sensors.

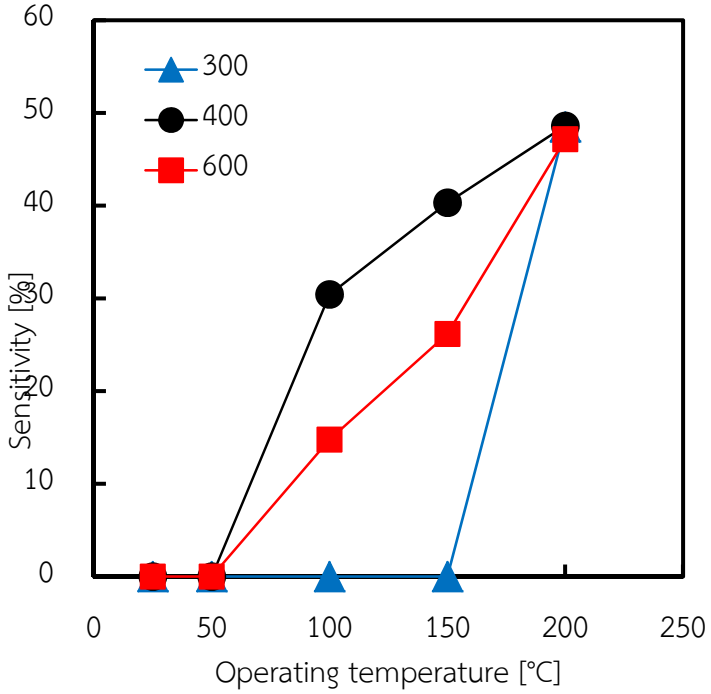

Figure 6.3 Sensitivity of the sensors fabricated from WO_3 calcined at different temperature

However it was worth to notice that the sensitivity of WO_3@400 °C sensor was higher than other sensors in all operating temperature (100 °C, 150 °C, and 200 °C). The higher sensitivity would be attributed to suitable characteristics of WO_3 nanoparticles. These characteristics would be small crystallite size and high surface area of WO_3 nanoparticles. Consequently this experimental finding strongly confirmed that the calcination condition at 400 °C for 1 hour was suitable condition for preparing WO_3 nanoparticles than that at 300 °C and 600 °C. Therefore this calcination condition was further used to prepare MWCNT-WO_3 composites as well as calcined MWCNTs.

6.4.2 Sensitivity of the sensors fabricated from MWCNTs

In previous section, WO_3 nanoparticles were solely used to prepare the sensor and test its sensing ability. Similarly, MWCNTs were also used to fabricate the sensor separately. The fabricated sensors would be tested in the same way as the sensors from WO_3 nanoparticles. This investigation mean would help us to understand the effects of additional MWCNTs and mechanisms of sensing materials when they were composited. Moreover the as-synthesized composites would be also calcined at 400 ℃ for 1 hour. Therefore, not only WO_3 nanoparticles but also MWCNTs were calcined before fabricating the sensor. The p-MWCNT sensor and c-MWCNT sensor denote the sensors prepared from pristine MWCNTs and MWCNTs calcined at 400 ℃ for 1 hour, respectively. Sensitivity of the sensors was shown in Figure 6.4. It was found that the c-MWCNT sensor would exhibit higher sensitivity than the p-MWCNT sensor. It was suggested that calcination process would help improve in higher surface area [80] and crystallinity of MWCNTs. This improvement could be attributed to decomposition of amorphous carbon in MWCNTs, resulting in development of higher pore structure as well as increase in crystallinity content. The decomposition behavior would be observed from weight loss of TGA results.

The higher surface area and crystallinity would provide larger capacity for CO_2 accommodation and also give higher electrical conductivity of the fabricated sensor. With these experimental finding, it was evident that calcination process could not provide negative effects on property of MWCNTs. Fortunately it improved the sensing property of MWCNTs. Therefore it was implied that the MWCNT-WO_3 composite would be improved with this calcination condition.

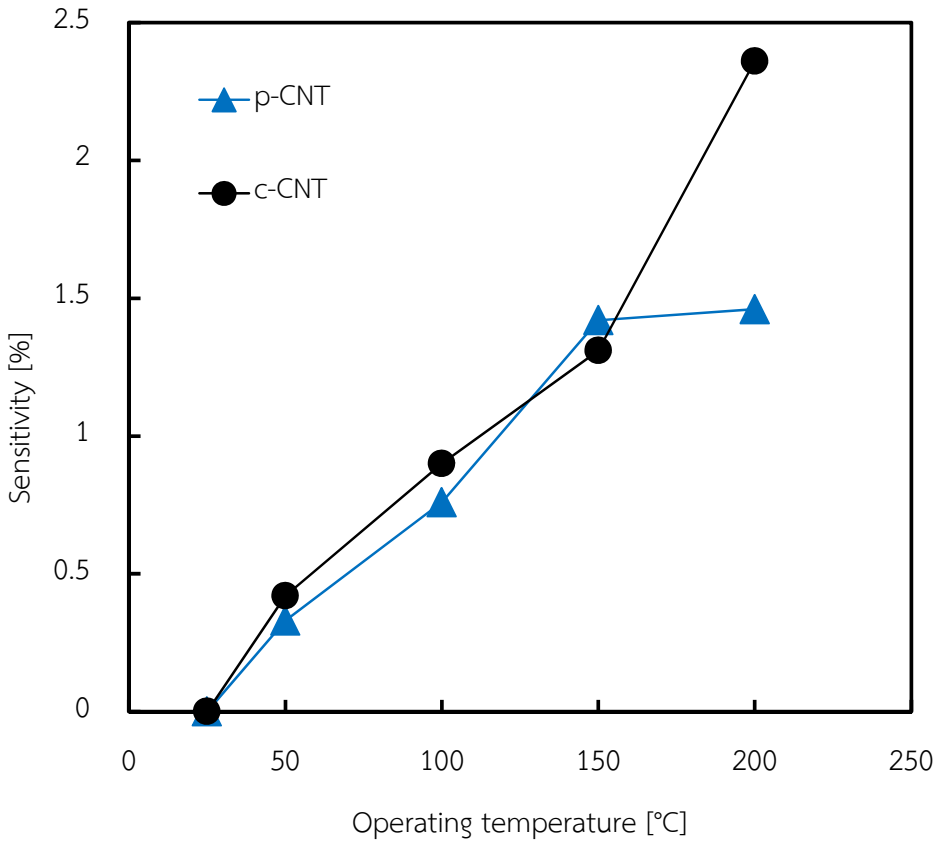

Figure 6.4 Sensitivity of the sensors fabricated from p-MWCNTs and c-MWCNTs

6.4.3 Sensitivity of the sensors fabricated from MWCNT-WO_3 composites

From two previous sections, the WO_3 sensor, the c-MWCNT sensor, and the p-MWCNT sensor were tested their sensing ability to use as reference sensors for comparing to the sensors prepared from the MWCNT-WO_3 composites. In this section, the five different mass ratios of MWCNTs to WO_3 nanoparticles including 0.4:100, 1.0:100, 1.5:100, 2.5:100, and 8.5:100 were employed to prepare the sensors. Therefore the 0.4:100@sensor, 1.0:100@sensor, 1.5:100@sensor, 2.5:100@sensor, and 8.5:100@sensor denote the sensors prepared from the MWCNT-WO_3 composites with mass ratio of 0.4:100, 1.0:100, 1.5:100, 2.5:100, and 8.5:100, respectively. Their sensitivity was shown in Figure 6.5.

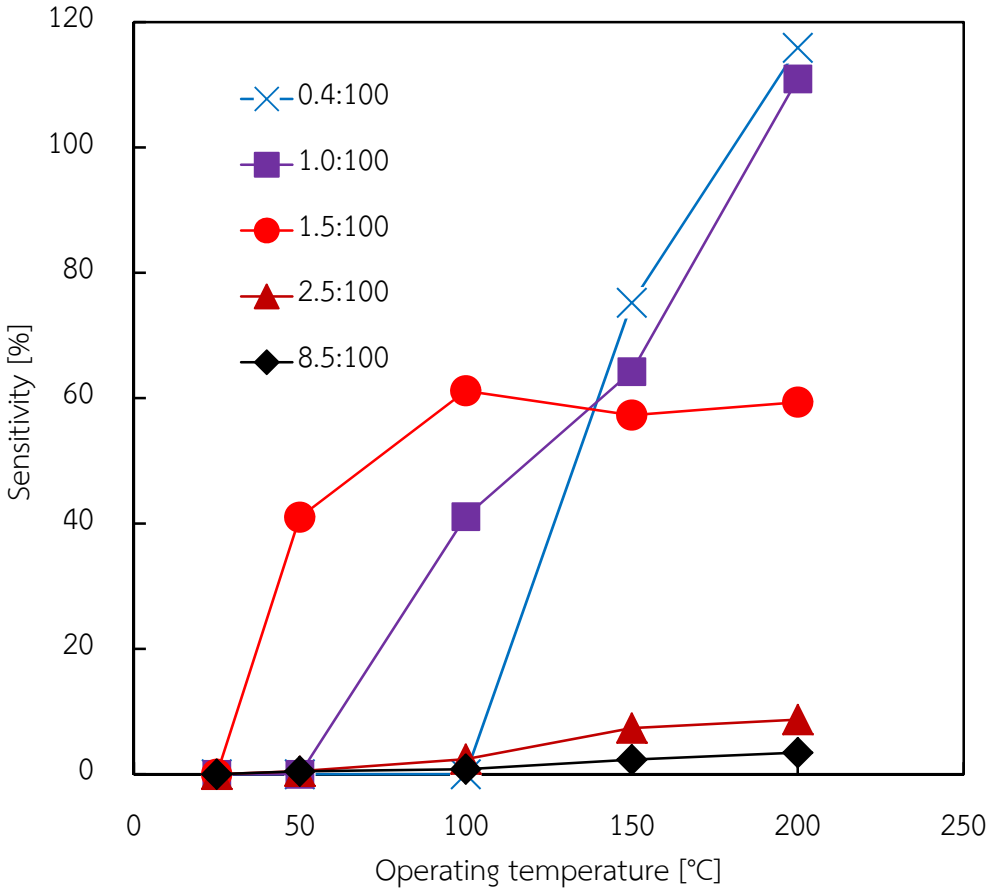

Figure 6.5 Sensitivity of the sensors fabricated from MWCNT-WO_3 composites with different ratio

With smallest ratio, the 0.4:100@sensor would exhibit the highest sensitivity at higher temperature range (150-200 °C). This would be attributed to WO_3 nanoparticles would play an important role in response to CO_2 gas due to the main matrix of sensor consisting of WO_3. However incorporation of such small amount of MWCNTs in the composites would help improve the sensitivity. It was found that the sensitivity increased two times from the WO_3 sensor at operating temperature of 200 °C as shown in Table 6.1. It could be implied from this results that MWCNTs would not only adsorb CO_2 molecules but also enhance the chemical reactions of CO_2 on the surface of sensors, resulting in higher sensitivity.

Meanwhile the 1.0:100@sensor could response to CO_2 with sensitivity of 40% at lower operating temperature of 100 °C. It was suggested that the more

addition of MWCNTs to the composites would improve the ability of sensor in term of sensing ability at lower operating temperature. With higher portion of MWCNTs in the composites, they would provide more capacity for adsorption of CO_2 due to high surface area of MWCNTs. This could be confirmed by the higher surface area of the as-prepared composited when the portion of MWCNTs added more (see chapter V). Meanwhile it is known that MWCNTs possesses high electrical conductivity attributed to crystalline property of graphitic carbons. The good electrical conductivity would help reduce the resistance of sensor when it performs at lower operating temperature. Therefore the two useful properties of MWCNTs would help improve the sensing ability in lower operating temperature with high sensitivity. However because of the majority of composite matrix is WO_3 nanoparticles, the sensitivity would increase upon increase in operating temperature.

With higher portion of MWCNTs in the composite, the 1.5:100@sensor would response to CO_2 at the lowest operating temperature of 50 ℃, which is near room temperature (25 ℃). This sensing ability is the aim of this work. As mentioned earlier, the main disadvantage of WO_3 sensor is only sensible in range of high operating temperature. Therefore it could hardly apply to use in real applications. At the lowest operating temperature (50 ℃), the sensitivity of the sensor was 41%, which was same value (45%) as the WO_3 sensor performing at the highest operating temperature of 200 ℃. It was suggested that the operating temperature was reduced four times (from 200 ℃ to 50 ℃) by incorporation useful properties of MWCNTs. This benefit was shown in Figure 6.6. However, this incorporation would not be resulted from only mixing MWCNTs and WO_3 nanoparticles together. It would be attributed to characteristics of the composites, which could be confirmed by TEM and Raman observations (see chapter V).

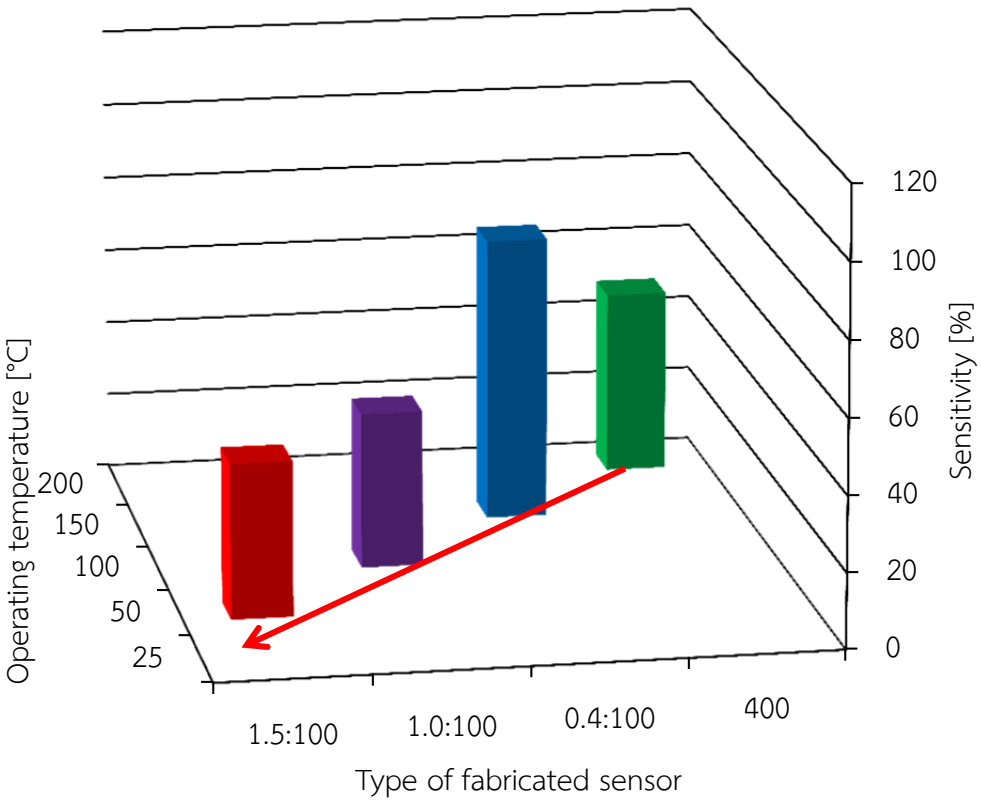

Figure 6.6 Sensitivity of the sensors prepared from the composites

Although the sensitivity increased when the operating temperature increased from 50 ℃ to 100 ℃, the sensitivity seemed to be constant at 60% upon increase in operating temperature from 100 ℃ to 200 ℃. It was suggested that the electrical conductivity of the sensor would achieve maximum point attributed to the portion of MWCNTs. The increase in operating temperature could not help enhance the electrical conductivity by reduction in resistance of WO_3 nanoparticles, resulting in constant sensitivity of sensor. This behavior would be also observed in the sensor with more MWNCTs as shown in Figure 6.7.

The 2.5:100@sensor and 8.5:100@sensor would exhibit lower sensitivity compared to other sensors that mentioned earlier. This low sensitivity would be caused from the higher electrical conductivity of sensors attributed to excess addition of MWCNTs. At such high conductivity, the resistance of sensor was low as its change could not be observed during exposure to CO_2. Although surface

area of composites with these ratios was higher than others, this higher surface area would play a minor role in increase in sensitivity. In contradict the resistance would be a main factor of the sensitivity. With this experimental observation, it was suggested that excess MWCNTs would significantly decrease the sensitivity of sensors, resulting from the high electrical conductivity of MWCNTs.

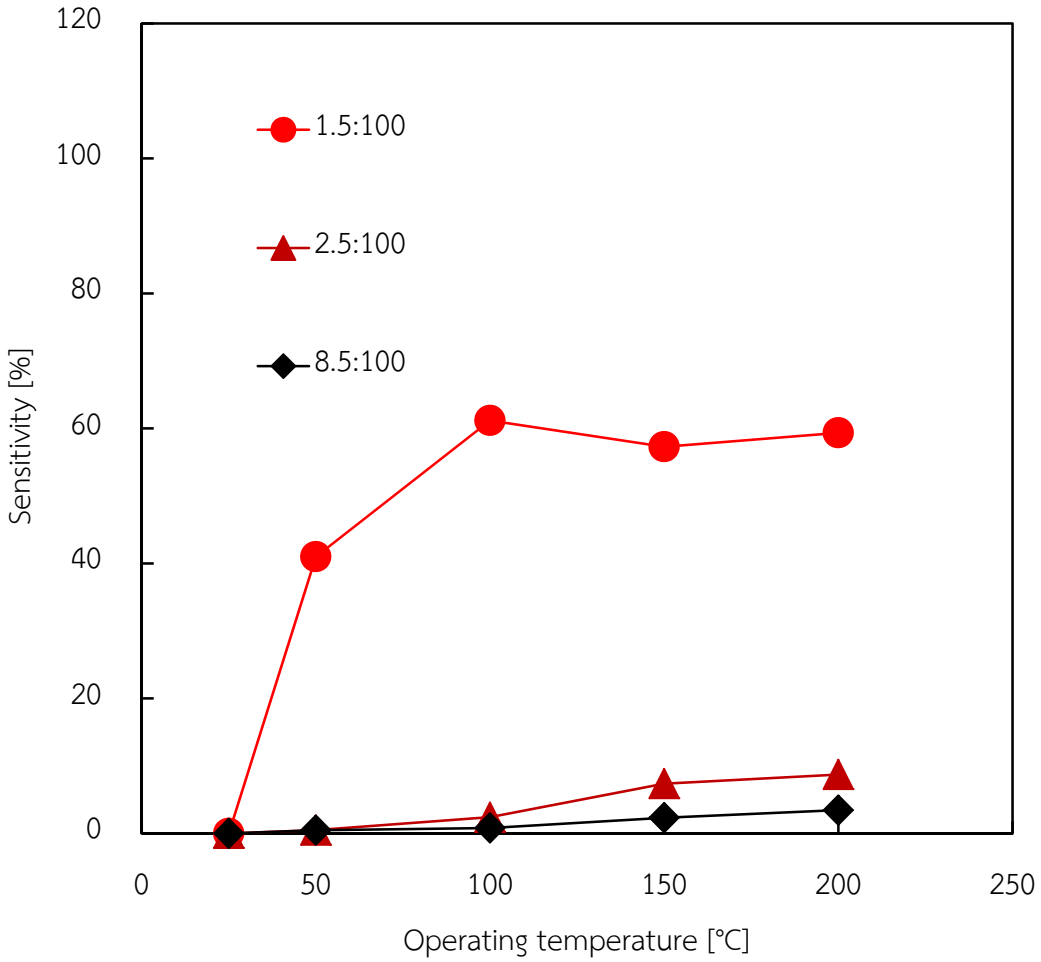

Figure 6.7 Sensitivity of the sensors fabricated from MWCNT-WO_3 composites with different ratio (higher ratio)

6.4.4 Sensitivity behavior at high operating temperature

At high range of operating temperature (150-200 °C), the sensitivity of sensor would decrease upon increase in a portion of MWCNTs in the composites as shown in Figure 6.8. At such high operating temperature, thermal energy would also help enhance chemical reactions (e.g. adsorption and desorption processes, surface coverage, co-adsorption, and chemical decomposition) on the surface of sensor as well as reduce its resistance due to increase charge-carrier concentration [79]. It was implied that WO_3 would play an important role to sensitivity of sensor at high operating temperature. Therefore the addition of high surface area MWCNTs which was expect to improve adsorption capacity of CO_2, could not exhibit its effect on sensitivity. Meanwhile good electrical conductivity of MWCNTs could reduce the resistance of sensor, resulting in low changing in resistance during exposure to CO_2 as well. Consequently the more addition of MWCNTs, the less sensitivity would be observed.

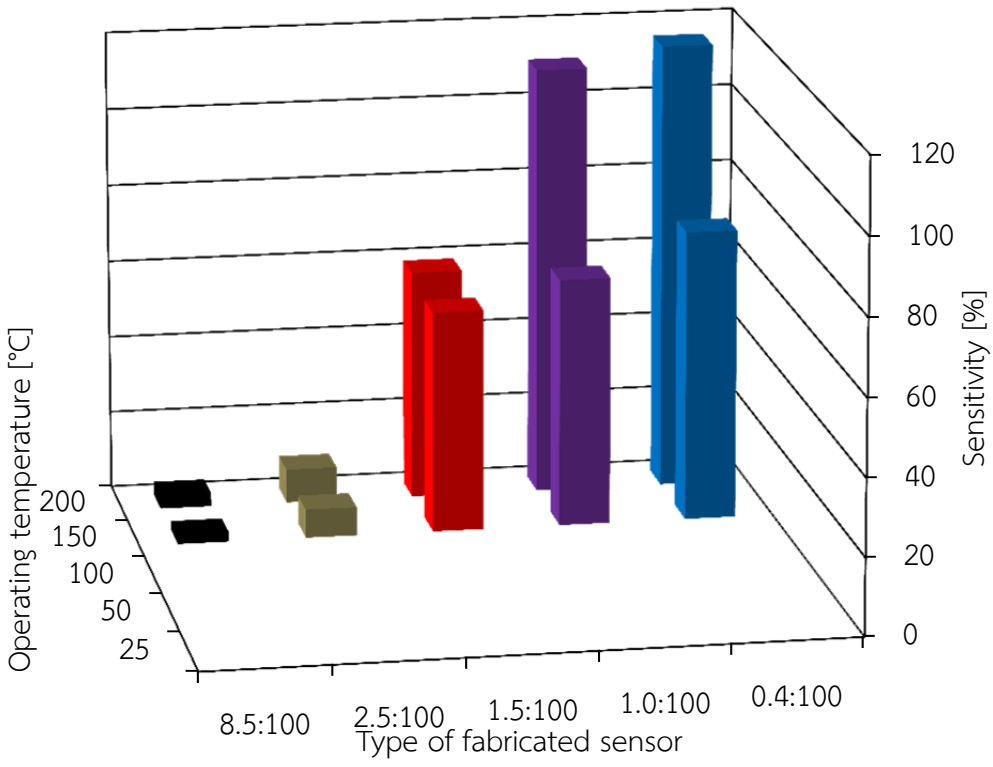

Figure 6.8 Sensitivity at high operating temperature

6.4.5 Sensitivity behavior at low operating temperature

Unfortunately all our fabricated sensors could not response to CO_2 at room temperature. However the addition of MWCNTs to the composites would exhibit good effect on sensitivity in term of reducing the operating temperature from 200 °C to 50 °C as mentioned earlier. At low range of operating temperature (50 – 100 °C), the trend of sensitivity was different from that at high operating temperature as shown in Figure 6.9. At operating temperature of 100 °C, the sensitivity was improved from zero to 41.1% when the ratio increased from 0.4:100 to 1.0:100. And the sensitivity reached maximum at the ratio of 1.5:100. It is turned to dramatically decrease upon increase in MWCNTs. For the operating temperature of 50 °C, the sensitivity was also maximum point at the ratio of 1.5:100. With observation of this trend, it was implied that the highest sensitivity at low operating temperature was obtained at the ratio of 1.5:100. It could be concluded that the optimum ratio for the highest sensitivity and low operating temperature is 1.5:100.

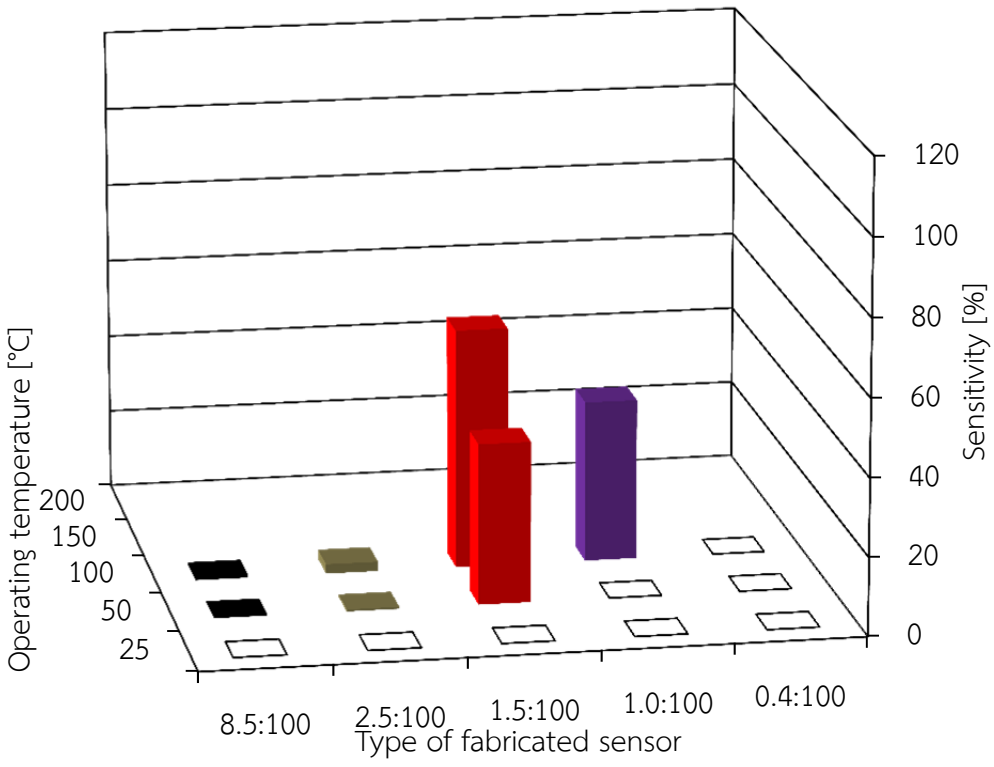

Figure 6.9 Sensitivity at low operating temperature

The sensitivity of the fabricated sensors was shown in Table 6.1. With the comparison of the sensors fabricated from the composites to those fabricated from pristine MWCNTs and WO_3 nanoparticles. With respect to the sensitivity, it was found that the sensors could perform in the higher and lower operating temperature in the different ways. At higher operating temperature, the WO_3 sensor could perform effectively with high sensitivity. However, the 0.4:100@sensor could detect CO_2 with higher sensitivity. It could be inferred that the MWNCTs in the composite could help improve the sensitivity. Moreover more addition of MWNCTs to the composite, it was found that the 1.5:100@sensor could respond to CO_2 at the lower operating temperature of 50 °C with the sensitivity of 41.0%. However the excess of MWCNTs could provide the negative effect to the sensitivity of the fabricated sensor, occurring when the ratio exceed 2.5:100 as shown in Table 6.1.

Table 6.1 Sensitivity (%) of composite sensors, pristine MWCNTs and WO_3 at various operating temperature

Sensor	Operating temperature (°C)				
	25	50	100	150	200
Pristine MWCNTs	-	0.3	0.8	1.4	1.5
Calcined MWCNTs	-	0.4	0.9	1.3	1.9
WO_3@300 °C	-	-	-	-	48.5
WO_3@400 °C	-	-	30.4	40.3	48.6
WO_3@600 °C	-	-	14.8	26.2	47.2
0.4:100	-	-	-	75.2	115.9
1.0:100	-	-	41.1	64.3	110.9
1.5:100	-	41.0	61.2	57.3	59.4
2.5:100	-	0.5	2.41	7.37	8.7
8.5:100	-	0.5	0.8	2.3	3.5

6.5 Response time of fabricated thick-film sensors

The response time of the WO_3@400 ℃ sensor at different operating temperature including 50, 150, 200 ℃ were 22.5, 22.2, and 21.4 seconds, respectively. It was found that the response time slightly decreased upon the increase in operating temperature. This prolonged response time at low operating temperature was corresponded to other research works on WO_3 sensor [29, 74]. The response times of the sensors in this work, however, were very fast in a range of 19-70 seconds. Moreover, the response time of the 1.5:100@sensor at lower operating temperature of 50 ℃ was the minimum response time in this work. It was suggested that this ratio could provide the sensor not only operation at low temperature, but also fast response time.

Table 6.2 Response time (s) of composite sensors, pristine MWCNTs and WO_3 at various operating temperature

Sensor	Operating temperature (℃)				
	25	50	100	150	200
Pristine MWCNTs	-	35.1	37.4	24.3	47.6
Calcined MWCNTs	-	44.1	34.2	68.5	50.1
WO_3@300 ℃	-	-	-	-	23.4
WO_3@400 ℃	-	-	22.5	22.2	21.4
WO_3@600 ℃	-	-	43.7	22.9	21.1
0.4:100	-	-	-	23.0	24.9
1.0:100	-	-	20.4	26.2	23.6
1.5:100	-	19.4	20.4	21.7	20.0
2.5:100	-	21.9	30.9	25.5	23.3
8.5:100	-	59.4	51.1	27.9	20.9

With increase in portion of MWCNTs in the composites, it was found that the response time of the 8.5:100@sensor slightly increased. It was suggested that

the more addition of MWCNTs would prolong the response time. This effect could be implied from the response time of pristine MWCNTs as shown in Table 6.2. However, it is known that sensing ability of the sensor has to be considered from various parameters. In this work, both sensitivity and response time were taken in account.

At higher operating temperature (150 – 200 °C), the 0.4:100@sensor could give the highest sensitivity of 75.2 % and 115.9%, respectively. However, the highest sensitivity of 41.0% and 61.2 % were achieved from 1.5:100@sensor at the lower operating temperature of 50 °C and 100 °C, respectively. With acceptable response time, it cloud be concluded that the 0.4:100@sensor could be performed effectively at high operating temperature with the highest sensitivity and fast response time. Meanwhile the 1.5:100@sensor could detect CO_2 effectively at the lower operating temperature with the fastest response time.

6.6 Conclusion

The last objective of this work is to investigate sensing ability of in-house fabricated thick-film sensors. Since WO_3 sensors could only perform effectively in a range of high operating temperature (200 – 800 °C) which is main disadvantage, the goal of this work is to utilize the synthesized MWCNT-WO_3 composites for fabricating gas sensors which could response to a target gas at lower operating temperature (< 200 °C). By using drop coating method, the in-house fabricated thick-film sensors were prepared from three sensing materials including as-synthesized WO_3 nanoparticles, pristine MWCNTs, MWCNT-WO_3 composites. The fabricated sensors were tested using CO_2 as a model target gas at low operating temperature of 25 °C to higher operating temperature of 200 °C. The responses are a change in resistance of sensors due to adsorption/desorption of CO_2 gas onto/out from their surface and nanostructure. In this work, it was found that the resistance (response) increased upon time of exposure and vice versa. It is indicated that these fabricated sensors are n-type semiconductor sensors. With different calcination temperatures (300, 400, and 600 °C), the WO_3@400 °C sensor could exhibit higher sensitivity than

others attribute their higher surface area and smaller crystallite that the WO_3@600 °C sensor. However the WO_3@300 °C sensor could only detect CO_2 at high operating temperature due to water remaining in its structure. Meanwhile the calcined MWCNTs could response to CO_2 with higher sensitivity than pristine MWCNTs attribute their decomposition of some amorphous carbon in their structure, resulting in higher crystallinity and surface area. With small portion of MWCNTs in the composites (the 0.4:100@sensor), it could provide higher sensitivity than those WO_3 nanoparticles attributed to incorporation of their useful characteristics. With higher portion of MWCNTs, it was found that the sensors could respond to CO_2 at lower operating temperature. At near same sensitivity, the 1.5:100@sensor could detect CO_2 at operating temperature of 50 °C, which reduce four times from 200 °C. However the addition of MWNCTs would become excess when the ratio exceed 2.5:100. This could be observed from sharp decrease in sensitivity of the sensors prepared from that ratio. The sensitivity behavior at high and low operating temperature was different way. At high operating temperature (150 – 200 °C), sensitivity would decrease upon increase in MWNCTs attributed to its high electrical conductivity. In contradictory, sensitivity was optimum at the appropriated ratio of 1.5:100 at low operating temperature (50 – 100 °C). Response time of all fabricated sensors was in range of 19 – 70 seconds. At the optimum ratio, the shortest response time of 19.4 seconds was obtained.

Chapter VII

CONCLUSION AND RECOMMENDATIONS

7.1 Conclusion

In this research work, the objective was divided into two main points. The first objective is to in situ synthesize multi-walled carbon nanotube-tungsten oxide (MWCNT-WO_3) composites by facile/inexpensive acid precipitation method for using as gas sensing materials. The second objective is to investigate sensing ability of the in-house fabricated sensors prepared from the synthesized sensing materials. In order to obtain the suitable conditions for synthesizing the MWCNT-WO_3 composites, tungsten oxide (WO_3) nanoparticles were synthesized solely to determine the highest yield and the optimal calcination conditions which have strong effect to the properties of sensing materials. The maximum percent yield was obtained at initial concentration of tungstate salt and nitric acid of 5.3 mM and 10 M, respectively. Therefore this condition was chosen for synthesizing WO_3 nanoparticles as well as MWCNT-WO_3 composites. In calcination process, it was confirmed that the calcination temperature of 400 °C and calcination time of 1 hour would be suitable condition to obtain appropriate WO_3 characteristics. Meanwhile this work is based on the assumption that physically mixed preparation of MWCNTs and WO_3 would not be sufficient for incorporating their useful nano-characteristics. To incorporate high surface area and good electrical conductivity of MWCNTs to WO_3, MWCNT-WO_3 composites, therefore, were in situ synthesized by acid precipitation method instead of only physically mixed together for fabricating sensing materials. Meanwhile the observation of composite morphology by SEM revealed that MWCNTs entangled with agglomerated WO_3 nanoparticles. Further observations of internal structure by TEM, it was found that WO_3 nanoparticles decorated on MWCNTs' surface and some of them embed on surface of nanotubes.

In conclusion, the MWCNT-WO_3 composites were successfully synthesized by facile/inexpensive acid precipitation method for employing as sensing materials. Their characteristics were thoroughly investigated by many analytical

techniques to determine suitable condition for precipitation, calcination, and composites preparation. With small ratio of MWCNTs to WO_3 (0.4:100), the as-prepared composites could provide three times higher sensitivity (S = 115.9%) than the sensors prepared from only WO_3 nanoparticles (S = 48.6%). With the optimum ratio of MWCNTs to WO_3 (1.5:100), the sensors could also respond to CO_2 at lower operating temperature of 50 °C with high sensitivity of 41.0%. With all these experimental finding, it could be a promising preparation method for synthesizing sensing materials for detecting gas in real applications.

7.2 Recommendations

The present work is the early step of investigation of in situ synthesis of MWCNT-WO_3 composites by facile/inexpensive acid precipitation method. Therefore, there are still a number of possible directions to extend, improve it. The followings are the recommendations for future work:

1) The present work pays more attention to the hydrolysis reaction in the acid precipitation process where a lot of WO_3 nanoparticles are expected to form by neglecting reactions after cooling to room temperature. Cleary, WO_3 nanoparticles seemed to precipitate more when they placed at static condition before rinsing process which would be attributed to high acid content with undergoing reactions. This could be solved by designing the new process with suddenly reducing the acid content.

2) The MWCNT-WO_3 composites have been proved to respond to CO_2 at lower operating temperature. It would be great that other hazardous gases would be used to test with these sensing materials.

3) In this present work, the concentration of CO_2 was fixed at 500 ppm. To investigate effect of gas concentration, the concentration should be varied in a range which related to real application.

4) After carbonization process, the MWCNT-WO_3 composites would still have some water content due to high surface area of MWCNTs. This high surface

area structure would provide higher capacity of water accommodation. This issue would be addressed by higher heat treatment to remove water molecules.

REFERENCES

[1] Chen, H. M., and Liu, R.-S., Architecture of Metallic Nanostructures: Synthesis Strategy and Specific Applications. The Journal of Physical Chemistry C 115,9(2011): 3513-3527.

[2] Zhang, L., and Webster, T. J., Nanotechnology and nanomaterials: Promises for improved tissue regeneration. Nano Today 4,1(2009): 66-80.

[3] Liu, Z., Miyauchi, M., Yamazaki, T., and Shen, Y., Facile synthesis and NO_2 gas sensing of tungsten oxide nanorods assembled microspheres. Sensors and Actuators B: Chemical 140,2(2009): 514-519.

[4] Zhan, Z., Lu, J., Song, W., Jiang, D., and Xu, J., Highly selective ethanol In_2O_3-based gas sensor. Materials Research Bulletin 42,2(2007): 228-235.

[5] Boudiba, A., Zhang, C., Navio, C., Bittencourt, C., Snyders, R., and Debliquy, M., Preparation of highly selective, sensitive and stable hydrogen sensors based on Pd-doped tungsten trioxide. Procedia Engineering 5,0(2010): 180-183.

[6] Wang, J., Li, M., Shi, Z., Li, N., and Gu, Z., Investigation of the electrocatalytic behavior of single-wall carbon nanotube films on an Au electrode. Microchemical Journal 73,3(2002): 325-333.

[7] Shanmugam, S., and Gedanken, A., An easy single step route to synthesize open-ended carbon nanotubes. Carbon 46,12(2008): 1615-1619.

[8] Hashishin, T., and Tamaki, J., Conductivity-Type Sensor Based on CNT-WO_3 Composite for NO_2 Detection. Journal of Nanomaterials 2008,(2008): 1-4.

[9] Espinosa, E. H., et al., Highly Selective NO_2 Gas Sensors Made of MWCNTs and WO_3 Hybrid Layers. Journal of The Electrochemical Society 154,5(2007): J141-J149.

[10] Bittencourt, C., et al., WO_3 films modified with functionalised multi-wall carbon nanotubes: Morphological, compositional and gas response studies. Sensors and Actuators B: Chemical 115,1(2006): 33-41.

[11] Bittencourt, C., et al., Evaporation of WO_3 on carbon nanotube films: a new hybrid film. Smart Materials and Structures 15,6(2006): 1555.

[12] Li, Y., Wang, H.-c., and Yang, M.-j., n-Type gas sensing characteristics of chemically modified multi-walled carbon nanotubes and PMMA composite. Sensors and Actuators B: Chemical 121,2(2007): 496-500.

[13] Roy, R. K., Chowdhury, M. P., and Pal, A. K., Room temperature sensor based on carbon nanotubes and nanofibres for methane detection. Vacuum 77,3(2005): 223-229.

[14] Ionescu, R., et al., Oxygen functionalisation of MWNT and their use as gas sensitive thick-film layers. Sensors and Actuators B: Chemical 113,1(2006): 36-46.

[15] Zhang, W.-D., and Zhang, W.-H., Carbon Nanotubes as Active Components for Gas Sensors. Journal of Sensors 2009,(2009).

[16] Llobet, E., et al., Carbon nanotube-TiO_2 hybrid films for detecting traces of O_2. Nanotechnology 19,37(2008): 375501.

[17] Baraton, M. I., Merhari, L., Ferkel, H., and Castagnet, J. F., Comparison of the gas sensing properties of tin, indium and tungsten oxides nanopowders: carbon monoxide and oxygen detection. Materials Science and Engineering: C 19,1-2(2002): 315-321.

[18] Yadav, L., Chandra Gupta, N., Dwivedi, R., and Singh, R. S., Sensing behavior and mechanism of titanium dioxide-based MOS hydrogen sensor. Microelectronics Journal 38,12(2007): 1226-1232.

[19] Aslam, M., et al., A highly selective ammonia gas sensor using surface-ruthenated zinc oxide. Sensors and Actuators A: Physical 75,2(1999): 162-167.

[20] Rout, C. S., Hegde, M., and Rao, C. N. R., H_2S sensors based on tungsten oxide nanostructures. Sensors and Actuators B: Chemical 128,2(2008): 488-493.

[21] Nimittrakoolchai, O.-u., and Supothina, S., High-yield precipitation synthesis of tungsten oxide platelet particle and its ethylene gas-sensing characteristic. Materials Chemistry and Physics 112,1(2008): 270-274.

[22] Breedon, M., et al., Synthesis of Nanostructured Tungsten Oxide Thin Films: A Simple, Controllable, Inexpensive, Aqueous Sol-Gel Method. Crystal Growth & Design 10,1(2009): 430-439.

[23] Kida, T., Nishiyama, A., Yuasa, M., Shimanoe, K., and Yamazoe, N., Highly sensitive NO_2 sensors using lamellar-structured WO_3 particles prepared by an acidification method. Sensors and Actuators B: Chemical 135,2(2009): 568-574.

[24] Solis, J. L., Saukko, S., Kish, L., Granqvist, C. G., and Lantto, V., Semiconductor gas sensors based on nanostructured tungsten oxide. Thin Solid Films 391,2(2001): 255-260.

[25] Sriyudthsak, M., and Supothina, S., Humidity-insensitive and low oxygen dependence tungsten oxide gas sensors. Sensors and Actuators B: Chemical 113,1(2006): 265-271.

[26] Srivastava, V., Srivastava, A. K., Sood, K. N., and Jain, K., Sol Gel Synthesis of Tungsten Oxide Thin Film in Presence of Surfactant for NO_2 Detection. Sensors & Transducers Journal 107,8(2009): 99-110.

[27] Wang, L., Pfeifer, J., Bal, zsi, C., and Gouma, P. I., Synthesis and Sensing Properties to NH_3 of Hexagonal WO_3 Metastable Nanopowders. Materials and Manufacturing Processes 22,6(2007): 773-776.

[28] Deliang, C., et al., The enhanced alcohol-sensing response of ultrathin WO_3 nanoplates. Nanotechnology 21,3(2010): 035501.

[29] Wang, S.-H., Chou, T.-C., and Liu, C.-C., Nano-crystalline tungsten oxide NO_2 sensor. Sensors and Actuators B: Chemical 94,3(2003): 343-351.

[30] Espinosa, E. H., et al., Hybrid metal oxide and multiwall carbon nanotube films for low temperature gas sensing. Sensors and Actuators B: Chemical 127,1(2007): 137-142.

[31] Supothina, S., Seeharaj, P., Yoriya, S., and Sriyudthsak, M., Synthesis of tungsten oxide nanoparticles by acid precipitation method. Ceramics International 33,6(2007): 931-936.

[32] Saleh, T. A., and Gupta, V. K., Functionalization of tungsten oxide into MWCNT and its application for sunlight-induced degradation of rhodamine B. Journal of Colloid and Interface Science 362,2(2011): 337-344.

[33] Tian, L., Ye, L., Liu, J., and Zan, L., Solvothermal synthesis of CNTs-WO_3 hybrid nanostructures with high photocatalytic activity under visible light. Catalysis Communications 17,0(2012): 99-103.

[34] Ng, C., Ye, C., Ng, Y. H., and Amal, R., Flower-Shaped Tungsten Oxide with Inorganic Fullerene-like Structure: Synthesis and Characterization. Crystal Growth & Design 10,8(2010): 3794-3801.

[35] Hidayat, D., Purwanto, A., Wang, W.-N., and Okuyama, K., Preparation of size-controlled tungsten oxide nanoparticles and evaluation of their adsorption performance. Materials Research Bulletin 45,2(2010): 165-173.

[36] Zheng, H., Ou, J. Z., Strano, M. S., Kaner, R. B., Mitchell, A., and Kalantar-zadeh, K., Nanostructured Tungsten Oxide - Properties, Synthesis, and Applications. Advanced Functional Materials 21,(2011): 2175-2196.

[37] Berger, O., Fischer, W.-J., and Melev, V., Tungsten-oxide thin films as novel materials with high sensitivity and selectivity to NO_2, O_3 and H_2S. Part I: Preparation and microstructural characterization of the tungsten-oxide thin films Journal of Materials Science: Materials in Electronics 15 7(2004): 463-482.

[38] Kadam, P. M., Tarwal, N. L., Mali, S. S., Deshmukh, H. P., and Patil, P. S., Enhanced electrochromic performance of f-MWCNT-WO3 composite. Electrochimica Acta 58,0(2011): 556-561.

[39] Yu, J., Qi, L., Cheng, B., and Zhao, X., Effect of calcination temperatures on microstructures and photocatalytic activity of tungsten trioxide hollow microspheres. Journal of Hazardous Materials 160,2-3(2008): 621-628.

[40] Ghasempour, R., and zad, A. I., Hybrid multiwalled carbon nanotubes and trioxide tungsten nanoparticles for hydrogen gas sensing. Journal of Physics D: Applied Physics 42,16(2009): 165105.

[41] Sharma, N., Deepa, M., Varshney, P., and Agnihotry, S. A., FTIR and absorption edge studies on tungsten oxide based precursor materials synthesized by sol-gel technique. Journal of Non-Crystalline Solids 306,2(2002): 129-137.

[42] Zhou, L., et al., Green Synthesis of Hexagonal-Shaped $WO_3.0.33H_2O$ Nanodiscs Composed of Nanosheets. Crystal Growth & Design 8,11(2008): 3993-3998.

[43] Boukriba, M., Sediri, F., and Gharbi, N., Hydrothermal synthesis of $WO_3.1/3H_2O$ nanorods and study of their electrical properties. Polyhedron 29,9(2010): 2070-2074.

[44] Kukkola, J., et al., Gas sensors based on anodic tungsten oxide. Sensors and Actuators B: Chemical 153,2(2011): 293-300.

[45] Senguttuvan, T. D., Srivastava, V., Tawal, J. S., Mishra, M., Srivastava, S., and Jain, K., Gas sensing properties of nanocrystalline tungsten oxide synthesized by acid precipitation method. Sensors and Actuators B: Chemical 150,1(2010): 384-388.

[46] Seeharaj, P., Synthesis of Tungsten Oxide Nanoparticle for iso-Butane Gas Sensing. King Mongkut's University of Technology North Bangkok Master Degree Thesis (2003).

[47] Sayago, I., et al., Carbon nanotube networks as gas sensors for NO2 detection. Talanta 77,2(2008): 758-764.

[48] Kreupl, F., Carbon Nanotubes in Microelectronic Applications, in C. Hierold (ed.), Advanced Micro & Nanosystems Weinheim: WILEY-VCH Verlag GmbH & Co. KGaA,2008.

[49] Dresselhaus, M. S., Dresselhaus, G., Charlier, J. C., and Hernandez, E., Electronic, thermal and mechanical properties of carbon nanotubes. Philosophical Transactions of the Royal Society of London. Series A:Mathematical, Physical and Engineering Sciences 362,1823(2004): 2065-2098.

[50] Baughman, R. H., Zakhidov, A. A., and Heer, W. A. d., Carbon Nanotubes-the Route Toward Applications. Science 297,(2002): 787-792.

[51] Arshak, K., Moore, E., Lyons, G. M., Harris, J., and Clifford, S., A review of gas sensors employed in electronic nose applications. Sensor Review 24,2(2004): 181 - 198.

[52] Pietruszka, B., Gregorio, F. D., Keller, N., and Keller, V., High-efficiency WO_3/carbon nanotubes for olefin skeletal isomerization. Catalysis Today 102–103,(2005): 94–100.

[53] Pietruszka, B., Di Gregorio, F., Keller, N., and Keller, V., High-efficiency WO_3/carbon nanotubes for olefin skeletal isomerization. Catalysis Today 102-103,(2005): 94-100.

[54] Balazsi, C., Sedlackova, K., Llobet, E., and Ionescu, R., Novel hexagonal WO_3 nanopowder with metal decorated carbon nanotubes as NO_2 gas sensor. Sensors and Actuators B: Chemical 133,1(2008): 151-155.

[55] Ionescu, R., et al., Novel hybrid materials for gas sensing applications made of metal-decorated MWCNTs dispersed on nano-particle metal oxides. Sensors and Actuators B: Chemical 131,1(2008): 174-182.

[56] Wang, S., Shi, X., Shao, G., Duan, X., Yang, H., and Wang, T., Preparation, characterization and photocatalytic activity of multi-walled carbon nanotube-supported tungsten trioxide composites. Journal of Physics and Chemistry of Solids 69,10(2008): 2396-2400.

[57] Sedlackova, K., Ionescu, R., and Balazsi, C., TEM Investigations on CNT-added hexagonal WO_3 films for sensing applications. NANO: Brief Reports and Reviews 3,4(2008): 223–227.

[58] Su, P.-G., and Pan, T.-T., Fabrication of a room-temperature NO_2 gas sensor based on WO_3 films and WO_3/MWCNT nanocomposite films by combining polyol process with metal organic decomposition method. Materials Chemistry and Physics 125,(2011): 351–357.

[59] Wongchoosuk, C., Wisitsoraat, A., Phokharatkul, D., Tuantranont, A., and Kerdcharoen, T., Multi-Walled Carbon Nanotube-Doped Tungsten Oxide Thin Films for Hydrogen Gas Sensing. Sensors 10,(2010): 7705-7715.

[60] Dembinska, B., and Kulesza, P. J., Multi-walled carbon nanotube-supported tungsten oxide-containing multifunctional hybrid electrocatalytic system for oxygen reduction in acid medium. Electrochimica Acta 54,(2009): 4682–4687.

[61] Lin, C.-K., Tseng, S.-C., Cheng, C.-H., Chen, C.-Y., and Chen, C.-C., Electrochromic performance of hybrid tungsten oxide films with multiwalled-CNT additions. Thin Solid Films 520,5(2011): 1375–1378.

[62] Livage, J., and Guzman, G., Aqueous precursors for electrochromic tungsten oxide hydrates. Solid State Ionics 84,3-4(1996): 205-211.

[63] Choi, Y. G., Sakai, G., Shimanoe, K., Miura, N., and Yamazoe, N., Preparation of aqueous sols of tungsten oxide dihydrate from sodium tungstate by an ion-exchange method. Sensors and Actuators B: Chemical 87,1(2002): 63-72.

[64] Choi, Y.-G., Sakai, G., Shimanoe, K., Teraoka, Y., Miura, N., and Yamazoe, N., Preparation of size and habit-controlled nano crystallites of tungsten oxide. Sensors and Actuators B: Chemical 93,1-3(2003): 486-494.

[65] Qamar, M., Gondal, M. A., and Yamani, Z. H., Synthesis of highly active nanocrystalline WO_3 and its application in laser-induced photocatalytic removal of a dye from water. Catalysis Communications 10,15(2009): 1980-1984.

[66] Bittencourt, C., Landers, R., Llobet, E., Correig, X., and Calderer, J., The role of oxygen partial pressure and annealing temperature on the formation of W=O bonds in thin WO_3 films. Semiconductor Science and Technology 17,6(2002): 522.

[67] Siciliano, T., Tepore, A., Micocci, G., Serra, A., Manno, D., and Filippo, E., WO_3 gas sensors prepared by thermal oxidization of tungsten. Sensors and Actuators B: Chemical 133,1(2008): 321-326.

[68] Santato, C., Odziemkowski, M., Ulmann, M., and Augustynski, J., Crystallographically Oriented Mesoporous WO_3 Films:Synthesis, Characterization, and Applications. Journal of the American Chemical Society 123,43(2001): 10639-10649.

[69] Daniel, M. F., Desbat, B., Lassegues, J. C., Gerand, B., and Figlarz, M., Infrared and Raman study of WO_3 tungsten trioxides and $WO_3.xH_2O$ tungsten trioxide tydrates. Journal of Solid State Chemistry 67,2(1987): 235-247.

[70] Cazzanelli, E., Vinegoni, C., Mariotto, G., Kuzmin, A., and Purans, J., Low-Temperature Polymorphism in Tungsten Trioxide Powders and Its Dependence on Mechanical Treatments. Journal of Solid State Chemistry 143,1(1999): 24-32.

[71] Iwasaki, M., and Park, W.-k., Synthesis of Nanometer-Sized WO_3 Particles by Facile Wet Process and Their Photocatalytic Properties. Journal of Nanomaterials 2008,(2008).

[72] Tamaki, J., et al., Grain-Size Effects in Tungsten Oxide-Based Sensor for Nitrogen Oxides. Journal of The Electrochemical Society 141,8(1994): 2207-2210.

[73] Yan, A., Xie, C., Zeng, D., Cai, S., and Hu, M., Synthesis, formation mechanism and sensing properties of WO_3 hydrate nanowire netted-spheres. Materials Research Bulletin 45,10(2010): 1541-1547.

[74] Kim, S.-J., Hwang, I.-S., Choi, J.-K., and Lee, J.-H., Gas sensing characteristics of WO_3 nanoplates prepared by acidification method. Thin Solid Films 519,6(2011): 2020-2024.

[75] Fine, G. F., Cavanagh, L. M., Afonja, A., and Binions, R., Metal Oxide Semi-Conductor Gas Sensors in Environmental Monitoring. Sensors 10,6(2010): 5469-5502.

[76] Wetchakun, K., et al., Semiconducting metal oxides as sensors for environmentally hazardous gases. Sensors and Actuators B: Chemical 160,1(2011): 580-591.

[77] Qin, Y., Hu, M., and Zhang, J., Microstructure characterization and NO_2-sensing properties of tungsten oxide nanostructures. Sensors and Actuators B: Chemical 150,1(2010): 339-345.

[78] Su, P. G., Ren-Jang, W., and Fang-Pei, N., Detection of nitrogen dioxide using mixed tungsten oxide-based thick film semiconductor sensor. Talanta 59,4(2003): 667-672.

[79] Mizsei, J., How can sensitive and selective semiconductor gas sensors be made? Sensors and Actuators B: Chemical 23,2-3(1995): 173-176.

[80] Li, C., et al., Oxidation of multiwalled carbon nanotubes by air: benefits for electric double layer capacitors. Powder Technology 142,2-3(2004): 175-179.

VITAE

Miss Siriporn Monchayapisut was born on June 5, 1980 in Bangkok. In 2002, she graduated Bachelor Degree of Engineering (Petrochemicals and Polymeric Materials) from Silpakorn University. After graduated, she worked as research assistant in Center of Excellence in Particle Technology, Department of Chemical Engineering, Faculty of Engineering, Chulalongkorn University for 6 years and enrolled in master course at Department of Chemical Engineering, Faculty of Engineering, Chulalongkorn University in 2008.